NASA CONTRACTOR REPORT

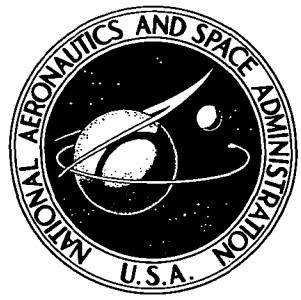

N73-24311
NASA CR-2230

NASA CR-2230

CASE FILE COPY

NEARLY SPHERICAL CONSTANT POWER DETONATION WAVES DRIVEN BY FOCUSED RADIATION

by Yves Henri George

Prepared by
CORNELL UNIVERSITY
Ithaca, N.Y. 14850
for Lewis Research Center

NATIONAL AERONAUTICS AND SPACE ADMINISTRATION • WASHINGTON, D. C. • APRIL 1973

1. Report No.	2. Government Accession No.	3. Recipient's Catalog No.
NASA CR-2230		

4. Title and Subtitle	5. Report Date
NEARLY SPHERICAL CONSTANT POWER DETONATION WAVES DRIVEN BY FOCUSED RADIATION	April 1973
	6. Performing Organization Code
7. Author(s)	8. Performing Organization Report No.
Yves Henri George	None
	10. Work Unit No.
9. Performing Organization Name and Address	
Cornell University Ithaca, New York 14850	11. Contract or Grant No. NGL 33-010-042
	13. Type of Report and Period Covered
12. Sponsoring Agency Name and Address	Contractor Report
National Aeronautics and Space Administration Washington, D.C. 20546	14. Sponsoring Agency Code

15. Supplementary Notes

Project Manager, John C. Evvard, NASA Lewis Research Center, Cleveland, Ohio

16. Abstract

The shape and the inner flow of a tridimensional spark created by focusing a laser beam in a gas are studied. The radiation is absorbed in a narrow layer preceded by a shock wave. The flow of inside plasma is assumed to be perfect gas, non-viscous, and non-heat conducting; thermal re-radiation can be neglected. Self-similarity is demonstrated for zero counterpressure and constant laser power in time; the time exponent is 3/5. An angular perturbation of a spherical spark is introduced by modifying the power addition in the angular direction. When the perturbation is small, flow equations and boundary conditions split into zeroth order and first order sets. The former is numerically integrated outward, thus checking results already known. The infinite temperature singularity at the origin is properly identified. The linear first order problem is decomposed in Fourier series of the angular variable. For harmonics one to five numerical results are obtained for the velocity components, density, and pressure profiles; the size of the perturbed spark is calculated. Maps are presented of the stream lines and constant density lines. An analysis of the large wave number case shows that the core of the flow has small tangential velocity and pressure perturbation, thus reducing the order of the system to two. A boundary layer appears near the wave front. The small perturbation expansions become singular near the focus, without, however, giving rise to sources of mass, momentum, or energy. A second order fully non-linear equation is derived for the radial velocity on the axis of symmetry in the neighborhood of the origin. Solutions to that equation display the existence of a forbidden

17. Key Words (Suggested by Author(s))	18. Distribution Statement
Detonation, constant power Laser-induced explosion Nearly-spherical shock	Unclassified - unlimited

19. Security Classif. (of this report)	20. Security Classif. (of this page)	21. No. of Pages	22. Price*
Unclassified	Unclassified	98	$3.00

* For sale by the National Technical Information Service, Springfield, Virginia 22151

region near the focus, thus indicating the limits of applicability of a small perturbation solution. An analysis of the forbidden region should include radiative heat transfer effects.

TABLE OF CONTENTS

INTRODUCTION

1. Literature Survey

The prospect of nuclear fusion recently has stimulated a great deal of interest in the production of clean, very high temperature plasmas. Focusing the beam of a Q-switched laser in a gaseous medium creates a microexplosion and an extremely hot plasma is formed. A typical laser pulse has a peak power of 100 MW and a width at half power of 20 ns. The necessary energy concentration for breakdown corresponds to electric fields of the order 10^6-10^7 V/cm; then gases normally transparent to laser light become ionized and hence absorbing.

The first reported such experiments are by Meyerand and Haught [1,2] and Damon and Tomlinson [3] in 1963. Since then a great many investigators have approached the problem from both experimental and theoretical points of view. The whole phenomenon is usually divided into three distinct phases: 1) breakdown mechanism 2) expansion of plasma during the laser pulse 3) decay of plasma after the pulse.

Experimental evidence is considerable and only a very brief survey will be attempted, more extensive descriptions can be found in the literature and a reference list is given in a very complete bibliographical review by C. DeMichelis [4] in 1969. Experiments concerning the first phase measure the threshold energy density as a function of various physical parameters: gas pressure [5,6,7], frequency of laser radiation [8,9], focal length of lens and hence energy losses by diffusion from the focal volume [6,7] and even space and time variations of the laser beam. The results show the threshold to decrease with increasing pressure with a minimum in the very high pressure range (5,000 psi), to exhibit a peak as function of frequency, to increase with decreasing focal length and to be fairly insensitive to variations of the laser beam. A large selection of gases were used: air, rare gases and some metal vapors.

The most striking feature of the second phase is the speed at which the front moves against the laser beam, typically 10^7-10^8 cm/s. This

motion has been recorded using techniques such as streak photograph (first by Ramsden and Davies [10] then various investigators [11,12,13]), Doppler shift of the radiation scattered by the plasma [10,14,15,16], Schlieren photographs [17] and scanning photographs [14,15,16].

All the experiments report longitudinal and lateral velocities as function of time. A note must be made about the experiments of Veyrie and Floux in 1968 [18] and Korobkin and al. in 1968 also [16] which show discontinuous motion of the front in direction of the lens suggesting a possibility of multiple breakdown. This effect has been explained by Evans and Grey Morgan [19,20]: primary spherical aberration of simple lenses causes peaks of intensity along the beam axis thus creating several possible regions of breakdown; the spacing between these regions is shown to agree very well with Korobkin's experiment. In fact Veyrie and Floux [18] reported that multiple breakdown did not occur when using a lens perfectly corrected for spherical aberrations. Other physical quantities pertaining to the second phase have been measured: electron density by interferometry [21,22] and temperature from X-ray emission of the plasma [15,23,24,13].

Experiments have been also performed during the third phase. Observed were the plasma motion [10,12,25], electron density from microwave transmission and reflection in a report by Askarayan and al. [26] (they also point out the existence of an ionized region ahead of the front), and temperature from spectroscopic studies [27,28,14].

The three phases have been subject to theoretical studies. The breakdown itself is generally described in terms of multiphoton ionization and cascade ionization. Since the probability of a free electron to occur naturally in the time interval considered (20 ns) is very low, the first electrons are believed to be created by a multiphoton ionization process in which several photons are simultaneously absorbed, their combined energy being sufficient to knock off an electron from a neutral atom. The probability of such an occurrence has been calculated and hence the threshold fields [29,30,31]. Except at very low pressure, order of

magnitude agreement with experiments is obtained only if the computation is limited to the creation of a single electron in the focal volume thereby indicating that another process takes over to achieve the plasma electron density (typically 10^{18} cm^{-3}), namely cascade ionization. Free electrons absorb energy from photons by inverse bremsstrahlung until they are sufficiently energetic to knock off a new electron by collision with a neutral atom giving two free electrons [32,33,34]. A cascade develops according to $N = N_o e^{t/\tau}$ with τ: cascade time constant depending on the electric field and breakdown occurs if N reaches a critical value during the laser pulse. It should be noted that neither of these two processes can account for the experimentally observed frequency dependence of the threshold field.

Before turning with somewhat more detail to the theoretical investigations of the second phase, it may be noted that the last phase has been described in terms of blast wave theory [35]. Panarella and Savic [36] developed a perturbation theory from a spherical blast wave assuming locally radial flow: the shape initially oblong due to asymmetric energy addition evolves to a spherical blast wave.

The second phase, expansion of the plasma under the influence of the laser pulse has been theoretically described in terms of three quasi one-dimensional mechanisms: a radiation supported detonation wave, a breakdown wave and a radiation transport wave.

The radiation supported detonation mechanism, first proposed by Ramsden and Savic in 1964 [35] assumes the wave front to be a shock wave followed by a layer in which the laser radiation is absorbed. Thermal reradiation from the hot plasma is neglected. Using quasi one-dimensional conservation laws across both the shock and the absorbing layer and postulating Chapman-Jouguet (normal detonation) conditions behind the discontinuity Ramsden and Savic arrived at

$$D = \left[2\ (\gamma^2-1)\ \frac{J_o}{\rho_o}\ \right]^{1/3} \qquad \text{(I-1)}$$

where D is the wave velocity, J_o the heat flux and ρ_o the density of the gas ahead of the wave. Taking into account the conical character of the

focused laser beam, $J_o \sim 1/r^2$ and integrating (I-1) with respect to time they showed that the radius of the detonation front grows as $t^{3/5}$ for a constant power laser and hence

$$D = K\left(\frac{P_L}{\rho_o}\right)^{1/3} t^{-2/5} \qquad \text{(I-2)}$$

where K is a constant and P_L the laser power. Raizer in 1965 [37] extended the model to general hydrodynamic discontinuities (not necessarily Chapman-Jouguet) and attempted to include the effect of lateral expansion of the plasma. In a not very clear paper by Champetier in 1965 [38] the purely one-dimensional plane motion of the gas behind the detonation wave is investigated: an expansion wave follows the front whereas an entropy line and a shock wave travel in the direction opposite to the lens. The effect of time dependence of the laser pulse was considered by Daiber and Thompson in 1967 [12]: in the case of a Gaussian pulse shape the time exponent of the radius of the detonation is shown to be ~3/5 when initial breakdown takes place near the peak of the Gaussian and larger for breakdown occurring at earlier instants. They also developed a model for gases (like hydrogen and deuterium at pressure less than 3 atm) almost transparent to laser radiation. A last improvement was made by Key in 1969 [39]: ionization was included in the gas law, the net effect being to lower the wave velocity and gas temperature for the same heat flux.

Champetier and al. in 1968 [40] and Wilson and Turcotte in 1970 [41a] independently studied the flow behind a spherical laser-driven detonation for constant power addition. Both used a self similar analysis of the kind Sedov [42] first proposed for regular blast wave; the hydrodynamic equations were integrated in a temperature-velocity plane starting from the saddle point corresponding to the origin. It was found that the wave front is not Chapman-Jouguet but rather overdriven (i.e. the gas behind the detonation is subsonic with respect to the front). Wilson [41b] also considered the case of linearly increasing power as well as plane and cylindrical geometries.

The breakdown wave mechanism is based on the idea that during the increasing part of the laser pulse breakdown conditions which were satified

at time t_o, at the focus assumed to be of cross sectional area A_o, will be met further up the beam at location r of larger cross section A at a later time t. In 1965 Raizer [37] postulating that breakdown occurs by cascade ionization from an original number of free electrons present in the cold gas proposed as breakdown criterion that the electron density reaches a certain critical value. If the cascade time constant τ is simply inversely proportional to the heat flux this criterion yields a breakdown wave motion characterized by the time integral from zero, beginning of the pulse to t of the heat flux at location r being a constant. For the rising part of a triangular pulse of maximum power P_{max} at time t_{max} the front velocity is obtained

$$D = K \left(\frac{P_{max}}{t_{max}}\right) \quad \frac{1}{\text{tn } \alpha} \qquad \text{(I-3)}$$

where K is a constant function only of the electron cascade and the critical electron density; α is half the divergence angle of the laser beam. Alcock and al. in 1968 [43] remarked that the free electrons necessary to initiate the cascade could be produced by precursor ionization due to the thermal radiation emitted by the hot plasma. They modified Raizer's model by saying that the initial electrons exist only at time t_1 just ahead of the wave; the breakdown motion is then described by the time integral from t_1 to t of the heat flux being constant. Alcock and al. [43] further assumed (without any theoretical basis) that the time lapse $t - t_1$ between pre-ionization and actual breakdown at any station is a constant t_b. Under these hypotheses the wave velocity for a triangular pulse is obtained

$$D = K \left(\frac{P_{max}}{t_{max}}\right)^{1/2} \quad \frac{1}{\text{tn}\alpha} \quad \frac{t_b^{1/2}}{(2t - t_b)^{1/2}} \qquad \text{(I-4)}$$

It differs from (I-3) by the inverse square root time dependence of the velocity.

Another and simpler breakdown criterion was proposed in 1965 by Ambartsumyan and al. [44]: if breakdown occurs at the lens focus for a laser power P_n, it will occur at station r for a power P equal to P_n times the ratio of the beam cross sectional area at r to that at the focus. Again for a triangular pulse the wave velocity comes out to be

$$D = K' \left(\frac{P_{max}}{t_{max}}\right)^{1/2} \quad \frac{1}{tn\,\alpha} \quad \frac{1}{t^{1/2}} \qquad \text{(I-5)}$$

where K' is a constant containing P_n as well as the focal cross section area. Canto, Reuss and Veyrie in 1968 [45] introduced the cascade time τ in a similar model: breakdown occurs at station r and time t if the heat flux at r and time $t - \tau$ was a critical value J_s. The wave velocity is modified from (I-5) only by changing $t^{1/2}$ into $(t - \tau)^{1/2}$. They also pointed out the possibility for transparent gases of a breakdown wave based on the transmitted power traveling in the direction opposite to the lens.

In summary, as shown by (I-3) to (I-5), whatever the breakdown criterion used, the wave velocity is large for steep pulses (large $\frac{P_{max}}{t_{max}}$) and long focal lengths (small $tn\alpha$); the time dependence is more sensitive to a detailed description of the breakdown mechanism.

The radiation transport wave was also proposed by Raizer in 1965 [37]. This elegant idea has not been subject to further developments since then. Raizer observed that in air, although the hot plasma is transparent to the thermal photons it emits, these have a very short free path in the cold gas ahead of the front. Therefore an ionizing precursor is formed; when the level of ionization in this precursor becomes sufficiently high the laser light is intensely absorbed and a new layer of hot plasma forms. The whole process is continuous and can be characterized as a radiation diffusion process involving two radiation absorption lengths: the mean free path of laser photons in the hot gas and the mean free path of thermal photons in the cold gas. Raizer computed the forward emitted thermal radiation from the plasma by assuming its shape to be a semi-infinite cylinder the cross section of which is the focal cross section of the beam. He arrived at a velocity dependence on heat flux $D \sim J_o^{0.364}$.

The three mechanisms for the expansion of the plasma under the influence of the laser beam are in competition and it is believed that the fastest velocity corresponding to a particular physical situation is the one which is observed in an actual experiment. Slow rising pulses and short focal lengths are associated with radiation driven detonations whereas

fast rising pulses and long focal lengths are explained by a breakdown wave mechanism. Indeed in an experiment by Floux, Guyot and Langer in 1968 [46] a laser pulse was used which exhibited two distinct slopes in the rising part; the wave speed corresponding to the steep slope was shown to agree with a breakdown wave model whereas the wave speed associated with the lesser slope agreed with the detonation theory. The only case where the radiation transport wave has been used is by Raizer [37]; he found that for the particular physical situation corresponding to the experiment of Mandel'shtam [14] the radiation wave velocity came out very close to the detonation wave velocity.

2. Present Work

As seen from the above bibliographical survey, theoretical studies of the plasma expanding under the action of the laser beam have been dealing mostly with the wave front and have been limited to one-dimensional models. The only descriptions of the flow inside the plasma have been for a spherically symmetric spark whereas in experimental conditions oblong asymmetric shapes were reported. From the point of view of nuclear fusion the geometrical and temporal distributions of physical variables are important, in particular temperature and density. As far as plasma containment is concerned an understanding of the spark shape as a function of the laser power distribution would be helpful.

The present work is concerned with the fluid mechanical theory of the developing spark during energy deposition from the laser beam; the wave front is assumed to be a radiation-driven detonation wave. Consider the cylindrically symmetric geometry of fig. 1: the laser beam focused at the origin O has a certain heat flux distribution in the azimuthal coordinate θ. A non-spherical plasma is formed and grows with time being led by the detonation front. The purpose of this thesis is to investigate the flow inside the spark as well as the front shape dependence on the angular distribution of the laser power. The general equations describing the flow and the boundary conditions corresponding to an energy absorbing narrow

layer are presented in Chapter I. A self similar analysis is proposed as well as conditions required for it. In Chapter II a perturbation scheme is derived for a small perturbation of the laser power from a purely spherical distribution. The zeroth order spherically symmetric solution is reviewed and the first order perturbation from it is obtained in a series of Legendre polynomials in cos θ. Numerical integration from the origin to the boundary was used. The dependence of the detonation front shape on the power distribution is presented together with velocity, density and pressure profiles inside the spark. This first order perturbation solution exhibits a singularity at the focus which is analyzed and discussed in Chapter III. Finally, Chapter IV contains a summary and some concluding remarks.

CHAPTER I

GENERAL EQUATIONS AND BOUNDARY CONDITIONS

1. Boundary Conditions for an Absorbing Layer

The plasma boundary is described as a moving energy absorbing layer constituted by a high velocity curved shock wave followed by a narrow region in which the energy carried by the laser photons is deposited. The laser beam is focused on the origin 0 and is characterized by a θ - distribution of heat flux; the power may also be time dependent. The strong shock elevates the gas temperature and density so that the laser photon mean free path becomes very small (Raizer [37] mentions for air at normal density and temperature of ~ 5 10^5°K mean free paths of the order of 5 10^{-3} cm.). Rankine-Hugoniot jump conditions will be derived from the undisturbed gas "o" to the hot gas behind the absorption layer "d". Three cases are considered: normal steady wave, oblique steady wave and unsteady wave.

The following assumptions are made: a) the thermal reradiation from the plasma is neglected on the basis that the emission length (typically several cm for conditions above) is much larger than the plasma dimension (a few mm at the end of the pulse) thus making the plasma transparent to its own thermal emission; b) the layer width is small compared to the front radius of curvature and to any length associated with changes of heat flux along the surface: this allows the application of locally one dimensional jump conditions c) the perfect gas law is used which is not an unreasonable description of a fully ionized plasma d) radiation pressure and energy are neglected; Zeldovich and Raizer ([47] p. 141) show that in air at normal density, due to multiple ionization, temperatures of $0(3.10^6$ °K) must be reached for the equilibrium radiant energy to become comparable to the fluid energy.

Steady normal wave:

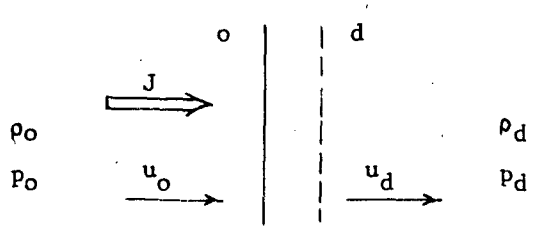

Consevation of mass, momentum and energy from "o" to "d" yields the following set of jump conditions: (see e.g. Raizer [37])

$$\rho_o u_o = \rho_d u_d \tag{1}$$

$$p_o + \rho_o u_o^2 = p_d + \rho_d u_d^2 \tag{2}$$

$$\frac{1}{2} u_o^2 + \varepsilon_o + \frac{p_o}{\rho_o} + \frac{J}{\rho_o u_o} = \frac{1}{2} u_d^2 + \varepsilon_d + \frac{p_d}{\rho_d} \tag{3}$$

ρ is density, u is velocity, p is pressure and ε is internal energy per unit mass. It is noted that $J/\rho_o u_o$ is the energy per unit mass associated with the laser heat flux J. To obtain boundary conditions on the physical variables at "d" equations (1) to (3) are solved for u_d, ρ_d, p_d making use of the perfect gas law and defining the Mach number ahead of the wave $M_o^2 = \frac{\rho_o u_o^2}{\gamma p_o}$ (γ is the ratio of specific heats at constant pressure and volume)

$$u_d = u_o f \tag{4}$$

$$\rho_d = \rho_o f^{-1} \tag{5}$$

$$p_d = p_o + \rho_o u_o^2 (1 - f) \tag{6}$$

from which the Mach number behind the wave can be obtained as

$$M_d^2 = \frac{f}{\gamma[\frac{1}{\gamma M_o^2} + 1 - f]} \tag{7}$$

where f is defined by

$$f \equiv \frac{1}{\gamma + 1} [\gamma + \frac{1}{M_o^2} \pm \sqrt{(1 - \frac{1}{M_o^2})^2 - 2(\gamma^2 - 1) \frac{J}{\rho_o u_o^3}}\,] \tag{8}$$

When J = 0 the + sign in formula (8) corresponds to the trivial solution whereas the - sign gives the familiar density jump across a shock wave. The necessity for the radicand in (8) to be positive yields a minimum possible wave velocity: for example for a very strong wave $M_o \to \infty$ one gets $u_o \geq [\, 2 (\gamma^2 - 1) \frac{J}{\rho_o}\,]^{1/3}$. The equal sign corresponds to the Chapman-Jouguet detonation velocity obtained by Ramsden and Savic (I-1). The choice of the - sign in (8) gives an overdriven detonation characterized by a subsonic downstream flow ($M_d < 1$); the + sign corresponds to an underdriven detonation with a supersonic ($M_d > 1$) downstream flow. For constant

upstream flow conditions and varying heat flux it is seen that the gas velocity behind an overdriven detonation is less than behind a Chapman-Jouguet detonation which in turn is less than that behind an underdriven detonation; on the contrary density and pressure are larger behind an overdriven detonation than behind a Chapman-Jouguet one, the latter being larger than those behind an underdriven one.

In the model adopted here only Chapman-Jouguet or overdriven conditions are physically acceptable; behind the leading shock wave the flow is subsonic and further energy addition can only increase the Mach number towards one. The crossing of the sonic point is impossible unless heat is somehow removed in the supersonic region (e.g. by radiation losses). It should be noted that for continuous changes from "o" to "d" (i.e. without shock) like a breakdown wave or a radiation-supported wave the - sign would be the appropriate one and thus would correspond to an underdriven deflagration.

Steady oblique wave:

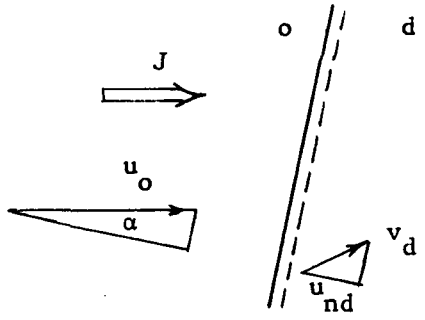

The upstream velocity, parallel to the heat flux vector forms an angle α with the direction normal to the wave front. The jump conditions (1) to (3) apply now the normal velocity and heat flux components and the velocity component v parallel to the front is preserved. Boundary conditions are obtained, with u_{nd} the normal velocity behind the wave:

$$u_{nd} = u_o \cos \alpha \, f \tag{9}$$

$$v_d = u_o \sin \alpha \tag{10}$$

$$\rho_d = \rho_o / f \tag{11}$$

$$p_d = p_o + \rho_o (u_o \cos \alpha)^2 (1 - f) \tag{12}$$

The total Mach number behind the wave is

$$M_d^2 = \frac{f^2 + tn^2\,\alpha}{\gamma f \left[\frac{1}{M_{on}^2} + 1 - f\right]} \tag{13}$$

M_{on} is the upstream Mach number based on the normal velocity component $u_o \cos\alpha$; f is now defined as

$$f \equiv \frac{1}{\gamma+1}\left[\gamma + \frac{1}{M_{on}^2} \pm \sqrt{\left(1 - \frac{1}{M_{on}^2}\right)^2 - 2(\gamma^2 - 1)\frac{J}{\rho_o u_o^3 \cos^2\alpha}}\right] \tag{14}$$

The Chapman-Jouguet wave is again defined by the radical in (14) being zero. This can be seen to correspond to a normal downstream Mach number of one. A minimum possible wave speed is associated $u_o = \left[2(\gamma^2-1)\frac{J}{\rho_o}\frac{1}{\cos^2\alpha}\right]^{1/3}$ (for $M_o \to \infty$)which is larger than the corresponding normal minimum wave velocity. The flow behind a Chapman-Jouguet wave is supersonic ($M_d > 1$) and can be supersonic, sonic or subsonic behind an overdriven wave depending on the magnitude of the radical.

Unsteady wave:

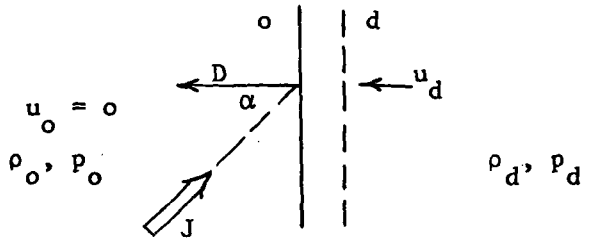

The upstream flow from the two steady cases is brought to rest by superposing a velocity $-u_o$. Regardless of whether the steady wave was normal or oblique, the unsteady velocity u_d behind the wave is normal to the front; D is defined as the normal component of the front velocity. Of course the heat flux will generally form an angle α with the normal. The following unsteady boundary conditions are obtained, where J represents the magnitude of the heat flux:

$$u_d = D(1 - f) \tag{15}$$

$$\rho_d = \rho_o / f \tag{16}$$

$$p_d = p_o + \rho_o D^2 (1 - f) \tag{17}$$

$$f \equiv \frac{1}{\gamma+1}\left[\gamma + \frac{1}{M_D^2} \pm \sqrt{\left(1 - \frac{1}{M_D^2}\right)^2 - 2\,(\gamma^2 - 1)\,\frac{J\cos\alpha}{\rho_o D^3}}\right] \tag{18}$$

M_D is the Mach number based on D, ρ_o and p_o. It is noticed that contrary to ordinary shocks f does not go to a constant when $M_D \to \infty$ but generally remains a function of the wave velocity and front location (through $J \sim 1/r^2$ and $\cos\alpha$). This feature makes boundary conditions rather more difficult to apply than for ordinary blast waves.

2. Basic Differential Equations

The differential equations describing the flow behind the absorption wave are those for compressible non-viscous, non-heat conducting fluid. Neglecting thermal reemission makes the flow adiabatic and hence isentropic. Perfect gas law is assumed to apply. Equations are simultaneously presented in spherical and cylindrical coordinates; r is the spherical or cylindrical radius, θ the azimuthal angle measured from the axis of symmetry in spherical geometry and a fixed reference direction in cylindrical geometry; u_r is the radial velocity component, u_θ the tangential velocity component. Axial symmetry exists in spherical geometry and physical quantities are independent of the z - coordinate in cylindrical geometry. No swirl is present. If ν is defined such that $\nu = 1$ applies to the cylindrical case and $\nu = 2$ to the spherical case, the continuity, r - momentum, θ - momentum and isentropy equations are:

$$\frac{\partial\rho}{\partial t} + \frac{\partial}{\partial r}(\rho u_r) + \frac{\nu}{r}\rho u_r + \frac{1}{r}\frac{\partial}{\partial\theta}(\rho u_\theta) + \frac{\nu-1}{r}\cot\theta\,\rho u_\theta = 0 \tag{19}$$

$$\frac{\partial u_r}{\partial t} + u_r\frac{\partial u_r}{\partial r} + \frac{1}{r}u_\theta\frac{\partial u_r}{\partial\theta} - \frac{u_\theta^2}{r} = -\frac{1}{\rho}\frac{\partial p}{\partial r} \tag{20}$$

$$\frac{\partial u_\theta}{\partial t} + u_r\frac{\partial u_\theta}{\partial r} + \frac{1}{r}u_\theta\frac{\partial u_\theta}{\partial\theta} + \frac{u_r u_\theta}{r} = -\frac{1}{\rho}\frac{1}{r}\frac{\partial p}{\partial\theta} \tag{21}$$

$$\left(\frac{\partial}{\partial t} + u_r\frac{\partial}{\partial r} + u_\theta\frac{\partial}{\partial\theta}\right)\left(\frac{p}{\rho\gamma}\right) = 0 \tag{22}$$

3. Self-similar Processes

The solution of the set of four non-linear partial differential equations (19) to (22) in three independent variables r, θ, t subject to

boundary conditions (15) to (18) which not only apply at an a priori unknown location r_d (θ, t) but also contains the unknown quantity r_d through D, cos α, J, appears a formidable task indeed. Furthermore, initial conditions have to be supplied which depend on the complicated starting process, namely the initial breakdown mechanism briefly discussed in the introduction. Under appropriate conditions self-similarity will be shown to apply, this allows to reduce the number of independent variables to two: θ and the similarity variable $\lambda = r/t^n$. In a self-similar process the values of the physical variables describing the flow at station r and time t can also be used to describe the flow at earlier time and larger r or later time and smaller r, provided the value of λ remains the same. Self-similar flows do not need initial conditions and because of that generally fail to properly include the initial stages of a physical phenomenon.

Spherical and cylindrical cases will be treated simultaneously. The laser beam is characterized by its angular and temporal power distribution $\mathcal{P}(\theta, t)$ from which the heat flux hitting the wave front is

$$J(\theta,t) = \frac{\mathcal{P}(\theta,t)}{[r_d(\theta,t)]^\nu} \tag{23}$$

Self-similarity is obtained when the two following conditions are satisfied: a) $\mathcal{P}$ is specialized to a power-law time dependence

$$\mathcal{P}(\theta,t) = P_L t^\kappa g(\theta) \tag{24}$$

where P_L is a constant representing power per unit time to the κ and $g(\theta)$ is a non-dimensional function of the azimuth; b) very strong waves are considered i.e. $M_D \to \infty$ and $p_o \to 0$. This in fact means neglecting the static pressure ahead of the wave compared to its dynamic pressure; for high velocity waves as those experimentally observed this assumption is certainly valid. An analysis is made in Appendix A which includes finite pressure p_o for a spherically symmetric spark: the results are presented in the form of a perturbation in $1 / M_D^2$ from the self-similar solution.

Dimensional arguments can be used to determine the proper similarity variable (see Sedov [42]). The overall physical problem possesses only

two dimensional parameters: P_L of dimension mass times length to the ν divided by time to the $(\kappa + 3)$ and the undisturbed density ρ_o of dimension mass over length cubed. It is seen that the ratio P_L/ρ_o contains only the dimensions of length and time. The non-dimensional similarity variable is thus defined

$$\lambda = \frac{r}{At^n} \tag{25}$$

with

$$n = \frac{\kappa + 3}{\nu + 3} \quad \text{and} \quad A = \left[\frac{P_L}{\rho_o} \, (\gamma - 1) \, a \right]^{\frac{1}{\nu + 3}} \tag{26}$$

a is a constant to be obtained as part of the solution. It will be chosen such that the boundary of the spherically symmetric spark is $\lambda = 1$. From (25) it is seen that the boundary is now located at

$$\lambda = h(\theta) \tag{27}$$

or in physical variables $r_d = h(\theta) \, A \, t^n$.

The self-similar variable can also be obtained by considering the boundary conditions; in particular it is necessary that the density ratio across the wave be time-independent. Looking at the last term of the radicand of (18) it is required that the quantity $\frac{t^\kappa}{r_d^\nu \, (\dot{r}_d)^3}$ (the dot represents time-derivative) be not a function of time. Integrating that quantity with respect to time one obtains $r_d \sim t^{\frac{\kappa + 3}{\nu + 3}}$; defining λ as r/r_d one recovers (25) - (26) when all constants are taken into account.

The explicit time dependence in the set of differential equations (19) - (22) can be shown to cancel out when the velocities, density and pressure are respectively non-dimensionalized by $A \, t^{n-1}$, ρ_o and $\rho_o \, (A \, t^{n-1})^2$ (see e.g. Rae and Kirchner [48]). This result actually holds for any values of A and n. This type of self-similarity although limited to spherically symmetric geometry was first proposed by Taylor [49] for ordinary blast waves, it differs slightly from Sedov's [42] type in which the non-dimensionalization is carried with respect to r/t, ρ_o and $\rho_o \, (r/t)^2$.

The self-similar equations are obtained by changing variables in equations (19) - (22) from r, θ, t to λ, θ and introducing the self-similar physical quantities (represented by capital letters) functions only

of λ, θ :

$$u_r = n A t^{n-1} V(\lambda,\theta) \tag{28}$$

$$u_\theta = n A t^{n-1} W(\lambda,\theta) \tag{29}$$

$$\rho = \rho_o R(\lambda,\theta) \tag{30}$$

$$p = \rho_o (n A t^{n-1})^2 P(\lambda,\theta) \tag{31}$$

canceling out the explicit t - dependence in all equations one gets

$$D_{\lambda\theta} \cdot R + R\left[V_\lambda + \nu \frac{V}{\lambda} + \frac{1}{\lambda} W_\theta + (\nu - 1) \cot\theta \frac{1}{\lambda} W\right] = 0 \tag{32}$$

$$D_{\lambda\theta} \cdot V + \frac{n-1}{n} V - \frac{W^2}{\lambda} + \frac{1}{R} P_\lambda = 0 \tag{33}$$

$$D_{\lambda\theta} \cdot W + \frac{n-1}{n} W + \frac{V W}{\lambda} + \frac{1}{R} \frac{1}{\lambda} P_\theta = 0 \tag{34}$$

$$D_{\lambda\theta} \cdot P + 2 \frac{n-1}{n} P + \gamma P \left[V_\lambda + \nu \frac{V}{\lambda} + \frac{1}{\lambda} W_\theta + (\nu - 1) \cot\theta \frac{1}{\lambda} W\right] = 0 \tag{35}$$

where $D_{\lambda\theta}$ is a linear differential operator defined by

$$D_{\lambda\theta} \equiv (V - \lambda) \frac{\partial}{\partial \lambda} + W \frac{1}{\lambda} \frac{\partial}{\partial \theta} \tag{36}$$

The boundary conditions (15) - (18) are also recast in self-similar form. First, from (27) the normal component of the wave velocity and the angle α, defined positive from the external normal direction to the front to radial direction, turn out to be:

$$D = n A t^{n-1} \left(1 + \frac{h'^2}{h^2}\right)^{-1/2} \tag{37}$$

$$\cos\alpha = \left(1 + \frac{h'^2}{h^2}\right)^{-1/2} \tag{38}$$

$$\sin\alpha = -\frac{h'}{h} \left(1 + \frac{h'^2}{h^2}\right)^{1/2} \tag{39}$$

h' is the derivative of $h(\theta)$ with respect to θ . Then, remarking that the velocity behind the wave which is perpendicular to the front yields both a radial and a tangential component the final boundary conditions come out: at $\lambda = h(\theta)$

$$V_d = (1 - f)\, h \left(1 + \frac{h'^2}{h^2}\right)^{-1} \tag{40}$$

$$W_d = -(1 - f) h' \left(1 + \frac{h'^2}{h^2}\right)^{-1} \tag{41}$$

$$R_d = \frac{1}{f} \tag{42}$$

$$P_d = (1 - f)\, h^2 \left(1 + \frac{h'^2}{h^2}\right)^{-1} \tag{43}$$

$$\text{with } f = \frac{1}{\gamma + 1} \left[\gamma - \sqrt{1 - 2 \frac{\gamma + 1}{a\, n^3} \frac{g(\theta)}{h^5(\theta)} \left(1 + \frac{h'^2}{h^2}\right)} \right] \tag{44}$$

Only the - sign will be retained in f, consistent with the chosen detonation wave model. The problem has now been reduced to a system of four non-linear partial differential equations in two independent variables. The boundary conditions still contain an unknown function h (θ).

It may be noticed that the self-similarity presented here is the same as for spherically symmetric geometry; this results from the fact that the angular distribution of power g (θ) does not introduce any new physical length in the problem.

CHAPTER II

SMALL PERTURBATION OF A SPHERICAL SPARK

1. Small Perturbation Assumption

Throughout this chapter only constant power in time will be considered i.e. $\kappa = 0$ and hence $n = 3/5$. The geometry will be spherical: $\nu = 2$. Consider the following arrangement: a battery of lasers all focused at the same point creates a slightly non-spherical angular distribution of power:

$$g(\theta) = \frac{1}{4\pi} [\, 1 + \varepsilon G\,(\theta)\,] \tag{45}$$

where ε is a non-dimensional parameter much less than one. The object of this investigation is to determine the spark shape and the plasma flow resulting from such a power distribution. Since a uniform change in power level can easily be treated by a perturbation of the definition of λ (see eq. (25)) the function $G\,(\theta)$ will be chosen such that the total power P_L remains unchanged. This is expressed by the condition

$$\int_0^{\pi} G\,(\theta)\,\sin\theta\, d\theta = 0 \tag{46}$$

It is assumed that the displacement of the boundary of the initially spherical spark, resulting from the imposed power perturbation is also proportional to ε ; the wave front is thus

$$\lambda = h\,(\theta) = 1 + \varepsilon\, H\,(\theta) \tag{47}$$

where $H\,(\theta)$ is an a priori unknown function to be found as part of the solution.

In the light of equations (45) and (47) the boundary conditions previously derived (40) to (44) can be expanded in a power series in ε . First it is observed that, provided the radicand in (44) is different from zero in the spherically symmetric case, and this will be shown later in this chapter, the function f can be expanded as

$$f = f^{(o)} + \varepsilon\, K\, [G(\theta) - 5H(\theta)] + O(\varepsilon^2) \tag{48}$$

where $f^{(o)}$ and K are constants depending only on the spherically symmetric solution (which from now on will also be referred to as "zeroth - order solution") defined by

$$f^{(o)} = \frac{1}{\gamma+1}\left[\gamma - \left(1 - \frac{\gamma+1}{2\pi n^3 a}\right)^{1/2}\right] \tag{49}$$

and $$K = \frac{1}{4\pi n^3 a}\left(1 - \frac{\gamma+1}{2\pi n^3 a}\right)^{-1/2} \tag{50}$$

Expanding in powers of ε equations (40) to (44) yields the boundary conditions where terms of 0 (ε^2) have been dropped: at $\lambda = 1 + \varepsilon H(\theta)$

$$V_d = 1 - f^{(o)} + \varepsilon\left[-K G(\theta) + (1 - f^{(o)} + 5K) H(\theta)\right] \tag{51}$$

$$W_d = -\varepsilon (1 - f^{(o)}) H'(\theta) \tag{52}$$

$$R_d = \frac{1}{f^{(o)}} - \varepsilon \frac{K}{f^{(o)2}}[G(\theta) - 5 H(\theta)] \tag{53}$$

$$P_d = 1 - f^{(o)} + \varepsilon\left[-K G(\theta) + \{2 (1 - f^{(o)}) + 5 K\} H(\theta)\right] \tag{54}$$

The form of the boundary conditions (51) to (54) naturally suggests expansions in powers of ε of the physical variables everywhere in the flow field

$$V(\lambda,\theta) = V^{(o)}(\lambda) + \varepsilon V^{(1)}(\lambda,\theta) \tag{55}$$

$$W(\lambda,\theta) = \varepsilon W^{(1)}(\lambda,\theta) \tag{56}$$

$$R(\lambda,\theta) = R^{(o)}(\lambda) + \varepsilon R^{(1)}(\lambda,\theta) \tag{57}$$

$$P(\lambda,\theta) = P^{(o)}(\lambda) + \varepsilon P^{(1)}(\lambda,\theta) \tag{58}$$

The zeroth-order functions representing the spherically symmetric case are dependent only on λ. It is noticed that, although the expansions of the boundary conditions are exact, provided that assumption (47) is valid, there is no guarantee that the expansions of the field variables (55) to (58) are uniformly valid. In fact it will be shown that they do break down in the neighborhood of the focus: $\lambda = 0$.

Proceeding with the substitution of (55) to (58) into the flow equations (32) to (36) one collects the 0 (1) and 0 (ε) terms to obtain the following two systems of differential equations:

$$(V^{(o)} - \lambda) R^{(o)\prime} + R^{(o)} V^{(o)\prime} + 2\frac{R^{(o)} V^{(o)}}{\lambda} = 0 \tag{59}$$

$$\frac{n-1}{n} V^{(o)} + (V^{(o)} - \lambda) V^{(o)\prime} + \frac{1}{R^{(o)}} P^{(o)\prime} = 0 \tag{60}$$

$$2\frac{n-1}{n} P^{(o)} + (V^{(o)} - \lambda) P^{(o)\prime} + \gamma P^{(o)} V^{(o)\prime} + 2\gamma \frac{P^{(o)} V^{(o)}}{\lambda} = 0 \tag{61}$$

In the above zeroth-order non-linear system of ordinary differential equations $'$ stands for $\frac{d}{d\lambda}$.

The first order system is a linear system of partial differential equations, the non-constant coefficients of which are function of the zeroth-order variables. It reads:

$$R^{(o)}\, V^{(1)}_{\lambda} + \left(R^{(o)'} + 2\,\frac{R^{(o)}}{\lambda}\right) V^{(1)} + \frac{1}{\lambda} R^{(o)} \left(W^{(1)}_{\theta} + \cot\theta\ W^{(1)}\right) + \left(V^{(o)} - \lambda\right) R^{(1)}_{\lambda} + \left(V^{(o)'} + 2\,\frac{V^{(o)}}{\lambda}\right) R^{(1)} = 0 \tag{62}$$

$$\left(V^{(o)} - \lambda\right) V^{(1)}_{\lambda} + \left(\frac{n-1}{n} + V^{(o)'}\right) V^{(1)} - \frac{P^{(o)'}}{R^{(o)2}}\, R^{(1)} + \frac{1}{R^{(o)}}\, P^{(1)}_{\lambda} = 0 \tag{63}$$

$$\left(V^{(o)} - \lambda\right) W^{(1)}_{\lambda} + \left(\frac{n-1}{n} + \frac{V^{(o)}}{\lambda}\right) W^{(1)} + \frac{1}{R^{(o)}}\, \frac{1}{\lambda}\, P^{(1)}_{\theta} = 0 \tag{64}$$

$$\gamma\, P^{(o)} V^{(1)}_{\lambda} + \left(P^{(o)'} + 2\gamma\,\frac{P^{(o)}}{\lambda}\right) V^{(1)} + \gamma\,\frac{1}{\lambda}\, P^{(o)} \left(W^{(1)}_{\theta} + \cot\theta\, W^{(1)}\right) + \left(V^{(o)} - \lambda\right) P^{(1)}_{\lambda} + \left(2\,\frac{n-1}{n} + \gamma\, V^{(o)'} + 2\gamma\,\frac{V^{(o)}}{\lambda}\right) P^{(1)} = 0 \tag{65}$$

The boundary conditions on the two systems are readily obtained from (51) to (54); for convenience, they will be transferred to the fixed location $\lambda = 1$ by means of Taylor expansions around $\lambda = 1 + \varepsilon H(\theta)$. One thus obtains the following zeroth order and first order sets of boundary conditions:

$$V^{(o)}(1) = 1 - f^{(o)} \tag{66}$$

$$R^{(o)}(1) = \frac{1}{f^{(o)}} \tag{67}$$

$$P^{(o)}(1) = 1 - f^{(o)} \tag{68}$$

and

$$V^{(1)}(1,\theta) = -KG(\theta) + \left[1 - f^{(o)} + 5K - V^{(o)'}(1)\right] H(\theta) \tag{69}$$

$$W^{(1)}(1,\theta) = -\left(1 - f^{(o)}\right) H'(\theta) \tag{70}$$

$$R^{(1)}(1,\theta) = -\frac{K}{f^{(o)2}}\, G(\theta) + \left[5\,\frac{K}{f^{(o)2}} - R^{(o)'}(1)\right] H(\theta) \tag{71}$$

$$P^{(1)}(1,\theta) = -KG(\theta) + \left[2\left(1 - f^{(o)}\right) + 5K - P^{(o)'}(1)\right] H(\theta) \tag{72}$$

2. Spherical Spark - Zeroth-order Solution

Although the spherical spark problem was treated by Champètier and al. [40] and Wilson and Turcotte [41a] a new investigation was prompted by the necessity of a readily available solution in order to compute the coefficients of the first order set. It was also observed that a slight discrepancy exists between the pressure profiles obtained by the above

investigators: Wilson's and Turcotte exhibit a dip around $\lambda \simeq 0.5$ which is not present in Champetier's and furthermore Wilson and Turcotte's pressure at the origin is about fifteen percent higher than Champetier's. The density profile in Champetier and al. [40] appears to be erroneous; although they correctly indicate that the wave front is overdriven, they mention a density ratio across the wave: $f = \frac{\gamma}{\gamma+1}$ which, of course, is that of a Chapman-Jouguet detonation.

The approach used here is quite different from the previous investigations: the set of equations (59) - (61) is directly integrated as a function of λ from the origin out to the boundary. This necessitates a detailed study of the behavior of the physical variables in the neighborhood of the origin; the understanding of this singularity at the origin also throws some light on the more complicated singularity arising in the first order perturbation problem. Since the boundary conditions (66) to (68) with $f^{(o)}$ defined in (49) contain the unknown constant a, and hence provide only two known boundary conditions, expansions near the origin are needed which contain only two independent constants.

2.1 Expansions near $\lambda = 0$

For convenience a change of variables is made:

$$\mu = \lambda^{\alpha} \tag{73}$$

$$V_i^{(o)} = \lambda\, y_1(\mu) \tag{74}$$

$$R^{(o)} = \frac{1}{\lambda^2}\, y_2(\mu) \tag{75}$$

$$P^{(o)} = y_3(\mu) \tag{76}$$

where α is, at this point, an arbitrary constant. Transforming equations (59) to (61) and canceling out all explicit λ - dependence, one obtains: (with $' \equiv \frac{d}{d\mu}$)

$$(y_1 + 2)\, y_2 + \alpha\mu[y_2\, y_1' + (y_1 - 1)\, y_2'] = 0 \tag{77}$$

$$y_1 \left(y_1 - \frac{1}{n}\right) y_2 + \alpha\,\mu[(y_1 - 1)\, y_2\, y_1' + y_3'] = 0 \tag{78}$$

$$\left(3\gamma\, y_1 + 2\,\frac{n-1}{n}\right) y_3 + \alpha\,\mu[\gamma\, y_3 y_1' + (y_1 - 1)\, y_3'] = 0 \tag{79}$$

Expansions near $\lambda = 0$ are sought of the form:

$$y_1 = a_o + a_1\,\mu + a_2\,\mu^2 + a_3\,\mu^3 + \cdots \tag{80}$$

$$y_2 = b_1\mu + b_2\mu^2 + b_3\mu^3 + \cdots \tag{81}$$

$$y_3 = c_o + c_1\mu + c_2\mu^2 + c_3\mu^3 + \cdots \tag{82}$$

Note that the constant term in the expansion of y_2 being zero renders the density $R^{(o)}$ bounded at the origin. The leading term in equations (77) to (79) yields respectively:

$$[a_o + 2 + \alpha(a_o - 1)]\, b_1 = 0 \tag{83}$$

$$a_o\left(a_o - \frac{1}{n}\right) b_1 + \alpha c_1 = 0 \tag{84}$$

$$\left(3\gamma a_o + 2\frac{n-1}{n}\right) c_o = 0 \tag{85}$$

Therefore the expansions near the origin contain two arbitrary constants b_o and c_1, the value of a_o is found and α is determined:

$$a_o = -\frac{2}{3\gamma}\frac{n-1}{n} \qquad \alpha = -\frac{a_o + 2}{a_o - 1} \tag{86}$$

c_1 is readily obtained from (84):

$$c_1 = -\left(a_o - \frac{1}{n}\right) a_o \frac{1}{\alpha} b_1 \tag{87}$$

Numerical values corresponding to $\gamma = 5/3$ (and recalling $n = 3/5$) are $a_o = 4/15$ and $\alpha = 34/11$. α being non-integer makes all functions singular at the origin in the sense that although the function itself is bounded, there always exists some derivative which is not (e.g. $R^{(o)''}$ is infinite.)

The self-similar velocity, density and pressure are seen to have a leading term respectively proportional to λ, $\lambda^{12/11}$ and a constant. From the definitions (28) to (31) the r, t dependence of the physical velocity, density and pressure are obtained respectively as r/t, $r^{12/11} \cdot t^{-12/11}$, $t^{-4/5}$. This kind of flow where the velocity is proportional to r and the pressure is independent of r is usually referred to as uniform spherical expansion. It is worth noting that the temperature is unbounded at the origin ($r^{-12/11} \cdot t^{16/55}$) as it indeed must in a self-similar spherical non-heat conducting process. The initial stage of a spark is characterized by an infinite front velocity, $D \sim t^{-2/5}$; this raises the entropy of the gas particle at the focus to infinity. But, by symmetry this particle stays at the focus so that entropy cannot be convected away from the origin; on the other hand it cannot diffuse away since non-heat conducting fluid is assumed. Thus the temperature at the origin has to remain infinite at all times.

In order to improve the accuracy of the numberical solution several more terms are computed in expansions (80) to (82). For $\gamma = 5/3$ the following numerical coefficients are obtained where $\beta \equiv b_1/c_o$:

$$y_1 = \frac{4}{15} + 2.69692\ 10^{-2}\ \beta\ \mu + 3.10402\ 10^{-3}\ \beta^2\mu^2 + 2.01178\ 10^{-4}\ \beta^3\mu^3 \quad (88)$$

$$y_2 = b_1\mu\ (1 + 8.54504\ 10^{-2}\ \beta\ \mu + 1.2256\ 10^{-2}\ \beta^2\mu^2 + 1.56620\ 10^{-3}\ \beta^3\mu^3\ ) \quad (89)$$

$$y_3 = c_o\ (1 + 1.20784\ 10^{-1}\ \beta\ \mu + 1.99936\ 10^{-2}\ \beta^2\mu^2 + 2.91446\ 10^{-3}\ \beta^3\mu^3\ ) \quad (90)$$

These expansions containing two arbitrary constants are sufficient to start a numerical solution which has to satisfy two boundary conditions. However, it could be argued that the system (59) - (61) is third order and a third solution has been implicitly discarded. In fact, by inspection a solution depending on one arbitrary constant C can be found (for $\gamma = 5/3$)

$$V^{(o)} = \frac{5}{6}\lambda\ ;\quad R^{(o)} = C\ \lambda^{15}\ ;\quad P^{(o)} = \frac{25}{36}\frac{1}{17}\ C\ \lambda^{17} \quad (91)$$

This solution has to be discarded indeed since it does not have the required physical feature of an infinite temperature at the origin.

2.2. Numerical Integration and Results

The system of three non-linear ordinary differential equations (77) to (79) is integrated from 0.01 to 1 using a standard fourth-order Runge-Kutta technique with a step-size of 10^{-2} or less. Expansions (88) to (90) are used to move away from the origin. Two boundary conditions are to be satisfied, for example:

$$y_1\ (1) = y_3\ (1)\ ;\ y_1\ (1) = \frac{1}{y_2(1)} \quad (92)$$

The values of the constants b_1 and c_o are obtained by a linear correction procedure: considering the y's to be function not only of μ but also of b_1 and c_o , their values corresponding to a new guess b_1^N, c_o^N are related to the values corresponding to the old guess b_1^o, c_o^o by a Taylor expansion:

$$y\ (\mu\ ;\ b_1^N,\ c_o^N) = y\ (\mu\ ;\ b_1^o,\ c_o^o) + \frac{\partial y}{\partial b_1}\ (\mu\ ;\ b_1^o,\ c_o^o)\ \Delta b_1 + \frac{\partial y}{\partial c_o}\ (\mu\ ;\ b_1^o,\ c_o^o)\ \Delta c_o \quad (93)$$

with $\Delta b_1 = b_1^N - b_1^o$ and $\Delta c_o = c_o^N - c_o^o$. The system (77) to (79) and the

expansions (88) to (90) must be supplied with six extra equations and six extra expansions for the derivatives of the y's with respect to b_1 and c_o; these are obtained simply by taking derivatives of (77) - (79) with respect to b_1 and c_o as well as of equations (88) to (90). The full system of nine equations is then integrated for an initial guess of the pair b_1^o, c_o^o. The values of the y's and their derivatives for the initial guess are now known at the boundary. Application of the boundary conditions (92) on the values of y's at the new guess gives a system of two inhomogeneous algebraic equations for Δb_1 and Δc_o. Solving this the Δ's are found and hence the new guess. The procedure is repeated until both Δ's become smaller than a prescribed value, namely 10^{-12} in the present case. This correction scheme was found to converge fairly rapidly requiring fifteen iterations to bring b_1 and c_o from an initial guess of 1.0 to their final values:

$$b_1 = 0.9299591 \qquad c_o = 0.173074414$$

The self-similar velocity, density and pressure profiles obtained are plotted on figure 2 as a function of the self-similar variable λ. The boundary values are

$$R^{(o)}(1) = 1.85043402;\ V^{(o)}(1) = P^{(o)}(1) = 0.459586242$$

where all digits are significant. From that the constant a related to the wave front speed can be found

$$a = 1.990$$

2.3. Discussion and Conclusions

A highly accurate numerical solution has been obtained; this results from the use of several terms expansions near the origin as well as a severe convergence criterion combined with step-size as small as $5\ 10^{-4}$ in the last iterations. No pressure dip similar to Wilson and Turcotte's is observed and the ratio of the pressure at the origin to that just behind the absorption wave is 0.37659 compared to Wilson and Turcotte's value of 0.441. Aside of these differences the velocity, density and pressure profiles and in particular the values at the boundary, agree fairly closely with Wilson and Turcotte's results.

The density ratio at the front $f^{(o)} = 0.540413758$ is less than $\frac{\gamma}{\gamma + 1}$

thereby indicating an overdriven detonation front. This result is important for the perturbation scheme since it justifies the previously cited eq. (48). Also note that the whole flow inside the spark is subsonic.

A comparison with ordinary constant energy blast waves is enlightening. From a mathematical point of view, their treatment would be very similar. Changes of n to 2/5 and of the definition of A are needed and the boundary conditions are modified by having $f^{(o)} = \frac{\gamma-1}{\gamma+1}$. Expansions near the origin are of the same form with $a_o = 3/5$ and $\alpha = 13/2$. It is observed that the boundary conditions do not contain the unknown wave velocity "a" and therefore appear to constitute three independent boundary conditions in contradiction with the expansion near $\lambda = 0$ containing only two independent constants. In fact by manipulating the equations (59) - (61) the following integral relation can be obtained:

$$(V^{(o)} - \lambda)\left[P^{(o)} + (\gamma-1)\frac{R^{(o)}V^{(o)2}}{2}\right]\Big|_{\lambda=1} + (\gamma-1)\,P^{(o)}V^{(o)}\Big|_{\lambda=1} + \frac{5n-2}{n}\int_o^1\left[P^{(o)} + (\gamma-1)\frac{R^{(o)}V^{(o)2}}{2}\right]\lambda^2\,d\lambda = 0 \qquad (94)$$

It states that the total energy swept in by the moving front plus the pressure work balance the change in total energy of the flow inside the spark. For a constant energy blast wave ($n = 2/5$) the integral in (94) drops out and hence a relation is obtained solely from the differential equations, between the values of the physical quantities at the boundary. Clearly only two boundary conditions need be applied.

Physically the constant power laser spark has a faster moving front than a constant energy blast wave which is natural in view of the continuously added energy. The mechanism pushing the leading shock wave is quite different: in a blast wave the energy released initially at the origin is redistributed as the blast grows whereas in the laser spark the energy is deposited right behind the shock driving it forward. This is the reason why the boundary conditions appear different: dependent on velocity for a laser spark and independent for a blast wave. The flow near the origin is very much alike in the two cases: constant pressure and $v \sim r/t$.

It should be noticed that for the same $\gamma = 5/3$ the density profile of a blast wave drops much more steeply near the boundary. This, actually, is only a manifestation of a very important difference between the two flows, namely the fact that when $\gamma \to 1$ a blast wave exhibits a Newtonian layer of concentrated mass near the shock, contrary to the laser spark which does not. Figure 3 shows the velocity, density and pressure profile of a constant power spherical spark for $\gamma = 1$; they clearly do not have a layer of concentrated mass near the boundary. The procedure to obtain these is the same as for $\gamma = 5/3$ although convergence appeared somewhat slower. The existence of a Newtonian layer for blast waves permits the considerable simplification of treating the flow as locally radial (i.e. dropping of θ - derivatives compared to r - derivatives), this possibility was exploited by Laumbach and Probstein [50,51] in their study of blast waves in non-homogeneous atmosphere. However, the author disagrees with their use of the same simplifying assumption in their treatment of blast waves in in-homogeneous atmosphere including the thermal radiation emanating from the inside of the blast: the boundary conditions are then modified to look like those derived in Chapter I (equations (4) to (8)) and this should destroy the possibility of a Newtonian layer.

The reason why a Newtonian layer is possible or not is readily seen from equations (15) to (18): when $\gamma \to 1$, in the case of a shock wave the density tends to infinity at the same time as the velocity u_d tends to D thereby trapping most of the mass inside the blast wave in a layer next to the shock. Therefore for a blast wave with $\gamma \to 1$ the velocity profile tends to a straight line $V^{(o)} = n^{\lambda}$ which implies that particle trajectories are also similarity lines: this feature allows the existence of a constant pressure, zero density core inside the blast wave into which the mass flow is zero. For a constant power laser spark none of these characteristic features hold and hence a Newtonian layer is ruled out.

In conclusion, the non-existence of a Newtonian layer for constant power excludes the possibility of using the locally radial approximation and a small perturbation scheme has been proposed instead.

3. Non-spherical Spark - First Order solution

3.1. Fourier Decomposition

Contrary to the zeroth order set, the first order set of differential equations (62) to (65) is linear; this feature is exploited by expanding the dependent variables in Fourier series in the coordinate θ. First the imposed power addition perturbation G (θ) is decomposed in a series of Legendre polynomials in cos θ:

$$G(\theta) = \sum_{\ell=1}^{\infty} P_\ell (\cos\theta) A_\ell \qquad (95)$$

where P_ℓ is the Legendre polynomial of order ℓ and the A_ℓ are known constants. Note that the requirement (46) that the total power should remain unchanged is satisfied since the constant term P_o is omitted in the series (95) and for $\ell > 1$, all Legendre polynomials satisfy

$$\int_o^\pi P_\ell (\cos\theta) \sin\theta \, d\theta = 0 \qquad (96)$$

The first term of the series $P_1 = \cos\theta$ corresponds to a maximum asymmetric perturbation: if $A_1 > 0$ the laser beam is altered such that the power is increased by a certain amount at $\theta = 0$ and decreased by the same amount at $\theta = \pi$. Higher order polynomials create a more evenly distributed power perturbation. When the order ℓ is even the distribution is symmetric with respect to the axis $\theta = \frac{\pi}{2}$ in addition to the original symmetry about θ 0,π and the whole flow presumably possesses two axis of symmetry.

The perturbation of the spark shape H (θ) is similarly decomposed in:

$$H(\theta) = \sum_{\ell=1}^{\infty} P_\ell (\cos\theta) X_\ell \qquad (97)$$

where the X_ℓ are unknown constants since the shape is to be determined as part of the solution.

In order to achieve Fourier decomposition of the differential equations and boundary conditions the following expansions are made for the velocities, density and pressure perturbations:

$$V^{(1)}(\lambda,\theta) = \sum_{\ell=1}^{\infty} P_\ell (\cos\theta) \bar{V}_\ell (\lambda) \qquad (98)$$

$$W^{(1)}(\lambda,\theta) = \sum_{\ell=1}^{\infty} \frac{d}{d\theta} [P_\ell (\cos\theta)] \bar{W}_\ell (\lambda) \qquad (99)$$

$$R^{(1)}(\lambda,\theta) = \sum_{\ell=1}^{\infty} P_\ell(\cos\theta)\,\bar{R}_\ell(\lambda) \qquad (100)$$

$$P^{(1)}(\lambda,\theta) = \sum_{\ell=1}^{\infty} P_\ell(\cos\theta)\,\bar{P}_\ell(\lambda) \qquad (101)$$

where the quantities $\bar{\ }$ are solely function of λ. Again the constant terms $P_o = 1$ have been omitted consistently with the remark made previously that they represent a purely spherical flow which can easily be treated by a perturbation of the definition of λ. The expansions (98) to (101) are inserted into equations (62) to (65). Making use of the defining differential relation for Legendre polynomials

$$\frac{d^2P_\ell}{d\theta^2} + \cot\theta\,\frac{dP_\ell}{d\theta} + \ell(\ell+1)\,P_\ell = 0 \qquad (102)$$

to express the quantity $(W_\theta^{(1)} + \cot\theta\, W^{(1)})$ as function of P_ℓ rather than its derivatives it is seen that $P_\ell(\cos\theta)$ can be factored out of equations (62), (63) and (65) and that $\frac{d}{d\theta} P_\ell(\cos\theta)$ can be factored out of (64) which is then integrated with respect to θ producing an arbitrary constant C. Each equation, which is now of the form $P_\ell(\cos\theta)$. function of λ, is multiplied by $P_k(\cos\theta)\sin\theta$ (with $k = 1,2,3\cdots$) and integrated from 0 to π. Using the orthogonality properties of Legendre polynomials:

$$\int_o^\pi P_k(\cos\theta)\,.\,P_\ell(\cos\theta)\sin\theta\,d\theta = \begin{cases} 0 & k \neq \ell \\ \dfrac{2}{2k+1} & k = \ell \end{cases} \qquad (103)$$

and remarking that the contribution of the arbitrary constant C is zero, for any value $k > 1$ one obtains:

$$R^{(o)}\bar{V}_k' + (R^{(o)'} + 2\frac{R^{(o)}}{\lambda})\bar{V}_k - \frac{R^{(o)}}{\lambda}k(k+1)\bar{W}_k + (V^{(o)}-\lambda)\bar{R}_k' + (V^{(o)'} + 2\frac{V^{(o)}}{\lambda})\bar{R}_k = 0 \qquad (104)$$

$$(V^{(o)}-\lambda)\bar{V}_k' + (\frac{n-1}{n} + V^{(o)'})\bar{V}_k - \frac{P^{(o)'}}{R^{(o)2}}\bar{R}_k + \frac{1}{R^{(o)}}\bar{P}_k' = 0 \qquad (105)$$

$$(V^{(o)}-\lambda)\bar{W}_k' + (\frac{n-1}{n} + \frac{V^{(o)}}{\lambda})\bar{W}_k + \frac{1}{R^{(o)}}\frac{1}{\lambda}\bar{P}_k = 0 \qquad (106)$$

$$\gamma P^{(o)}\bar{V}_k' + (P^{(o)'} + 2\gamma\frac{P^{(o)}}{\lambda})\bar{V}_k - \frac{P^{(o)}}{\lambda}\gamma k(k+1)\bar{W}_k + (V^{(o)}-\lambda)\bar{P}_k' + (2\frac{n-1}{n} + \gamma V^{(o)'} + 2\gamma\frac{V^{(o)}}{\lambda})\bar{P}_k = 0 \qquad (107)$$

In the above equations ' refers to $\frac{d}{d\lambda}$. The boundary conditions are treated likewise: the expansions (95) for G (θ), (97) for H (θ) and (98) to (101) for the physical variables are substituted into equations (69) to (72); after multiplication by P_k ($\cos\theta$) $\sin\theta$ and integration over θ from 0 to π one obtains the set of boundary conditions:

$$\bar{V}_k(1) = -KA_k + [\,1 - f^{(o)} + 5K - V^{(o)'}\,(1)\,]\,X_k \qquad (108)$$

$$\bar{W}_k(1) = -\,(1 - f^{(o)})\,X_k \qquad (109)$$

$$\bar{R}_k(1) = -\frac{K}{f^{(o)2}}\,A_k + [5\frac{K}{f^{(o)2}} - R^{(o)'}\,(1)\,]\,X_k \qquad (110)$$

$$\bar{P}_k(1) = -\,K\,A_k + [2\,(1 - f^{(o)}) + 5\,K - P^{(o)'}\,(1)\,]\,X_k \qquad (111)$$

The differential equations (104) to (197) and boundary conditions (108) to (111) apply separately for each value of k = 1,2,3...The problem has been completely split into its different harmonic components: the influence of each constituent harmonic of the power perturbation G (θ) can be investigated independently. The simplification is the result of adopting a linear perturbation scheme in ϵ and it is remarked that the full set of non-linear equations (32) to (35) is not amenable to such a treatment.

The problem now is reduced to that of obtaining the solution of the system of four linear homogeneous ordinary differential equations with variable (and known only numerically) coefficients subject to four non-homogeneous boundary conditions. These contain the unknown constant X_k which, in fact, reduces the number of known boundary conditions down to three, by eliminating X_k. The system being fourth order, this implies that a solution will have to be discarded on physical grounds.

3.2. Expansions near $\lambda = 0$

The set of equations (104) to (107) will be integrated outward from the origin to the boundary. Starting such a solution necessitates an investigation of the flow in the neighborhood of $\lambda = 0$. Only the leading term of the expansions of $\bar{V}_k$, $\bar{W}_k$, $\bar{R}_k$ and $\bar{P}_k$ is sought; to that effect

equations (104) to (107) are specialized to the neighborhood of the origin by retaining only the leading term in the expansion of their coefficients. Use is made of the previously obtained expansions of the zeroth order physical variables (80) to (82):

$$b_1 \lambda^{\alpha-2} \bar{V}_k' + b_1 \alpha \lambda^{\alpha-3} \bar{V}_k - k(k+1) b_1 \lambda^{\alpha-3} \bar{W}_k + (a_o - 1) \lambda \bar{R}_k' + 3 a_o \bar{R}_k = 0 \tag{112}$$

$$(a_o - 1) \lambda \bar{V}_k' + \left(\frac{n-1}{n} + a_o\right) \bar{V}_k - \frac{c_1 \alpha}{b_1^2} \lambda^{-\alpha+3} \bar{R}_k + \frac{1}{b_1} \lambda^{-\alpha+2} \bar{P}_k' = 0 \tag{113}$$

$$(a_o - 1) \lambda \bar{W}_k' + \left(\frac{n-1}{n} + a_o\right) \bar{W}_k + \frac{1}{b_1} \lambda^{-\alpha+1} \bar{P}_k = 0 \tag{114}$$

$$\gamma c_o \bar{V}_k' + 2 \gamma \frac{c_o}{\lambda} \bar{V}_k - \gamma k (k+1) \frac{c_o}{\lambda} \bar{W}_k + (a_o - 1) \lambda \bar{P}_k' + \gamma a_1 (\alpha + 3) \lambda^{\alpha} \bar{P}_k = 0 \tag{115}$$

It is observed that the coefficients of $\bar{P}_k'$ and $\bar{P}_k$ in equation (115) are respectively multiplied by λ^{α} and $\lambda^{2\alpha}$ compared to those in equations (113) and (114). These higher order terms may be dropped and equation (115) reduces to its first three terms. Equations (112) to (115) constitute a fourth order system, hence four solutions are sought, each of the form:

$$\bar{V}_k = A_{1k} \lambda^{m_k} \tag{116}$$

$$\bar{W}_k = A_{2k} \lambda^{m_k} \tag{117}$$

$$\bar{R}_k = A_{3k} \lambda^{m_k + \alpha - 3} \tag{118}$$

$$\bar{P}_k = A_{4k} \lambda^{m_k + \alpha - 1} \tag{119}$$

When these are substituted into the set (112) to (115) all terms in each equation come out to be of the same order in λ. Cancelling out all λ dependence a system of four algebraic equations is obtained for the constants A_{1k}, A_{2k}, A_{3k}, A_{4k}. Since the original differential equations are homogeneous the algebraic system is homogeneous too and m_k must be root of an indicial equation, namely the determinant of the system equals zero. After some manipulations in which use is made of the definition of α (86) it reads:

$$\begin{vmatrix} \alpha-2 & 0 & (m_k-1)\,(a_o-1) & 0 \\ (a_o-1)\,m_k + \frac{n-1}{n} + a_o & 0 & a_o(a_o - \frac{1}{n}) & m_k + \alpha - 1 \\ 0 & (a_o-1)\,m_k + \frac{n-1}{n} + a_o & 0 & 1 \\ m+2 & -k\,(k+1) & 0 & 0 \end{vmatrix} = 0 \qquad (120)$$

Developing this determinant yields a fourth order algebraic equation in m_k. Its coefficients do not contain the constants b_1 and c_o entering the expansions of the zeroth order quantities so that the values of m_k's are dependent only on the characteristic quantities a_o and α of the zeroth order numerical solution. However, the m_k's are seen to be function of γ and of the harmonic considered k. The fourth order equation has been solved numerically for $\gamma = 5/3$, the results are presented in table 1 for the first ten harmonics. A definite pattern for the numerical values of the roots seems to emerge for increasing k i.e. for perturbations tending to be more and more spherically symmetric: the first root is positive and increasing, the last root is negative and decreasing and the pair of complex conjugate roots has a real part negative and increasing for the first three harmonics and a real part positive and increasing from harmonic four on. An important feature of the complex roots is that their real part always remains less than one, even for large values of k. This will be demonstrated in section 3.4.

The system of four algebraic homogeneous equations for A_{1k} to A_{4k} is then solved for each root. One obtains, with the superscript i referring to each root i = 1, 2, 3, 4:

$$A^i_{2k} = \frac{m^i_k + 2}{k\,(k+1)}\, A^i_{1k} \qquad (121)$$

$$A^i_{3k} = -\frac{\alpha - 2}{(m^i_k - 1)(a_o - 1)}\, b_1\, A^i_{1k} \qquad (122)$$

$$A^i_{4k} = -\frac{m^i_k + 2}{k(k+1)}\left[(a_o-1)\, m^i_k + \frac{n-1}{n} + a_o\right] b_1\, A^i_{1k} \qquad (123)$$

For each root, A^i_{1k} has been arbitrarily chosen as the free constant. Note that for the pair of complex conjugate roots all A's are complex numbers.

harmonic k	roots: m_k		
1	1.114	- 0.6253 ± 0.5500 i	- 3.500
2	1.399	- 0.2491 ± 0.7055 i	- 4.537
3	1.941	- 0.0137 ± 0.6691 i	- 5.550
4	2.719	+ 0.0998 ± 0.5965 i	- 6.555
5	3.619	+ 0.1510 ± 0.5413 i	- 7.557
6	4.569	+ 0.1767 ± 0.5047 i	- 8.558
7	5.540	+ 0.1912 ± 0.4802 i	- 9.559
8	6.522	+ 0.2002 ± 0.4632 i	- 10.56
9	7.510	+ 0.2061 ± 0.4511 i	- 11.56
10	8.510	+ 0.2103 ± 0.4421 i	- 12.56

Table 1: Roots of the indicial equation for harmonics 1 to 10 and $\gamma = 5/3$.

From this, the expansions of $\overline{V}_k$, $\overline{W}_k$, $\overline{R}_k$, $\overline{P}_k$ near $\lambda = 0$ can be obtained as a sum of four linearly independent solutions. For convenience the notation is simplified to: m_k refers to the positive root and is associated with the real constants A_k's; m_k' refers to the negative root and is associated with the real constants D_k's; $m_{rk} \pm im_{ik}$ are the complex conjugate roots associated with the complex constants B_k's. The expansions of the k^{th} harmonic read:

$$\overline{V}_k(\lambda) = A_{1k}\lambda^{m_k} + B_{1k}\lambda^{m_{rk}+im_{ik}} + B^*_{1k}\lambda^{m_{rk}-im_{ik}} + D_{1k}\lambda^{m_k'} \quad (124)$$

$$\overline{W}_k(\lambda) = A_{2k}\lambda^{m_k} + B_{2k}\lambda^{m_{rk}+im_{ik}} + B^*_{2k}\lambda^{m_{rk}-im_{ik}} + D_{2k}\lambda^{m_k'} \quad (125)$$

$$\overline{R}_k(\lambda) = A_{3k}\lambda^{m_k+\alpha-3} + B_{3k}\lambda^{m_{rk}+\alpha-3+im_{ik}} + B^*_{3k}\lambda^{m_{rk}+\alpha-3-im_{ik}} + D_{3k}\lambda^{m_k'+\alpha-3} \quad (126)$$

$$\overline{P}_k(\lambda) = A_{4k}\lambda^{m_k+\alpha-1} + B_{4k}\lambda^{m_{rk}+\alpha-1+im_{ik}} + B^*_{4k}\lambda^{m_{rk}+\alpha-1-im_{ik}} + D_{4k}\lambda^{m_k'+\alpha-1} \quad (127)$$

* stands for complex conjugate. Note that in each relation the second and third terms always combine to form a real quantity as they should since they represent real physical quantities. The free constants are now A_{1k}, B_{1k}, D_{1k} and the A_{jk}, B_{jk}, D_{jk} ($j = 2,3,4$) are respectively related to the free constants by (121) to (123). The pair of middle terms, containing B's can also be rewritten as:

$$B\,\lambda^{m_{rk}+im_{ik}} + B^*\,\lambda^{m_{rk}-im_{ik}} = 2\lambda^{m_{rk}}\,(B_r \cos\xi - B_i \sin\xi) \qquad (128)$$

$$\xi = m_{ik} \log \lambda \qquad (129)$$

where B_r and B_i are respectively the real and imaginary parts of B. In this form the oscillatory character of the expansions is clearly displayed.

3.3 Numerical Integration and Results

The system of differential equations (104) to (107) is integrated from $\lambda = 0.01$ to $\lambda = 1$ using a standard fourth-order Runge-Kutta numerical scheme. The three boundary conditions are obtained from (108) to (111) by elimination of X_k. The solution is started using expansions (124) to (127) in which the terms corresponding to the worst singularity (i.e. the negative real root m_k') are discarded by setting $D_{1k} = 0$ and hence $D_{2k} = D_{3k} = D_{4k} = 0$. This will be justified in the next chapter on the physical ground that this singularity represents a source of mass and energy at the origin.

The linear character of the differential system and boundary conditions is exploited to determine the values of the free constants A_{1k}, B_{1kr}, B_{1ki} by application of the boundary conditions. First a solution is obtained starting with expansions (124) to (127) specialized to $A_{1k} = 1$, $B_{1kr} = 0$, $B_{1ki} = 0$. Call this solution $S_k^{(1)}$ where $S_k^{(1)}$ is a column matrix $\bar{V}_k$, $\bar{W}_k$, $\bar{R}_k$, $\bar{P}_k$. A second solution $S_k^{(2)}$ is obtained with $A_{1k} = 0$, $B_{1kr} = 1$, $B_{1ki} = 0$ as well as a third solution $S_k^{(3)}$ for $A_{1k} = 0$, $B_{1kr} = 0$, $B_{1ki} = 1$. The full solution is then sought in the form of a linear combination of $S_k^{(1)}$, $S_k^{(2)}$, $S_k^{(3)}$:

$$S_k = A_{1k}\,S_k^{(1)} + B_{1kr}\,S_k^{(2)} + B_{1ki}\,S_k^{(3)} \qquad (130)$$

The value of the constants are obtained by applying the boundary conditions on the full solution S_k. Since these are non-homogeneous, a third order non-homogeneous linear algebraic system is to be satisfied by A_{1k}, B_{1kr} and B_{1ki} and the velocities, density and pressure profiles are obtained as linear combinations of the specialized solutions $S_k^{(1)}$, $S_k^{(2)}$, $S_k^{(3)}$. As a check of the numerical accuracy the equations were integrated over again with the correct values of the free constants and it was found that the boundary conditions were accurately satisfied.

Note that the system (104) to (107) was supplied with the set of zeroth order equations (59) to (61) so as to have the numerical values of the coefficients at all grid points. The seven equations were integrated simultaneously starting with expansions (88) to (90) in which use is made of the correct values of b_1 and c_0 obtained in the previous section.

More details about this method of linear superposition of specialized solutions can be found in Appendix A where it is applied to a spherical perturbation due to finite external pressure.

The integration has been carried out for the first five harmonics, treating each as if it were alone i.e. the coefficient A_i (i = 1,2,3,4,5) in series (45) is set equal to one and all the others zero. An actual power perturbation G (θ) would include several coefficients different from zero and with numerical values distinct of one. The effect of such a perturbation can easily be obtained by a linear superposition of the results presented here.

The results describing the wave front and the physical variables behind it are presented in Table I; each harmonic is treated separately. As a reminder, the five first Legendre polynomials are given in the second column of Table I. The magnitude of the shape perturbation is given by the coefficient X_k of the Legendre expansion of H (θ). All X_k's are positive indicating that an increase of laser power creates an outward displacement of the wave front and hence an increase of its velocity D. For increasing values of k, the magnitude of X_k diminishes: this shows that the shape perturbation becomes less when the power is more evenly

distributed. The values of radial velocity, tangential velocity, density and pressure behind the absorption front are readily obtained from equations (51) to (54) combined with expansions in Legendre polynomials (95), (97), and (98) to (101). They read:

$$V_d = 1 - f^{(o)} + \varepsilon P_k (\cos\theta) [-KA_k + (1 - f^{(o)} + 5K) X_k] \quad (131a)$$

$$W_d = - \varepsilon \frac{dP_k (\cos\theta)}{d\theta} (1 - f^{(o)}) X_k \quad (131b)$$

$$R_d = \frac{1}{f^{(o)}} - \varepsilon P_k (\cos\theta) \frac{K}{f^{(o)2}} (A_k - 5 X_k) \quad (132a)$$

$$P_d = 1 - f^{(o)} + \varepsilon P_k (\cos\theta) [-KA_k + \{ 2 (1 - f^{(o)}) + 5 K \} X_k] \quad (132b)$$

Table I gives the numerical values of the coefficients of P_k or $\frac{dP_k}{d\theta}$ when A_k is set equal to one for each individual harmonic. The density perturbation corresponding to a power increase is negative: this simply results from the fact that the influence of the shape perturbation H (θ) is greater than that of the power perturbation G (θ) in all cases. As a result of the enhanced front velocity, the velocities and pressure perturbations at the boundary appear first positive, then negative. It must be pointed out that the absolute values of the perturbations of radial velocity, density and pressure increase with k; in fact they tend to asymptotic values for $k \to \infty$ as will be shown in section 3-4. The tangential velocity decreases with k as it should for a flow tending towards spherical symmetry.

The radial dependence of velocities, density and pressure are plotted on Figures 4,5,6 and 7 for harmonics 1 to 4. The θ - dependence is obtained by multiplying by the respective Legendre polynomials. Note that the radial variable λ used here is not the ratio of the current radius r to the wave front radius r_d, and consequently the wave front does not correspond exactly to $\lambda = 1$. The choice of λ was made so that the radial and tangential variables λ and θ remain independent of each other. The tangential velocity remains negative as was imposed by the boundary condition that the velocity vector be perpendicular to the wave front. Its

magnitude decreases over the whole range of λ for increasing k. The density perturbation exhibits a change of sign from negative to positive around $\lambda \times .3$.

Although the character of the singularity near the origin changes between harmonic three and four (the velocities become bounded from harmonic four and up, whereas they were unbounded for the first three) no drastic change in the profiles appears to take place. This is discussed in more detail in Chapter III, Section 1.

Density maps are presented in Figures 8 and 9; for the first two harmonics the constant density lines are shown. Compared to the spherical spark the mass repartition has been altered as follows: near the focus, an increase of density corresponds to enhanced power addition. In the main body of the flow, on the contrary, a decrease of density is associated with a positive power perturbation. Separating these two regions are circles of radius $\lambda = 0.34$ and $\lambda = 0.3$ for respectively $k = 1$ and $k = 2$. Near the boundary the density perturbation again follows the power perturbation. In the asymmetric case ($k = 1$) a net mass transfer appears to take place across the focal region from $\theta = \pi$ towards $\theta = 0$. It should be remembered, however, that the small perturbation scheme breaks down near the origin so that the validity of what happens there is questionable.

Figures 10 and 11 show velocity maps for $k = 1$ and $k = 2$. The vectors represent direction and magnitude of the velocity at different points of the field. Lines tangent to the velocity vectors are streamlines, not particle paths since the flow is unsteady. Physically, the vectors are proportional to the traces which would be left by flow particles made visible by flow visualization techniques on a short exposure time photograph. The bending of streamlines is determined by the distorted shape of the spark since velocity has to remain perpendicular to the wave front. In the asymmetric case, $k = 1$, there appears to be a net flow across the focal region from $\theta = 0$ towards $\theta = \pi$; the zero velocity point is displaced on the cylindrical symmetry axis towards higher laser powers.

This, of course, doe not happen in the case of symmetric perturbation, $k = 2$.

3.4. Limiting Case of Large Wave Numbers

For increasingly large wave numbers k it is observed in table 1 that the numerical value of the first root m_k of the indicial equation is positive and increasing without bounds; the fourth root m_k' is negative and its absolute value is also increasing boundlessly. On the contrary both the real part m_{rk} and the imaginary part m_{ik} of the complex conjugate roots tend to finite asymptotic values. These behaviors have been confirmed by calculating the roots corresponding to the next ten harmonics ($k = 10, 11, \ldots 20$). The values of m_{rk} and m_{ik} are displayed on Figure 8.

The purpose of this section is to show that in the limit $k \to \infty$ the original fourth order system of ordinary differential equations (104) to (108) reduces down to a second order system. Furthermore, the behavior of the physical quantities near the focus $\lambda = 0$ is entirely described by the asymptotic values of the complex conjugate roots which will be calculated exactly.

Physically, for large wave numbers, all quantities i.e. the power perturbation, the shape perturbation and the physical variables oscillate rapidly in the angular direction θ thus giving rise to large θ - derivatives. This is expressed by:

$$\frac{d}{d\theta} [P_k (\cos\theta)] \sim O(k) \quad \text{when } k \to \infty$$

Terms $W_\theta^{(1)} + \cot\theta\, W^{(1)}$ containing second derivatives of Legendre Polynomials in equations (62) and (65) become $O(k^2)$ in equations (104) and (107) and the whole equation (64) containing first derivatives of $P_k (\cos\theta)$ becomes $O(k)$. A new ordering of terms is called for in order for the expansions (55) to (58) in powers of ε to remain valid for large values of k. The perturbation quantities $V^{(1)}$, $W^{(1)}$, $R^{(1)}$, $P^{(1)}$ have to be $O(1)$ or less.

It is noticed that one should expect a singular perturbation problem when $k \to \infty$ due to the existence of two independent small parameters ε and $\frac{1}{k}$.

The new ordering of terms corresponding to large k is suggested by equations (104) to (107). $\bar{V}_k$ and $\bar{R}_k$ remain of 0 (1) but $\bar{W}_k$ is set of 0 $(\frac{1}{k^2})$ thus making $\bar{P}_k$ of $0(\frac{1}{k^2})$ through equation (106). New tangential velocity and pressure are defined:

$$\bar{W}_k\ (\lambda) = \frac{1}{k^2}\,\bar{\bar{W}}_k\ (\lambda) \tag{133}$$

$$\bar{P}_k\ (\lambda) = \frac{1}{k^2}\,\bar{\bar{P}}_k\ (\lambda) \tag{134}$$

Substituting (133) and (134) in equations (104) to (107) and neglecting in first approximation terms of 0 $(\frac{1}{k^2})$ one obtains:

$$R^{(o)}\bar{V}_k' + (R^{(o)'} + 2\,\frac{R^{(o)}}{\lambda})\,\bar{V}_k - \frac{k+1}{k}\,\frac{R^{(o)}}{\lambda}\,\bar{\bar{W}}_k + (V^{(o)} - \lambda)\,\bar{R}_k' + (V^{(o)'} + 2\,\frac{V^{(o)}}{\lambda})\,\bar{R}_k = 0 \tag{135}$$

$$(V^{(o)} - \lambda)\,\bar{V}_k' + (\frac{n-1}{n} + V^{(o)'})\,\bar{V}_k - \frac{P^{(o)'}}{R^{(o)2}}\,\bar{R}_k = 0 \tag{136}$$

$$\gamma P^{(o)}\bar{V}_k' + (P^{(o)'} + 2\gamma\,\frac{P^{(o)}}{\lambda})\,\bar{V}_k - \frac{k+1}{k}\,\gamma\,\frac{P^{(o)}}{\lambda}\,\bar{\bar{W}}_k = 0 \tag{137}$$

Equation (106) contains terms which are all 0 $(\frac{1}{k})$; it may be used as a decoupled relation to calculate $\bar{\bar{P}}_k$. The system (135) to (137) is only second order as can easily be seen by eliminating $\bar{R}_k$ and $\bar{\bar{W}}_k$.

Consideration of large wave numbers thus brings about the important simplification of reducing the order of the system by two. This is further exploited by specializing equations (135) to (137) to the neighborhood of the origin. Only the first term in the expansions of the coefficients is retained so as to obtain:

$$b_1\lambda^{\alpha-2}\bar{V}_k' + b_1\alpha\lambda^{\alpha-3}\bar{V}_k - \frac{k+1}{k}\,b_1\lambda^{\alpha-3}\,\bar{\bar{W}}_k + (a_o-1)\,\lambda\,\bar{R}_k' + 3\,a_o\,\bar{R}_k = 0 \tag{138}$$

$$(a_o - 1)\lambda\,\bar{V}_k' + (\frac{n-1}{n} + a_o)\,\bar{V}_k - c_1\,\frac{\alpha}{b_1^2}\,\lambda^{-\alpha+3}\,\bar{R}_k = 0 \tag{139}$$

$$\bar{V}_k' + 2\,\frac{\bar{V}_k}{\lambda} - \frac{k+1}{k}\,\bar{\bar{W}}_k = 0 \tag{140}$$

In complete analogy to what was done for the fourth order system, solutions to (138) and (140) are sought of the form:

$$\bar{V}_k = A_{1k}\lambda^{m_\infty} \tag{141}$$

$$\bar{\bar{W}}_k = A_{2k}\lambda^{m_\infty} \tag{142}$$

$$R_k = A_{3k}\, \lambda^{m_\infty} + \alpha - 3 \qquad (143)$$

An indicial equation is obtained for m_∞ . It is quadratic as it should for a second order system and reads after some manipulations in which it is remarked that $\frac{k+1}{k} \to 1$ when $k \to \infty$:

$$-(a_o-1)\, m_\infty^2 - \frac{2n-1}{n}\, m_\infty + [\alpha-2)a_o \frac{a_o - 1/n}{a_o - 1} + \frac{n-1}{n} + a_o\,] = 0 \qquad (144)$$

The solution is the pair of complex conjugate roots:

$$m_\infty = 0.227 \pm i\ 0.400 \qquad (145)$$

These values are plotted on Figure 12. They show excellent agreement with the asymptotic values obtained from the fourth order indicial equation when k gets large (k = 20). This also proves that the real part of m_∞ is less than one. The two purely real roots m_k and m_k' completely disappear in this limit; this looks reasonable since the contribution of λ^{m_k} tend to be very small and can thus be discarded and on the other hand $\lambda^{m_k'}$ gets very large, so violating the small perturbation assumption and has to be discarded too.

This approach provides a rational way to reduce the order of the system and will be used in Chapter III when dealing with the full non-linear equations (32) to (35).

It is easily recognized that boundary conditions (109) to (111) cannot be satisfied by equations (135) to (137). This comes as no surprise since the order of the system is only two and the number of independent boundary conditions is three. Specifically, in view of the definition (133) of $\bar{W}_k$ equation (109) implies that X_k is 0 $(\frac{1}{k^2})$. A contradiction then appears between the definition (134) of $\bar{P}_k$ and equation (111).

This difficulty can be resolved by introducing a narrow region near the front of the wave where derivatives with respect to λ become large. In fact the singular perturbation aspect of the expansions suggests such a boundary layer approach. The proper ordering in that region is to keep $\bar{V}_k$, $\bar{R}_k$, and $\bar{P}_k$ of 0 (1) compatible with the boundary conditions and to make $\bar{W}_k$ and the thickness of the boundary layer of 0 $(\frac{1}{k})$. One defines:

$$\bar{W}_k = \frac{1}{k}\tilde{W}_k \tag{146}$$

$$\lambda = 1 - \frac{1}{k}\tilde{\lambda} \tag{147}$$

This ordering makes $W^{(1)}$ of 0 (1) so that the expansion in series of ε is still valid. Furthermore (146) implies X_k of 0 $(\frac{1}{k})$ through boundary condition (109). Physically this corresponds to the perturbation of the wave front being much smaller, $\frac{1}{k}$, then the imposed power perturbation. Thus boundary conditions (108), (110), (111) take only into account, in first approximation, the power perturbation A_k. The perturbation in shape is reflected solely in the boundary condition (109) on the tangential velocity $\bar{W}_k$.

Equations (104) to (109) are transformed as follows. The coefficients dependent on the first order physical variables are expanded in Taylor series

$$F^{(o)}(\lambda) = F^{(o)}(1) - \frac{1}{k}\frac{dF^{(o)}}{d\lambda}(1)\,\tilde{\lambda} \tag{148}$$

where $F^{(o)}$ is any $V^{(o)}$, $R^{(o)}$, $P^{(o)}$. Use is made of the zeroth order boundary conditions (66) to (68). Terms of 0 (k) are retained in equations (104), (105), (107) compared to terms of 0 (1) and terms of 0 (1) are retained in equation (106) compared to terms of 0 $(\frac{1}{k})$. One obtains:

$$\frac{1}{f^{(o)}}\frac{d\bar{V}_k}{d\tilde{\lambda}} + \frac{k+1}{k}\frac{1}{f^{(o)}}\bar{V}_k - f^{(o)}\frac{d\bar{R}_k}{d\tilde{\lambda}} = 0 \tag{149}$$

$$-\frac{d\bar{V}_k}{d\tilde{\lambda}} + \frac{d\bar{P}_k}{d\tilde{\lambda}} = 0 \tag{150}$$

$$\frac{d\tilde{W}_k}{d\tilde{\lambda}} + \bar{P}_k = 0 \tag{151}$$

$$\gamma(1-f^{(o)})\frac{d\bar{V}_k}{d\tilde{\lambda}} + \frac{k+1}{k}\gamma(1-f^{(o)})\tilde{W}_k - f^{(o)}\frac{d\bar{P}_k}{d\tilde{\lambda}} = 0 \tag{152}$$

The last three equations are combined into a single equation for P_k, remarking that $\frac{k+1}{k} \to 1$ when $k \to \infty$.

$$\frac{d^2\bar{P}_k}{d\tilde{\lambda}^2} - \beta^2\bar{P}_k = 0 \tag{153}$$

where

$$\beta^2 = \gamma\frac{1-f^{(o)}}{\gamma(1-f^{(o)}) - f^{(o)}} \tag{154}$$

β^2 is a positive number and its numerical value, using the results of the spherically symmetric solution is: $\beta^2 = 3.390$ or $\beta = 1.840$.

Boundary conditions are given by (108) to (111) with $X_k = \frac{1}{k}\tilde{X}_k$:

$$\bar{V}_k(1) = - KA_k \tag{155}$$

$$\tilde{W}_k(1) = - (1 - f^{(o)})\, \tilde{X}_k \tag{156}$$

$$\bar{R}_k(1) = - \frac{KA_k}{\beta^2} \tag{157}$$

$$\bar{P}_k(1) = - KA_k \tag{158}$$

The solution of (153) gives an increasing exponential and a decreasing exponential in $\tilde{\lambda}$. The former is rejected since only bounded values of the physical variables are acceptable when $\tilde{\lambda} \to \infty$, that is at the inner edge of the boundary layer. The solution of (149) to (151) and (153) subject to boundary conditions (155) to (158) is:

$$\bar{V}_k = - KA_k\, e^{- \beta \tilde{\lambda}} \tag{159}$$

$$\tilde{W}_k = - \frac{KA_k}{\beta}\, e^{-\beta \tilde{\lambda}} \tag{160}$$

$$\bar{R}_k = - \frac{KA_k}{\gamma f^{(o)}\,(1-f^{(o)})}\, e^{- \beta \tilde{\lambda}} - \frac{1}{\beta^2} \frac{KA_k}{f(o)^2} \tag{161}$$

$$\bar{P}_k = - KA_k\, e^{-\beta \tilde{\lambda}} \tag{162}$$

and $$\tilde{X}_k = + \frac{KA_k}{\beta} \frac{1}{1-f(o)} \tag{163}$$

The validity of the boundary layer expansions near the front of the spark can be discussed in comparison with the numerical results obtained in Section 3.3. when k increases. Since calculations were carried out only for the first five harmonics, no accurate agreement should be expected but rather some general trends.

First the boundary layer ordering implies that $X_k = 0\ (\frac{1}{k})$; thus for large values of k the expected behavior of subsequent X_k's is given by

$$\frac{X_{k+1}}{X_k} = \frac{k}{k+1} \tag{164}$$

In comparison this ratio is calculated for the first five harmonics using the values of X_k obtained previously (equation (131). The result is shown in Table 2 and plotted on Figure 13.

k	$\frac{k}{k+1}$	$\frac{X_{k+1}}{X_k}$ calculated
1	0.5	0.921
2	0.667	0.904
3	0.750	0.8996
4	0.800	0.9015

Table 2

It is seen that the right trend appears in the numerical solutions when k equals 3: the ratio $\frac{X_{k+1}}{X_k}$ begins to increase and will presumably tend towards one. As an indication that k = 4 is still quite far away from the asymptotic limit $k \to \infty$ reference is made to Figure 12.

Secondly, the boundary values obtained from (159) to (163) are:

$$\bar{V}_k(1) = \bar{P}_k(1) = -0.789;\ \bar{R}_k(1) = -2.71;\ \bar{W}_k(1) \to 0 \qquad (165)$$

These are compared to those of the numerical solutions for the first five harmonics (see Figures 4 to 7). Again the correct trends emerge: $\bar{V}_k(1)$ is negative with an increasing absolute value for increasing k's and the value (165) for $k \to \infty$ fits in that pattern: see Figure 4; the same behavior is observed for $\bar{R}_k(1)$ and $\bar{P}_k(1)$. In contrast $\bar{W}_k(1)$ is negative with a decreasing absolute value (Figure 5) which is also in agreement with (165).

It may thus be concluded that the boundary layer expansions agree with the trends of the numerical solution for increasingly large k's.

The boundary layer solution (159) to (162) must be compatible in the limit $k \to \infty$ with the solution of the inside equations (138) to (140). In particular $\bar{W}_k$ and $\bar{P}_k$ must become of 0 $(\frac{1}{k^2})$ as $k \to \infty$: this is certainly possible in view of the exponential decay (160), (162) of both $\bar{W}_k$ and $\bar{P}_k$. It is noticed that $\bar{R}_k$ is finite at the inner edge of the boundary layer whereas $\bar{V}_k$ is exponentially small; this of course does not imply that $\bar{V}_k$ is small everywhere in the inner region.

Matching of the boundary layer solution with the inner region solution thus appears possible.

CHAPTER III

INVESTIGATION OF THE SINGULARITY AT THE FOCUS OF A NON-SPHERICAL SPARK

1. Nature of the Singularity

In Chapter II the behavior of all physical quantities was obtained near the focus $\lambda = 0$. Equations (124) to (127) together with Table 1 show that the two components of velocity $\bar{V}_k$ and $\bar{W}_k$ are oscillating and unbounded for the first three harmonics then become oscillating but of decreasing amplitude for subsequent harmonics. An analogous behavior is observed for the density $\bar{R}_k$ except that the transition from unbounded amplitude to bounded amplitude occurs between harmonics two and three. The pressure $\bar{P}_k$ is oscillating and decreasing for all harmonics.

Presented in this fashion the singularity at the origin may appear quite confusing. In order to get a better understanding of the physical situation, fluxes of basic properties such as mass, momentum and energy are computed across a sphere of small radius surrounding the focus. Since one of the basic assumptions made was that of non-viscous, non-heat conducting fluid, singularities of the type source or dipole are mathematically possible. In this problem, however, no source exists at the origin and such a singularity is not acceptable. This remark is used to provide a physical basis for the rejection of solutions depending on the fourth root of the indicial equation m'_k .

1.1. Integrated Flow Properties near the Focus

Consider the fluxes of mass $\mathcal{M}_s$, axial momentum $\mathcal{M}_m$ and energy $\mathcal{E}$ across a sphere defined by $\lambda = \lambda_o$ with $\lambda_o << 1$. This choice insures the reference sphere radius to be much smaller than the spark size at all times.

$$\mathcal{M}_s = \int_o^\pi \rho u_r \, 2\pi \, r_o^2 \sin\theta \, d\theta = 2\pi \, \rho_o \, n \, A^3 t^{3n-1} \int_o^\pi R \, V \, \lambda_o^2 \sin\theta \, d\theta \quad (166)$$

$$\mathcal{M}_m = \int_o^\pi \rho (u_r \cos\theta - u_\theta \sin\theta) \, u_r \, 2\pi \, r_o^2 \sin\theta \, d\theta = 2\pi \, \rho_o \, n^2 A^4 t^{4n-2} \int_o^\pi R \, (V\cos\theta - W\sin\theta) \, V \lambda_o^2 \sin\theta \, d\theta \quad (167)$$

$$\mathcal{E} = \int_o^\pi \rho\left(\frac{u_r^2 + u_\theta^2}{2} + \frac{1}{\gamma-1}\frac{p}{\rho}\right) u_r\, 2\pi\, r_o^2 \sin\theta\, d\theta = 2\pi\rho_o\, n^3 A^5\, t^{5n-3}$$

$$\int_o^\pi R\left(\frac{V^2 + W^2}{2} + \frac{1}{\gamma-1}\frac{P}{R}\right) V\lambda_o^2 \sin\theta\, d\theta \qquad (168)$$

The mass and momentum fluxes increase with increasing time (respectively as $t^{4/5}$ and $t^{2/5}$) whereas the energy flux remains constant. This, of course, is a consequence of the constant power assumption.

The θ - integrals in equations (166) to (168) give the dependence on λ_o. In the mass flux $\mathcal{M}_s$ the product RV contains successive powers of ε :

$$RV = R^{(o)}V^{(o)} + \varepsilon\,(R^{(o)}V^{(1)} + V^{(o)}R^{(1)}) + \varepsilon^2\,(R^{(o)}V^{(2)} + V^{(o)}R^{(2)} + R^{(1)}V^{(1)}) + 0\,(\varepsilon^3) \qquad (169)$$

Second order perturbations (superscript (2)) are treated in Appendix B; their behavior is described in the neighborhood of the origin by equations (B 13) to (B 16).

The integral from 0 to π of the zeroth order term of (169) yields a mass flux whose dependence on λ_o is: $\lambda_o^{\alpha+1}$. This simply corresponds to the spherically symmetric geometry. The θ - integral of the 0 (ε) term gives no contribution since the series of Legendre polynomials (98) to (101) start with $\ell = 1$ and Legendre polynomials satisfy the integral relation (96).

There is, however, a contribution to 0 (ε^2) since the series (B 5) to (B 8) and the product $R^{(1)}V^{(1)}$ contain the constant term $P_o(\cos\theta) = 1$.

If terms containing D's were retained in the first order expansions near the focus (124) to (127), the leading terms of $R^{(1)}V^{(1)}$ as well as those of $R^{(o)}V^{(2)}$ and $V^{(o)}R^{(2)}$ would be: $\lambda^{2m'_N + \alpha - 3}$, thus contributing a mass flux:

$$\mathcal{M}_s \sim \lambda_o^{2m'_N + \alpha - 1} \qquad (170)$$

It is readily remarked that this always corresponds to a source of mass at the focus; even for the smallest possible value of m'_k, that is k = 1, the exponent of (170) is equal to - 5.091.

Similarly it can be shown that the worst singularity m'_k of the first order expansions also yields a source of energy at the focus. It does not give a source of linear momentum for the first harmonic although it does

for all higher harmonics. Since the physical problem does not allow for any kind of source, these considerations provide sufficient ground for the rejection of solutions based on D's in Chapter II, Section 3.

It remains to show that the singularity related to the complex conjugate roots does not create sources of mass, linear momentum or energy.

The leading contribution to 0 (ε^2) in (169) corresponds to the complex conjugate roots of harmonic 1: $m_{r_1} \pm i m_{i_1}$ and gives a mass flux whose amplitude behaves as:

$$\mathcal{A}(\mathcal{M}_s) \sim \lambda_o^{2m_{r_1} + \alpha - 1} \tag{171}$$

The numerical value of the exponent is 0.840 which is physically acceptable. It may be remarked that if the leading harmonic happens to be higher than one, the exponent of λ_o will always be greater than the above numerical value, thus being a fortiori acceptable.

The linear momentum flux contains RV^2 and RVW which expand respectively as:

$$RV^2 = R^{(o)}V^{(o)2} + \varepsilon\,(V^{(o)2}R^{(1)} + 2R^{(o)}V^{(o)}V^{(1)}) + 0\,(\varepsilon^2) \tag{172}$$

$$RVW = \varepsilon\, R^{(o)}\, V^{(o)}\, W^{(1)} \tag{173}$$

The integral over θ in (167) has no zeroth order part as it should for a spherically symmetric situation and the 0 (ε) contribution is, taking into account only the first harmonic

$$\mathcal{M}_m = \varepsilon\, \lambda_o^2 \left[\frac{2}{3} V^{(o)2}\, \bar{R}_1 + \frac{4}{3} R^{(o)}V^{(o)}\, (\bar{V}_1 + \bar{W}_1) \right] \tag{174}$$

This gives an oscillating momemtum flux the amplitude of which behaves as:

$$\mathcal{A}(\mathcal{M}_m) \sim \varepsilon \lambda_o^{m_{r_1} + \alpha + 1} \tag{175}$$

The numerical value of the exponent is 3.466, which is acceptable.

The energy flux contains two parts: the flux of kinetic energy and the pressure work. Considerations analogous to what was done for and $\mathcal{M}_m$ allow to show that there exists a zeroth order contribution and a second order contribution. The latter has an amplitude behaving like:

$$(\mathcal{E}) \sim \varepsilon^2 \quad \lambda_o^{2m_{r_1} + \alpha + 1} \tag{176}$$

The exponent is equal to 2.840.

In summary the leading perturbations of the mass, momentum and energy fluxes were shown to be respectively of 0 (ε^2), 0 (ε) and 0 (ε^2).

Furthermore, the singularity m'_k gives rise to at least a source of mass and energy at the focus whereas the complex conjugate roots $m_{r_k} \pm i m_{i_k}$ yield bounded fluxes to leading order. This justifies setting D's = 0 in expansions (124) to (127).

1.2. Mathematical Description - Singular Perturbation

The treatment will be limited to the mass flux $\mathcal{M}_s$, the other fluxes being amenable to the same approach. Furthermore, only the leading harmonic of the first order perturbation, which will here be assumed to be harmonic one, is taken into account. Higher order perturbations ($\varepsilon^3, \varepsilon^4, \cdots$) could be computed; it is clear that higher order equations will look like equations (B 1) to (B 4) of Appendix B with right-hand sides containing more complex functions of the lower order perturbations. The λ - dependence of the amplitude of the third and fourth order quantities can be inferred to be:

$$\mathcal{A}(V^{(3)}) \sim \lambda^{3m_{r_1}-2} \qquad \mathcal{A}(V^{(4)}) \sim \lambda^{4m_{r_1}-3} \tag{177}$$

$$\mathcal{A}(W^{(3)}) \sim \lambda^{3m_{r_1}-2} \qquad \mathcal{A}(W^{(4)}) \sim \lambda^{4m_{r_1}-3} \tag{178}$$

$$\mathcal{A}(R^{(3)}) \sim \lambda^{3m_{r_1}+\alpha-5} \qquad \mathcal{A}(R^{(4)}) \sim \lambda^{4m_{r_1}+\alpha-6} \tag{179}$$

$$\mathcal{A}(P^{(3)}) \sim \lambda^{3m_{r_1}+\alpha-3} \qquad \mathcal{A}(P^{(4)}) \sim \lambda^{4m_{r_1}+\alpha-4} \tag{180}$$

The mass flux is then obtained from (166). The integral over θ gives terms of $0(1)$, $0(\varepsilon^2)$, $0(\varepsilon^3)\cdots$ The expansion has the form:

$$\mathcal{M}_s(\lambda_o) \doteq c_o \lambda_o^{\alpha+1} [\, 1 + \varepsilon^2 \lambda_o^{2(m_{r_1}-1)} f_2(\lambda_o) + \varepsilon^3 \lambda_o^{3(m_{r_1}-1)} f_3(\lambda_o) + \varepsilon^4 \lambda_o^{4(m_{r_1}-1)} f_4(\lambda_o) + \cdots\cdots \,] \tag{181}$$

where f_2, f_3 and f_4 are purely oscillating functions of λ_o whose arguments are respectively $2\, m_i \ln \lambda$, $3\, m_i \ln \lambda$ and $4\, m_i \ln \lambda$.

Similar series of powers of ε can be obtained for the linear momentum and energy fluxes.

Series (181) is uniformly convergent in Poincarre's sense as long as

$$\varepsilon \lambda_o^{m_{r_1}-1} < 1 \tag{182}$$

Thus there exists a region in the neighborhood of the origin of size

$$0\left(\varepsilon^{-\frac{1}{m_{r_1}-1}}\right) = 0\left(\varepsilon^{0.615}\right) \tag{183}$$

in which expansions (55) to (58) in powers of ε break down. It must be remarked that the region of non-uniformity exists however small ε is. The problem is thus a singluar perturbation problem (reference [52], Chapter V). It is interesting to observe that the usual warning sign of singular perturbation (reference [52]), namely ε being the ratio of two independent lengths is not present in this particular case.

Equation (182) indicates that for any $m_{r_k} < 1$, there is a region of non-uniformity near the focus. Since it was shown (equation (145)) that m_{r_k} is always less than one the singular perturbation exists for all harmonics, including the limit $k \to \infty$.

2. Model Equations Near the Origin

2.1. Attempt to use a Poincare-Lighthill-Kuo Method

The usual Poincare-Lighthill-Kuo (P.L.K.) method, as presented for example in reference [52], Chapter 6, is not applicable to a system of four equations for four unknowns. This, of course, is due to the fact that a single straining of the independent variable cannot take care of the singularity of four dependent variables. What is needed is an individual straining for each dependent variable. The proper strainings can be obtained using a method derived from Pritulo's remarks [53]. It requires the knowledge of the second order solution, as is done in Appendix B.

The method is founded on the following consideration. A function $F(\lambda,\theta)$ is expanded in series of ε:

$$F(\lambda,\theta) = F^{(1)}(\lambda,\theta) + \varepsilon F^{(2)}(\lambda,\theta) + 0(\varepsilon^3) \tag{184}$$

$F^{(1)}$ is singular near $\lambda = 0$ and $F^{(2)}$ even more singular. The dependent variables are also expanded in series of ε :

$$\lambda = s + \varepsilon \lambda_1(s,\phi) + 0(\varepsilon^2) \tag{185}$$

$$\theta = \phi + \varepsilon \Phi_1(s,\phi) + 0(\varepsilon^2) \tag{186}$$

Substituting (185) and (186) into (184) one collects powers of ε after making use of the Taylor expansion of $F^{(1)}$. The determination of the straining functions λ_1 and Φ_1 is such that the $0(\varepsilon)$ term of the expansion

in the new independent variables s, ϕ is no more singular than the 0 (1) term. This is written as:

$$\frac{\partial F^{(1)}}{\partial \lambda}(s,\phi)\,\lambda_1 + \frac{\partial F^{(1)}}{\partial \theta}(s,\phi)\cdot\Phi_1 + F^{(2)}(s,\phi) = \mathcal{F}_1 \qquad (187)$$

where $\mathcal{F}_1$ is any function of s, ϕ no more singular than $F^{(1)}$; usually it is set equal to zero.

In order to apply this method to the problem at hand, four functions F are defined from the physical variables, by subtracting the regular zeroth order term:

$$V^* = \frac{V-V^{(o)}}{\varepsilon} = V^{(1)} + \varepsilon V^{(2)} \quad \text{and} \quad W^* = \frac{W}{\varepsilon} = W^{(1)} \qquad (188)$$

R* and P* are formed similarly. Using the results (124) to (127) of Chapter II and (B 13) to (B 16) of Appendix B, individual relations (184) can be written for V*, W*, R* and P* from which individual strainings are obtained.

However, no functions λ_1 and Φ_1 could be found such that the mapping s,ϕ to λ,θ is one to one thus insuring functions V* to P* to be single-valued in λ,θ. As an example consider V* and choose Φ_1 to be zero; λ_1 is then obtained:

$$\lambda(s_1\theta) = -\frac{V^{(2)}(s,\theta)}{\frac{\partial V^{(1)}}{\partial \lambda}(s,\theta)} \qquad (189)$$

Owing to the oscillating character of $V^{(1)}$ and hence of its derivative $V^{(1)}_\lambda$ in both λ and θ, λ_1 takes up infinite values of either sign, which in turn gives a non-acceptable transformation s to λ.

Notice that this difficulty with a P.L.K. method is not specific to this particular problem but rather appears in any situation where the first order function $F^{(1)}$ is oscillating.

The method of matched asymptotic expansions could be used. As indicated by equation (183) an inner independent variable $\tilde{\lambda}$ is defined:

$$\lambda = \varepsilon^{\chi}\tilde{\lambda} \quad \text{with} \quad \chi = -\frac{1}{m_r - 1} = 0.615 \qquad (190)$$

Expansions (124) to (127) show the ordering of the inner dependent variables to be:

$$V = \varepsilon^{\chi}\mathcal{V};\ W = \varepsilon^{\chi}\mathcal{W};\ R = \varepsilon^{\chi}\mathcal{R};\ P = \mathcal{P}^{(o)} + \varepsilon^{\alpha\chi}\mathcal{P}^{(1)} \qquad (191)$$

$\mathcal{P}^{(o)}$ turns out to be constant and $\mathcal{V}, \mathcal{W}, \mathcal{R}, \mathcal{P}^{(1)}$ are solution of a fourth order non-linear system of partial differential equations. This system was found to be no more tractable than the original non-linear system (32) to (35) so that this approach was interrupted.

2.2. First Order Non-linear Models

In view of the difficulties encountered with the above standard techniques non-linear model equations are considered with the hope to determine if the singularity at the focus originates in the mathematical treatment of the problem or in the basic physical assumptions.

The full non-linear equations (32) to (35) are used in the neighborhood of $\lambda = 0$. For convenience they are slightly modified by extracting the leading part of the spherically symmetric solution near the origin:

$$V = a_o \lambda + v \tag{192}$$

$$W = w \tag{193}$$

$$\frac{1}{R} = S = \frac{1}{\lambda^{\alpha-1}} \left(\frac{1}{b_1} \lambda + s \right) \tag{194}$$

$$P = c_o + \lambda^{\alpha-1} (c_1 \lambda + p^*) \tag{195}$$

The system of non-linear partial differential equations for v, w, s, p* is derived in Appendix C, equations (C 6) to (C 10). It is used as the source of model equations.

Notice that for small λ's developing the physical quantities in powers of ϵ is equivalent to linearizing system (C 6) to (C 10). Model equations must thus be chosen so as to include non-linear terms.

A first model is obtained by retaining only the linear and non-linear radial velocity terms in the r-momentum equation (C 8). After dividing through by $(a_o + \frac{n-1}{n})$ and absorbing the multiplicative constant in a new definition of v, one gets:

$$N \lambda v_\lambda + v = v v_\lambda \tag{196}$$

with

$$N = \frac{a_o - 1}{a_o + \frac{n-1}{n}} > 0 \tag{197}$$

The numerical value of N is 11/6. The general solution of (196) is

obtained by inverting independent and dependent variables; with K an arbitrary constant it reads:

$$\lambda = Kv^{-N} + \frac{1}{N+1} v \tag{198}$$

If this solution is to be matched with the numerical solution of Chapter II developed in powers of ε outside the region of non-uniformity, v must be of 0 (ε), Thus

$$v = \varepsilon v^* \tag{199}$$

The solution for v^*, now directly comparable to $\bar{V}^{(1)}$ or V_k is:

$$\lambda = Kv^{*-N} + \frac{\varepsilon}{N+1} v^* \tag{200}$$

A schematic plot of v^* (λ) is presented in Figure 14 for positive K. The first term in (200) corresponds to the dotted line and indicates that v^* goes to infinity when λ goes to zero. This is the sort of behavior observed for the amplitude of $\bar{V}_1$ in Chapter II. This, however, is strongly modified by the existence of the second term in (200) which corresponds to the non-linear right-hand side of (198). It forces the solution to turn around before reaching $\lambda = 0$; v^* then tends to infinity along an oblique asymptote: $v^* = \frac{N+1}{\varepsilon} \lambda$. Thus, however small ε ; there exists a forbidden region near $\lambda = 0$ which the solution cannot enter; its size is given by:

$$\lambda_c = \varepsilon^{\frac{N}{N+1}} [K (N+1)]^{\frac{1}{N+1}} N^{-\frac{N}{N+1}} \tag{201}$$

Notice that the characteristic power of ε: $\frac{N}{N+1} = 0.647$ is fairly close to the power X = 0.615 corresponding to the region of non-uniformity of the singular perturbation(see equation (190)).

In this case it can be shown that the P.L.K. method gives exactly the answer (200); this is not surprising since the solution appears in the form of λ being a function of v^* expanded in powers of ε.

The non-linear term of (196), even though it is small, radically changes the character of the solution near $\lambda = 0$. Unfortunately, this change depends on the exact nature of the non-linear term. Suppose that instead of equation (196) another first order model equation is chosen:

$$N \lambda v_\lambda + v = \frac{1}{\lambda} v^2 \qquad (202)$$

This is quite plausible in view of the existence of a term $\frac{w^2}{\lambda}$ in equation (C 8) which very likely behaves as v^2/λ . The solution of (202) is reduced to a quadrature at the transformation $v = \lambda z$ and $\xi = \ln\lambda$; expressed in terms of v* it comes out to be, with K an arbitrary constant:

$$v^* = K (N+1) \frac{\lambda}{\lambda^{\frac{N}{N+1}} + K} \qquad (203)$$

This is schematically plotted on Figure 14. The dotted line corresponds to equation (203) with ε set equal to zero; it is exactly the same as the dotted line corresponding to the first term of (200). The non-linear term introduces a change near $\lambda = 0$ which is quite different from the one observed with the first model equation: v* goes to zero with a slope of $\frac{N+1}{\varepsilon}$ thus exhibiting a typical boundary layer behavior. The boundary layer thickness, defined as the value of λ for which v^*_λ is zero, comes out:

$$\lambda_c = \varepsilon^{\frac{N}{N+1}} (NK)^{\frac{N}{N+1}} \qquad (204)$$

Notice that the same power of ε appears in both models. The P.L.K. method applied to equation (202) does not properly describe the boundary layer effect: instead of going to zero for $\lambda \to 0$, v* goes to a finite value of $0 (\varepsilon^{\frac{-1}{N+1}})$.

The examination of these two non-linear first order model equations shows that the correct behavior of the solution near $\lambda = 0$ is very sensitive to the exact nature of the non-linear terms retained. It is thus desirable to use a rational way to derive a model equation.

2.3. Second Order Non-linear Model

The second order model equation must have the feature that its linear part yields the oscillating behavior in λ characteristic of $\bar{V}_k$. The pertinent non-linear terms can be rationally chosen in the limit of large wave number (k). In that case, the linear system (104) to (107) reduces down from fourth order to second order. The non-linear system (C 6) to (C 10) is similarly reduced.

For large k, the ordering of tangential velocity and pressure

perturbation is obtained by carrying over the results of the linear analysis (equations (133) and (134)) to the non-linear system:

$$w \sim 0 \left(\frac{1}{k}\right) \tag{205}$$

$$p^* \sim 0 \left(\frac{1}{k^2}\right) \tag{206}$$

Equations (C 6) to (C 10) are specialized to the axis of symmetry $\theta = 0, \pi$ on which the θ derivatives of v and s vanish. Further, only equations in the neighborhood of $\lambda = 0$ are of interest. For small λ, provided that v and w_θ are leading over $\lambda^{\alpha+1}$, equation (C 10) simply reads:

$$\Phi = 0 \tag{207}$$

The large k center line equations near $\lambda = 0$ obtained from (C 7) and (C 8) are:

$$-(\alpha - 2)\frac{1}{b_1} v + (a_o - 1)(\lambda s_\lambda - s) - v s_\lambda - (\alpha - 1)\frac{vs}{\lambda} = 0 \tag{208}$$

$$(a_o - 1)\lambda v_\lambda + \left(a_o + \frac{n-1}{n}\right) v + \alpha c_1 s + v v_\lambda = 0 \tag{209}$$

Elimination of s provides the second order equation in v:

$$(\alpha - 2)\frac{\alpha c_1}{b_1} v + (a_o - 1)^2 \lambda^2 v_{\lambda\lambda} + \left(a_o + \frac{n-1}{n}\right)(a_o - 1)(\lambda v_\lambda - v)$$
$$+ 2(a_o - 1)\lambda v v_{\lambda\lambda} + v^2 v_{\lambda\lambda} + (a_o - 1)\lambda v_\lambda^2 + v v_\lambda^2$$
$$+ \left(3 a_o + \frac{2n-1}{n}\right) v v_\lambda - (\alpha - 1)\frac{1}{\lambda} v^2 v_\lambda - (\alpha - 1)\left(a_o + \frac{n-1}{n}\right)\frac{v^2}{\lambda} = 0 \tag{210}$$

This equation contains a rather long series of non-linear terms all of which must be retained. It is seen from the ordering (190), (191) of dependent and independent variables in the region of non-uniformity of the series of powers of ϵ that all terms, linear and non-linear, in equation (210) are of $0(\epsilon^{\alpha})$.

The explicit λ- dependence in (210) can be eliminated by the transformation

$$v = \lambda z \tag{211}$$

$$\xi = \ln \lambda \tag{212}$$

With $' \equiv \frac{d}{d\xi}$ the equation reads:

$$N_1^2 z'' + N_2 z' + N_3 z$$
$$- 2N_1 z z'' + z^2 z'' - N_1 z'^2 + z z'^2 - M_1 z z' + M_2 z^2 z' + M_3 z^2 -$$
$$- M_4 z^3 = 0 \tag{213}$$

The quantities N's and M's are defined positive:

$$N_1 = (a_o - 1) = .7333 \quad ; \quad M_1 = 7\, a_o - \frac{2n+1}{n} = 1.800$$

$$N_2 = (a_o - 1)\left(2\, a_o - \frac{1}{n}\right) = .8311 \quad ; \quad M_2 = 4 - \alpha = .9091$$

$$N_3 = -(\alpha - 2)\, a_o \left(a_o - \frac{1}{n}\right) = .4073 \quad ; \quad M_3 = 4\, a_o + \frac{n-1}{n} - (\alpha - 1)\left(a_o + \frac{n-1}{n}\right) = 1.236 \tag{214}$$

$$M_4 = \alpha - 2 = 1.091$$

In form (213) the second order equation for z is amenable to phase-plane techniques. See for instance reference [54]. With the standard notation:

$$X_1 \equiv z \tag{215}$$

$$X_2 \equiv z' \tag{216}$$

equation (213) becomes:

$$\frac{dX_2}{dX_1} = \frac{-(X_1 - N_1)\, X_2^2 - M_2 (X_1 - R_3)(X_1 - N_1)\, X_2 + M_4\, X_1 (X_1 - R_1)(X_1 + a_o)}{X_2 (X_1 - N_1)^2} \tag{217}$$

$$\frac{d\xi}{dX_1} = \frac{1}{X_2} \tag{218}$$

The quantities R_1 and R_3 are defined as:

$$R_1 = \frac{N_3}{a_o M_4} = 1.3965 \tag{219}$$

$$R_3 = \frac{N_2}{N_1 M_2} = 1.2445 \tag{220}$$

In principle, equation (217) is to be integrated in the phase plane X_1, X_2 taking singular points into account. The physical location λ is then found by integrating equation (218).

For example, consider only the linear terms in equation (210); equation (217) simply reads:

$$\frac{dX_2}{dX_1} = \frac{-N_2 X_2 - N_3 X_1}{N_1^2 X_2} \tag{221}$$

It has one singular point (0,0) which is a focus, the characteristic roots of which are: $-0.773 \pm 0.400i$. The corresponding solution for v is:

$$v = A_1\, \lambda^{.227 + i0.400} + A_2\, \lambda^{.227 - i0.400} \tag{222}$$

which is in agreement with the results of Chapter II, Section 3.4.

The complete equation (217) exhibits five singular points: S_1 (0,0) which is a focus; S_2 (R_1,0), S_3 ($-a_o$,0) and S_5(∞, ∞) which are saddle points; and the singular point S_4 (N_1,∞).

The local solutions in the neighborhood of S_4 are given by:

$$X_2 = \frac{c_1}{X_1 - N_1} \tag{223}$$

The corresponding solutions for v are obtained from integration of equation (218):

$$(v - N_1 \lambda)^2 = \lambda^2 (c_1 \ln \lambda + c_2) \tag{224}$$

c_1 and c_2 are arbitrary constants.

This result is interpreted in the following way: singularity S_4 is associated with points v_c, λ_c on the straight line $v = N_1 \lambda$ of the v, λ plane. Consider the integral curves going through such a point; their behavior in the immediate neighborhood of v_c, λ_c is obtained from equation (224) with:

$$\lambda = \lambda_c + \lambda' \tag{225}$$

$$v = v_c + v' \tag{226}$$

Expanding the ln λ for small λ', one obtains:

$$v' = + N_1 \lambda' \pm \sqrt{c_1 \lambda_c \lambda'} \tag{227}$$

Thus the integral curves cross the line $v = N_1 \lambda$ with an infinite slope. Furthermore, there exists, on the axis of symmetry, a forbidden region near the origin: an integral curve coming from the half plane $\lambda > \lambda_c$ turns back toward that region after crossing $v = N_1 \lambda$.

The integral curves defined by equation (227) depend on two parameters: the position λ_c at which the crossing occurs and the curvature (related to c_1) of the square root function.

The size of the forbidden region could, in principle, be determined by matching the small perturbation solution (222), depending on the constants A_1 and A_2 to be determined from the boundary conditions, to the local non-linear solution (227) also depending on two free constants. As a first approximation of the relation of the size of the forbidden region to ε , it may be assumed that the linear solution (222) is continued until it

crosses the line $v = N_1 \lambda$. This yields a size $\lambda_c \sim 0\ (\varepsilon^{1.291})$ which is in agreement with the ordering used in the singular perturbation approach: see equation (190) with $m_r = 0.227$.

In summary it is seen that a forbidden domain of approximate size $0\ (\varepsilon^{1.291})$ occurs on the axis of symmetry. It seems likely that this conclusion also applies to other θ - directions.

3. Interpretation and Discussion

The above analysis brings about the true nature of the singularity at the focus: rather than possessing unbounded oscillatory physical variables, as indicated by the linear theory, the flow displays a forbidden region or hole near the origin. This, of course, is not physically acceptable. Since the mathematical treatment can no longer be criticized from the standpoint of singular perturbation, the source of the difficulty must be sought in the basic assumptions made to derive the flow equations.

Self-similarity in this particular problem, besides other conditions, requires neglecting the counterpressure p_o as well as neglecting viscosity and heat-conduction. The latter two are responsible for the infinite temperature and zero density obtained in the spherically symmetric geometry. It is shown in Appendix A that when counterpressure p_o is included in the problem as a small perturbation τ away from self-similarity, these features still prevail (see equations (A 37) and (A 39)).

It is believed that the infinite temperature is the physical origin of difficulties appearing in non-spherically symmetric geometry.

Each gas particle retains the entropy it got when it was processed by the narrow absorption layer. In particular, there exists always a point of zero velocity on the cylindrical symmetry axis, for example the focus itself if the power perturbation has a second symmetry axis at $\theta = 90^o$. Consider the gas particles immediately adjacent to that point; they have a high entropy because they were processed at early time and have a different entropy according to the angle θ at which they crossed the spark front. Very strong θ - gradient of entropy (or temperature) are therefore present near the focus. Physically it seems that these must be smoothed out by

diffusion processes including radiative heat transfer.

It is thus concluded that a proper physical approach of the flow near the focus should probably include momentum transfer and heat transfer effects.

CHAPTER IV

SUMMARY AND CONCLUSIONS

Most experiments on laser breakdown of gases until now have relied upon a single focused beam, thus creating very asymmetric sparks and theories have been limited to one dimensional models. In this study, angular variations of power are introduced. Furthermore, from the point of view of energy concentration in a single spark it would be highly desirable to use a spherical array of lasers surrounding the plasma. This, of course, will provide a nearly spherically symmetric distribution of power to which the small perturbation analysis presented here is exactly applicable.

Boundary conditions are derived for a narrow absorbing layer preceded by a shock wave. The inner plasma is described as a non-viscous, non-heat conducting, and perfect gas. The thermal radiation emitted by the hot plasma is neglected compared to the laser beam power input, thus making the inner flow isentropic. Self-similarity is possible provided the counterpressure can be neglected and assuming constant power addition in time; the size of the spark then grows like $t^{3/5}$.

The angular dependence is introduced as a perturbation in the power addition, of magnitude ε, a small quantity. The self-similar equations and boundary conditions are split into a zeroth order set and a first order set. The former describes a purely spherical spark. A numerical outward integration yields the velocity, density and pressure profiles which are comparable to those obtained by Champetier and Al. [40] and Wilson and Turcotte [41]. The temperature at the origin is infinite and the pressure bounded. The singularity at the origin is identified as depending on the self-similarity variable λ according to $\lambda^{34/11}$.

The first order perturbation equations and boundary conditions are linear and can be decomposed in Fourier series of the angular variable θ. For the first five harmonics an outward numerical integration yields the velocity components, density and pressure profiles in function of λ. The

size of the perturbed spark is determined; it turns out to be much smaller than the power perturbation which corresponds to a redistribution of the added energy in the whole flow. The wave front is strengthened by enhanced power addition, thus making velocity, density and pressure perturbations positive behind the front. Maps are presented of the stream lines and constant density lines for the first two harmonics. In the case of harmonic one, a mass transfer occurs near the focus towards the increased power addition; similarly the stream lines are pulled in that direction.

The case of large wave numbers is examined. The tangential velocity and pressure perturbations become small in most of the field and the system of differential equations describing the flow reduces down from fourth order to second order. A boundary layer forms near the wave front to accommodate the boundary conditions.

The small perturbation solution is valid away from the focus of the laser in which neighborhood the physical variables exhibit a singular behavior: they oscillate with reducing wave length. Analytical expansions in the variable λ show that the singularity does not, to leading order, yield a source of mass, momentum and energy. The expansion in powers of ϵ is, however, a singular perturbation near the focus.

Several first order and second order model equations are considered with the aim of including non-linear effects near the origin. In particular, for large wave numbers, a second order equation is rationally obtained which describes the velocity perturbation on the axis of symmetry of the spark. Solution of the first order to that equation suggests, and study of the second order equation confirms, the existence of a forbidden region near the focus.

Further improvements of the analysis presented here would include a detailed derivation of the size of the forbidden region by properly matching the non-linear solution with the small perturbation linear solution, in the large wave-number limit. This, however, still does not completely describe the physical situation. The basic assumptions should be reviewed; self-similarity likely should be excluded to properly take into account

heat transfer during early phases of the spark history when the infinite temperature singularity is established. Experimental evidence indicates the existence, inside the spark, of a hot core in which radiative transfer effects are probably strong; this may suggest the use of a constant temperature region near the origin.

BIBLIOGRAPHY

[1] R. G. Meyerand Jr and A. F. Haught: "Gas breakdown at optical frequencies" Proc. of 6th Intern. Conf. on Ionization Phenomena in Gases, Paris 1963, Vol. II, p. 479

[2] R. G. Meyerand Jr and A. F. Haught: "Gas breakdown at optical frequencies" Phys. Rev. Letters 11, 401 (1963)

[3] E. K. Damon and R. G. Tomlinson: "Observation of ionization in gases by a ruby laser" Appl. Opt. 2, 546 (1963)

[4] C. Demichelis: "Laser induced gas breakdown: a bibliographical review" IEEE J. of Quantum Electronics 5, 188 (1969)

[5] D. H. Gill and A. A. Dougal: "Breakdown minima due to electron impact ionization in super high pressure gases irradiated by a focused giant laser pulse" Phys. Rev. Letters 15, 845 (1965)

[6] A. F. Haught, R. G. Meyerand Jr and D. C. Smith: "Electrical breakdown of gases by optical frequency radiation" in Physics of Quantum Electronics, P. L. Kelley, B. Lax and P.E. Tannenwald, Eds., New York: McGraw-Hill, 1966, p. 509

[7] V. E. Mitsuk, V. I. Savdskin and V. A. Chernikov: "Breakdown at optical frequencies in the presence of diffusion losses" JETP Letters 4, 88 (1966)

[8] C. Barthelemy, M. Leblanc and M. T. Boucalt: "Variation du seuil de claquage de l'air en fonction de la longueur d'onde de l'irradiation laser" Comp. Rend. Acad. Sci. (Paris) 266B, 1234 (1968)

[9] H. T. Buscher, R. G. Tomlinson and E. K. Damon: "Frequency dependence of optically induced gas breakdown" Phys. Rev. Letters 15, 847 (1965)

[10] S. A. Ramsden and W. E. R. Davies: "Radiation scattered from the plasma produced by a focused ruby laser beam" Phys. Rev. Letters 13, 227 (1964)

[11] F. Floux and P. Veyrie: "Etude expérimentale du plasma créé par focalisation d'un faisceau laser dans l'air" Compt. Rend. Acad. Sci. (Paris) 261, 3771 (1965)

[12] J. W. Daiber and H. M. Thompson: "Laser driven detonation waves in gases" Phys. Fluids 10, 1162 (1967)

[13] J. W. Daiber and H. M. Thompson: "X-ray temperatures from laser-induced breakdown plasmas in air" J. Appl. Phys. 41, 2043 (1970)

[14] S. L. Mandel'shtam, P. P. Pashinin, A. V. Prokhindeev, A. M. Prokhorov and N. K. Sukhodrev: "Study of the spark produced in air by focused laser radiation" Sov. Phys. JETP 20, 1344 (1965)

[15] S. L. Mandel'shtam, P. P. Pashinin, A. M. Prokhorov, Yu. P. Raizer and N. K. Sukhodrev: "Investigation of the spark discharge produced in air by focusing laser radiation, II" Sov. Phys. JETP 22, 91 (1966)

[16] V. V. Korobkin, S. L. Mandel'shtam, P. P. Pashinin, A. V. Prokhindeev, A. M. Prokhorov, N. K. Sukhodrev and M. Ya. Schelev: "Investigation of the air spark produced by focused laser radiation, III" Sov. Phys. JETP 26, 79 (1968)

[17] A. J. Alcock, C. Demichelis and K. Hamal: "Subnanosecond Schlieren photography of laser induced gas breakdown" Appl. Phys. Letters 12, 148 (1968)

[18] P. Veyrie and F. Floux: "Breakdown wave, shock wave and radiation wave in laser created plasma" AIAA Fluid and Plasma Dynamics Conference. Los Angeles 1968 AIAA paper No. 68-678

[19] L. R. Evans and C. Grey Morgan: "Multiple collinear laser-produced sparks in gases" Nature (London) 219, 712 (1968)

[20] L. R. Evans and C. Grey Morgan: "Lens aberrative effects in optical frequency breakdown in gases" Phys. Rev. Letters 22, 1099 (1969)

[21] A. J. Alcock, E. Panarella and S. A. Ramsden: "An interferometric study of laser induced breakdown in air" Proc. 7th International Conf. on Phenomena in Ionized Gases Vol. 3 (Beograd, Yugoslavia) B. Perovic and D. Tosic eds., Gradevinska Kujiga Publ. House (1966) p. 224

[22] A. J. Alcock and S. A. Ramsden: "Two wave length interferometry of a laser induced spark in air" Appl. Phys. Letters 8, 187 (1966)

[23] A. J. Alcock, P. P. Pashinin and S. A. Ramsden: "Temperature measurements of a laser spark from soft X-ray emission" Phys. Rev. Letters 17, 528 (1966)

[24] M. P. Vanyukov, V. A. Venchikov, V. I. Isaenko, P. P. Pashinin and A. M. Prokhorov: "Production of a high temperature dense plasma by gas breakdown with the aid of a laser" JETP Letter 7, 251 (1968)

[25] T. P. Evtushenko, A. N. Zaidel, G. V. Ostrovskaya and T. Ta. Chelidze: "Spectroscopic studies of a laser spark I: Laser spark in helium" Sov. Phys. - Tech. Phys. 11, 1126 (1967)

[26] G. A. Askar'yan, M. S. Rabinovich, M.M. Savchenko and V. K. Stepanov: "Fast overlap of microwave radiation by an ionization aureole of a spark in a laser beam" JETP Letters 3, 303 (1966)

[27] V. Durand and P. Veyrie: "Etude spectroscopique d'un plasma d'hélium créé par le faisceau d'un laser" Compt. Rend. Acad. Sci. (Paris) 262B, 1283 (1966)

[28] M. M. Litvak and D. F. Edwards: "Electron recombination in laser produced hydrogen plasmas" J. Appl. Phys. 37, 4462 (1966)

[29] H. B. Bebb and A. Gold: "Multiphoton ionization of hydrogen and rare gases atoms" Phys. Rev. 143, 1 (1966)

[30] P. Nelson: "Calcul de l'ordre de gandeur des processus multiphotoniques" Compt. Rend. Acad. Sci. (Paris) 259, 2185 (1964)

[31] B. A. Tozer: "Theory of the ionization of gases by laser beams" Phys. Rev. 137A, 1665 (1965)

[32] P. F. Browne: "Mechanism of gas breakdown by lasers" Proc. Phys. Soc. 86, 1323 (1965)

[33] J. K. Wright: "Theory of the electrical breakdown of gases by intense pulses of light" Proc. Phys. Soc. 84, 41 (1964)

[34] Y. B. Zel'dovich and Yu. P. Raizer: "Cascade ionization of a gas by a light pulse" Sov. Phys. JETP 20, 772 (1965)

[35] S. A. Ramsden and P. Savic: "A radiative detonation model for the development of a laser induced spark in air" Nature 203, 1217 (1964)

[36] E. Panarella and P. Savic: "Blast waves from a laser induced spark in air" Can. J. Phys. 46, 183 (1968)

[37] Yu. P. Raizer: "Heating of a gas by a powerful light pulse" Sov. Phys. JETP 21, 1009 (1965)

[38] J. L. Champetier: "Interprétation théorique de l'évolution du plasma créé par focalisation d'un faisceau laser dans l'air" Compt. Rend. Acad. Sci. (Paris) 261, 3954 (1965)

[39] M. H. Key: "Ionization effects in a hydrodynamic model of radiation-driven breakdown wave propagation" J. Phys. B ser. 2 2, 544 (1969)

[40] J. L. Champetier, M. Couairon and Y. Vendenboomgaerde: "Sur les boules de claquage créées par lasers" Compt. Rend. Acad. Sci. (Paris) 267, 1133 (1968)

[41a] C. R. Wilson and D. L. Turcotte: "Similarity solution for a spherical radiation-driven shock wave" JFM 43, 399 (1970)

[41b] C. R. Wilson: "Radiation-driven shock waves" Ph.D. dissertation, Cornell University (1970)

[42] L. I. Sedov:"Similarity and dimensional analysis in mechanics" M. Holt ed., Academic Press (New York - London) 1959 p. 152

[43] A. J. Alcock, C. Demichelis, K. Hamal and B. A. Tozer: "Expansion mechanism in a laser-produced spark" Phys. Rev. Letters 20, 1095 (1968)

[44] R. V. Ambartsumyan, N. G. Basov, V. A. Boiko, V. S. Zuev, O. N. Krokhin, P. G. Kryukov, Yu. V. Senat-Skii and Yu.Yu. Stoilov: "Heating of matter by focused laser radiation" Sov. Phys. JETP 21, 1061 (1965)

[45] C. Canto, J. - D. Reuss and P. Veyrie: "Etude théorique de l'ionization du deutérium sous l'action d'un laser à impulsion courte" Compt. Rend. Acad. Sci. (Paris) 267, 878 (1968)

[46] F. Floux, D. Guyot and Ph. Langer: "Etude expérimentale de l'ionization du deutérium sous l'action d'un laser à impulsion courte" Compt. Rend. Acad. Sci. (Paris) 267, 416 (1968)

[47] Ya. B. Zeldovich and Yu. P. Raizer: "Physics of shock waves and high temperature hydrodynamics" W. D. Hayes and R. F. Probstein eds., Academic press (New York) 1966

[48] W. J. Rae and H. P. Kirchner: "Final report on meteoroid impact phenomena" CAL report n° RM 1655-M-4 (1963)

[49] G. I. Taylor: "The formation of a blast wave by a very intense explosion" Proc. Roy. Soc. London A201, 159 (1950)

[50] D. D. Laumbach and R. F. Probstein: "A point explosion in a cold exponential atmosphere" JFM 35, 53 (1969)

[51] D. D. Laumbach and R. F. Probstein: "A point explosion in a cold exponential atmosphere. Part 2. Radiating flow" JFM 40, 833 (1970)

[52] Milton Van Dyke: "Perturbation methods in fluid mechanics" Academic Press (1964)

[53] M. F. Pritulo: "On the determination of uniformly accurate solutions of differential equations by the method of perturbation of coordinates" J. Appl. Math. Mech. 26, 661 (1962)

[54] P. M. De Russo, R. J. Roy and C. M. Close: "State variables for engineers" Wiley (1964)

APPENDIX A

SPHERICAL LASER SPARK WITH COUNTERPRESSURE

A 1. General Equations and Boundary Conditions

The inclusion of counterpressure p_o introduces a new parameter containing mass, length and time; this invalidates the dimensional arguments leading to self-similarity (see Chapter I). The governing flow equations are thus the full time dependent equations (19) to (22). The analysis is restricted to purely spherical geometry i.e. $\frac{\partial}{\partial \theta} = 0$ and $u_\theta = 0$ and constant power $\kappa = 0$. Defining λ as previously (eq. (25) and (26)) and a modified time variable τ as

$$\tau \equiv \gamma \frac{p_o}{\rho_o} \frac{1}{(n A t^{n-1})^2} \tag{A1}$$

and non dimensionalizing the physical quantities as

$$u_r = n A t^{n-1} V(\lambda, \tau) \tag{A2}$$

$$\rho = \rho_o R(\lambda, \tau) \tag{A3}$$

$$p = \rho_o n^2 A^2 t^{2n-2} P(\lambda, \tau) \tag{A4}$$

equations (19), (20) and (22) can be rewritten, after cancellation of explicit t-dependence

$$(V - \lambda) R_\lambda + R V_\lambda + 2 \frac{RV}{\lambda} - 2 \frac{n-1}{n} \tau R_\tau = 0 \tag{A5}$$

$$(V - \lambda) V_\lambda + \frac{n-1}{n} V + \frac{1}{R} P_\lambda - 2 \frac{n-1}{n} \tau V_\tau = 0 \tag{A6}$$

$$(V - \lambda) P_\lambda + 2 \frac{n-1}{n} P + \gamma P V_\lambda + 2\gamma \frac{PV}{\lambda} - 2 \frac{n-1}{n} \tau P_\tau = 0 \tag{A7}$$

Note that the new independent variable τ (which goes as $t^{4/5}$) can be interpreted as the inverse square of a fictitious Mach number based on the sound velocity in the undisturbed gas and the wave front velocity that would pertain to a self-similar spherical spark. It was found more convenient, for perturbation purposes, to use this fictitious Mach number rather than the Mach number based on the actual front velocity as was done by Sakurai [I, II] in his study of ordinary blast waves.

The spark boundary is an unknown function of time that may be expressed as

$$r_d = A\, t^n\, m(\tau) \tag{A8}$$

The wave velocity is obtained by derivation with respect to time:

$$D = n\, A\, t^{n-1} \left(m - \frac{2n-2}{n}\, \tau\, m' \right) \tag{A9}$$

in which $m' = \frac{dm}{d\tau}$. Defining $\tilde{m}$, which depends only on the unknown function m as:

$$\tilde{m}(\tau) = m - \frac{2n-2}{n}\, \tau\, m' \tag{A10}$$

the boundary conditions are obtained from (15) to (18) for constant power P_L and uniform heat flux $J = \frac{P_L}{4\pi}$: at $\lambda = At^n\, m(\tau)$

$$V_d = m(\tau)\,(1-f) \tag{A11}$$

$$R_d = 1/f \tag{A12}$$

$$P_d = \frac{1}{\gamma}\,\tau + [\tilde{m}(\tau)]^2\,(1-f) \tag{A13}$$

with

$$f = \frac{1}{\gamma+1}\left[\gamma + \frac{\tau}{\tilde{m}^2} - \sqrt{\left(1 - \frac{\tau}{\tilde{m}^2}\right)^2 - \frac{\gamma+1}{2\pi a n^3}\,\frac{1}{m^2 \tilde{m}^3}}\,\right] \tag{A14}$$

A.2. Small perturbation Assumption

A small perturbation scheme from the self-similar spherical solution (zeroth order) is proposed by considering τ as the small parameter. This type of approach can be regarded as a late time solution for which the velocity of the self-similar wave (which goes as $t^{-2/5}$) has decreased sufficiently so that the undisturbed sound speed is no longer negligible with respect to it and the effect of non-infinite Mach number $1/\tau$ has to be taken into account.

The function $m(\tau)$ is expanded in a MacLaurin series, the first term of which is only retained

$$\lambda_d = m(\tau) = 1 + \lambda_2 \tau \tag{A15}$$

The density ratio f is expanded in powers of τ making use of the fact that the radical in (A 14) is non-zero for the overdriven zeroth order wave. One arrives at:

$$f = f^{(o)} + \tau\,(K + K_2\,\lambda_2) \tag{A16}$$

where $f^{(o)}$ and K are defined as in Chapter II (equations (49) and (50)) and

K_2 is another constant solely dependent on the zeroth order wave speed as:

$$K_2 = -\frac{6-n}{n} \frac{1}{4\pi\, an^3} \left(1 - \frac{\gamma+1}{2\pi an^3}\right)^{-1/2} \tag{A17}$$

The boundary conditions on velocity, density and pressure are then developed in powers of τ . This naturally suggests expansions of the flow variables over the whole field of λ:

$$V(\lambda,\tau) = V^{(o)}(\lambda) + \tau\, V^{(1)}(\lambda) \tag{A18}$$

$$R(\lambda,\tau) = R^{(o)}(\lambda) + \tau\, R^{(1)}(\lambda) \tag{A19}$$

$$P(\lambda,\tau) = P^{(o)}(\lambda) + \tau\, P^{(1)}(\lambda) \tag{A20}$$

Expansions (A 18) to (A 20) are substituted into the flow equations (A 5) to (A 7) and the boundary conditions (A 11) to (A 14). Collecting the terms of 0 (1) yields the zeroth-order problem which has already been solved in Chapter II § 2. The 0 (τ) terms give rise to a system of three ordinary differential equations with variable coefficients for $V^{(1)}$, $R^{(1)}$ and $P^{(1)}$. They read with' $\frac{d}{d\lambda}$:

$$R^{(o)}V^{(1)}{}' + (R^{(o)}{}' + 2\frac{R^{(o)}}{\lambda})\, V^{(1)} + (V^{(o)} - \lambda)\, R^{(1)}{}' + (V^{(o)}{}' + 2\frac{V^{(o)}}{\lambda} - 2\frac{n-1}{n})\, R^{(1)} = 0 \tag{A21}$$

$$(V^{(o)} - \lambda)\, V^{(1)}{}' + (V^{(o)}{}' - \frac{n-1}{n})\, V^{(1)} - \frac{P^{(o)}{}'}{R^{(o)2}}\, R^{(1)} + \frac{1}{R^{(o)}}\, P^{(1)}{}' = 0 \tag{A22}$$

$$\gamma P^{(o)}V^{(1)}{}' + (P^{(o)}{}' + 2\gamma\frac{P^{(o)}}{\lambda})\, V^{(1)} + (V^{(o)} - \lambda)\, P^{(1)}{}' + (\gamma\, V^{(o)}{}' + 2\gamma\frac{V^{(o)}}{\lambda})\, P^{(1)} = 0 \tag{A23}$$

The 0 (τ) terms are collected in the boundary conditions which are further transferred from the unknown location $\lambda_d = 1 + \lambda_2\, \tau$ to the known location $\lambda = 1$ by a Taylor expansion. One obtains:

$$V^{(1)}(1) = -K + [(1-f^{(o)})\frac{2-n}{n} - K_2 - V^{(o)}{}'(1)]\, \lambda_2 \tag{A24}$$

$$R^{(1)}(1) = -\frac{K}{f^{(o)2}} - [\frac{K_2}{f^{(o)2}} + R^{(o)}{}'(1)]\, \lambda_2 \tag{A25}$$

$$P^{(1)}(1) = \frac{1}{\gamma} - K + [(1-f^{(o)})\frac{2-n}{n}2 - K_2 - P^{(o)}{}'(1)]\, \lambda_2 \tag{A26}$$

A 2.1. Expansions near $\lambda = 0$

The system of differential equations (A 21) to (A 23) is to be integrated

subject to boundary conditions (A 24) to (A 26). By elimination of the unknown constant λ_2, these reduce down to only two, rendering impractical an inward numerical integration from the boundary $\lambda = 1$. Instead the three linearly independent solutions are sought in the neighborhood of the origin. One is to be discarded as corresponding to a physically inacceptable singularity. A numerical integration is conducted outwards with the two remaining solutions so as to satisfy boundary conditions at $\lambda = 1$.

Keeping only the leading term in the expansions of the coefficients of equations (A 21) to (A 23), the flow equations near the origin read:

$$b_1 \lambda^{\alpha-2} V^{(1)\prime} + b_1 \alpha \lambda^{\alpha-3} V^{(1)} + (a_o - 1)\, \lambda\, R^{(1)\prime} + \left(3 a_o - 2\,\frac{n-1}{n}\right) R^{(1)} = 0 \tag{A27}$$

$$(a_o - 1)\, \lambda\, V^{(1)\prime} + \left(a_o - \frac{n-1}{n}\right) V^{(1)} - \frac{c_1^{\alpha}}{b_1^{2}}\, \lambda^{-\alpha+3} R^{(1)} + \frac{1}{b_1}\, \lambda^{-\alpha+2} P_1^{(1)\prime} = 0 \tag{A28}$$

$$\gamma c_o\, V^{(1)\prime} + 2\, \gamma c_o\, \frac{V^{(1)}}{\lambda} + (a_o - 1)\, \lambda\, P^{(1)\prime} + 3\gamma\, a_o\, P^{(1)} = 0 \tag{A29}$$

Note that for $P^{(1)}$ behaving like a power of λ the last two terms of equation (A 29) are of 0 (λ^{α}) compared to the last term of (A 28). They may thus be dropped to leading order. Three linearly independent solutions are sought, each of the form:

$$V^{(1)} = A_1\, \lambda^{x} \tag{A30}$$

$$R^{(1)} = A_2 \lambda^{x + \alpha - 3} \tag{A31}$$

$$P^{(1)} = A_3 \lambda^{x + \alpha - 1} \tag{A32}$$

Substituting these into (A 27) to (A 29) gives, after cancellation of all λ dependence, a system of three linear homogeneous algebraic equations for A_1, A_2, A_3. x is solution of the indicial equation obtained by setting the determinant of this system equal to zero:

$$\begin{vmatrix} b_1 (x + \alpha) & (a_o - 1)(x-1) - 2\frac{n-1}{n} & 0 \\ (a_o - 1) & x + a_o - \frac{n-1}{n} & a_o (a_o - \frac{1}{n}) \quad x + \alpha - 1 \\ x + 2 & 0 & 0 \end{vmatrix} = 0 \quad \text{(A33)}$$

The three roots are immediately found:

$$x_1 = -2 \; ; \; x_2 = -(\alpha - 1) \; ; \; x_3 = 1 + 2\frac{n-1}{n}\frac{1}{a_o} \quad \text{(A34)}$$

The first root $x_1 = -2$ yields an infinite velocity at the origin as well as an infinite density. It can be seen that to order τ^2 the origin is a point source of mass and energy; this feature is not acceptable and the solution corresponding to the root $x_1 = -2$ is rejected by setting the A's equal to zero. The system of algebraic equations is solved for the A's corresponding to roots two and three. For x_2, one obtains

$$A_1 = 0 \; ; \quad A_2 = 0 \; ; \; A_3 = \text{arbitrary} \quad \text{(A35)}$$

and for x_3, the solution is:

$$A_1 = 0 \; ; \; A_2 = \text{arbitrary} \; ; \; A_3 = -\frac{a_o (a_o - \frac{1}{n})}{x_3 + \alpha - 1} A_2 \quad \text{(A36)}$$

Note that in both cases none of the physical quantities blow up at the origin. In order to increase the accuracy of the numerical solution, the first non-zero term of the expansions is sought. To that effect, the first two terms in the expansions of the coefficients of equations (A 21) to (A 23) are retained and it is easily seen that the next order terms of $V^{(1)}$ and $R^{(1)}$ are respectively $\lambda^{x + \alpha}$, $\lambda^{x + 2\alpha - 3}$. Denote the coefficients of these terms by B's. Remarking that for $\gamma = 5/3$ the numerical values of the retained roots are $x_2 = -\frac{23}{11}$ and $x_3 = \frac{31}{11}$ the expansions read:

$$V^{(1)} = B_1^1 \lambda + B_1^2 \lambda^{65/11} \quad \text{(A37)}$$

$$R^{(1)} = B_2^1 \lambda^{12/11} + A_2^2 \lambda^{32/11} \quad \text{(A38)}$$

$$P^{(1)} = A_3^1 + A_3^2 \lambda^{54/11} \quad \text{(A39)}$$

where superscript 1 refers to the root x_2 and superscript 2 refers to the root x_3. It is interesting to remark that the solution corresponding to the root x_2 has exactly the same type of singularity as the zeroth order self-similar solution, namely linear velocity in λ and constant pressure; it is

noted however that the coefficients are different. Choosing B_1^1 and B_1^2 as the arbitrary constants the four constants B_2^1, A_2^2, A_3^1 and A_3^2 are solution of an homogeneous algebraic third order system; for $\gamma = 5/3$ and using equations (88) to (90) one obtains:

$$B_2^1 = - \frac{135}{44} b_1 B_1^1 \tag{A40}$$

$$A_3^1 = - \frac{15}{4} c_o B_1^1 \tag{A41}$$

and

$$A_2^2 = \frac{2025 \times 2175}{154 \times 374} c_o B_1^2 \tag{A42}$$

$$A_3^2 = \frac{2175}{374} c_o B_1^2 \tag{A43}$$

A 2.2. Numerical Integration and Results

The system of six ordinary first order differential equations formed by the zeroth order system plus equations (A 21) to (A 23) is integrated starting from the origin with expansions (88) to (90) and (A 37) to (A 39). A fourth order Runge-Kutta scheme is used. The boundary conditions are obtained from equations (A 24) to (A 26) by elimination of the unknown constant λ_2:

$$\frac{V^{(1)}(1) - X_1}{X_2} = \frac{R^{(1)}(1) - X_3}{X_4} = \frac{P^{(1)}(1) - X_5}{X_6} \tag{A44}$$

in which the X's are known constants:

$$X_1 = - K \; ; \; X_2 = (1-f^{(o)}) \frac{2-n}{n} - K_2 - V^{(o)'}(1) \tag{A45}$$

$$X_3 = - \frac{K}{f^{(o)2}} \; ; \; X_4 = - \frac{K_2}{f^{(o)2}} - R^{(o)'}(1) \tag{A46}$$

$$X_5 = \frac{1}{\gamma} - K \; ; \; X_6 = (1-f^{(o)}) \, 2 \frac{2-n}{n} - K_2 - P^{(o)'}(1) \tag{A47}$$

Use is made of the linear character of the system (A 21) to (A 23) to determine the constants B_1^1 and B_1^2. A first integration is carried out with $B_1^1 = 1$ and $B_1^2 = 0$, call that solution $V_1^{(1)}$, $R_1^{(1)}$, $P_1^{(1)}$; the numerical values of these quantities at the boundary $\lambda = 1$, of course, do not satisfy the boundary conditions. A second integration is made for $B_1^1 = 0$ and $B_1^2 = 1$, call that solution $V_2^{(1)}$, $R_2^{(1)}$, $P_2^{(1)}$. The full solution which must satisfy the boundary conditions is expressed as a linear combination of these

two specialized solutions i.e.:

$$V^{(1)} = V_1^{(1)} B_1^1 + V_2^{(1)} B_1^2 \tag{A48}$$

$$R^{(1)} = R_1^{(1)} B_1^1 + R_2^{(1)} B_1^2 \tag{A49}$$

$$P^{(1)} = P_1^{(1)} B_1^1 + P_2^{(1)} B_1^2 \tag{A50}$$

The constants B_1^1 and B_1^2 are solution of the second order algebraic system obtained by applying boundary conditions (A 44) on the full solution (A 48) to (A 50). It reads:

$$\left(\frac{V_1^{(1)}(1)}{X_2} - \frac{R_1^{(1)}(1)}{X_4}\right) B_1^1 + \left(\frac{V_2^{(1)}(1)}{X_2} - \frac{R_2^{(1)}(1)}{X_4}\right) B_1^2 = \frac{X_1}{X_2} - \frac{X_3}{X_4} \tag{A51}$$

$$\left(\frac{V_1^{(1)}(1)}{X_2} - \frac{P_1^{(1)}(1)}{X_6}\right) B_1^1 + \left(\frac{V_2^{(1)}(1)}{X_2} - \frac{P_2^{(1)}(1)}{X_6}\right) B_1^2 = \frac{X_1}{X_2} - \frac{X_5}{X_6} \tag{A52}$$

As a check the system was integrated once more using the so obtained values of B_1^1 and B_1^2 in expansions (A 37) to (A 39) and it was found that the boundary conditions were accurately satisfied.

The velocity, density and pressure perturbation profiles are plotted on Figure A and λ_2 is obtained

$$\lambda_2 = -0.1993 \tag{A53}$$

A 2.3. Discussion and Conclusions

The numerical value of λ_2 is negative indicating an inward displacement of the boundary of the spark as well as a weakening of the wave characterized by a slower front velocity. This fact is also reflected in the perturbations of the physical quantities just behind the front. It should be noted that this applies at the actual front $\lambda = 1 - 0.1993\,\tau$ and not at the fictitious point $\lambda = 1$ (which is not even inside the spark) where boundary conditions are applied in the analysis. The value of a perturbation physical variable $F^{(1)}$ at the front is easily obtained:

$$F_d^{(1)} = F^{(1)}(1) + F^{(o)'}(1) \cdot \lambda_2 \tag{A54}$$

The particle velocity is seen to be lowered behind the detonation front and so is the density as might be expected for a weakened wave. The pressure,

however, is higher showing that the contribution of the added external static pressure overrides the lowering of the dynamic pressure (see for example eq. (17)).

The perturbation velocity is negative over the whole range of λ and its profile remains remarkably linear up to $\lambda \approx 0.5$ which is not surprising in view of the expansion (A 37) the linear part of which is expected to dominate over the power law part with the high exponent 65/11. The perturbation density and pressure are positive and a pressure increase is present at the origin. Note that since the density goes to zero, the temperature remains infinite at the origin as it should because no diffusion mechanism has been provided in this perturbation scheme.

Comparing these results with Sakurai's [I, II] for constant energy blast waves, it seems apparent that a considerable simplification in the analysis and numerical solution has been gained by the adoption of the perturbation parameter τ, inverse of a fictitious Mach number, rather than the actual front Mach number. This is reflected in the fact that the unknown constant does not enter the differential equations but is only present in the boundary conditions, thereby avoiding the difficulty of having to deal with unbounded functions in the integration procedure.

A direct comparison of the physical quantities distribution with those of a blast wave presented by Sakurai would require expressing the dependent variables in terms of a new independent variable, say $x = \frac{r}{r_d}$, where r_d is the actual front. Noting that x is related to λ by $x = \lambda (1 - \tau \lambda_2)$ this could easily be done

$$F(x) = F^{(o)}(\lambda) + \tau [F^{(1)}(\lambda) - F^{(o)'}(\lambda) \lambda_2 \lambda] \qquad (A55)$$

Nevertheless, the trends can be qualitatively described without that transformation. The perturbation profiles for density and pressure are markedly less steep near the boundary than for a blast wave. This, of course, is connected with the remark made in Chapter II § 2 that a Newtonian layer is not possible when energy is deposited right behind the leading shock wave. The velocity profiles exhibit the same negative behavior throughout and the density profiles appear to have the same trend in both cases. The

difference seems more marked in the pressure profiles: at the center a decrease in pressure is obtained for blast waves rather than the increase present here and a diminution of the pressure gradient just behind the shock wave is reported by Sakurai; it is not so for constant power laser sparks.

The applicability of this perturbation solution including counter-pressure for laser sparks can be found in certain special cases. Parameter τ becomes significant when the sound speed in the undisturbed gas is high, for example if the gas is preheated. This physical situation has been actually realized in an experiment conducted by Ahmad and Key in 1969 [III]. Instead of focusing the laser beam in a cold gas they first created a primary laser detonation wave in helium at 8 atm, after a 2 μ sec delay they focused the beam of a second laser on the hot gas just behind the front of the primary spark (which by then had degenerated into an ordinary blast wave). A secondary spark was obtained which developed in the heated gas inside the blast wave.

Another application is related to the possibility of maintaining a laser spark, once initial breakdown has taken place, by using much smaller powers than those commonly used in experiments and hence creating much slower moving fronts. Raizer discussed that situation for air in 1968 [IV], the criterion being that the gas should remain sufficiently hot ($\sim 20{,}000^{\circ}$ K) to be able to absorb the laser photons on a short distance. Front velocities of the order of a few km/sec seem possible, thus making the inverse Mach number non-negligible with respect to one.

Bibliography

[I] A. Sakurai: "On the propagation and structure of the blast wave, I" J. Phys. Soc. Japan 8, 662 (1953)

[II] A. Sakurai: "On the propagation add structure of a blast wave, II" J. Phys. Soc. Japan 9, 256 (1954)

[III] N. Ahmad and M. H. Key: "Enhanced plasma heating in laser induced gas breakdown at the shock front of a blast wave" Appl. Phys. Letters 14, 243 (1969)

[IV] Yu. P. Raizer: "Possibility of igniting a traveling laser spark at beam intensities much below the breakdown threshhold" JETP Letters 7, 55 (1968)

APPENDIX B

SOME REMARKS ABOUT THE SECOND ORDER SOLUTION

B.1. Second Order Equations

Expansions (55) to (58) in powers of ε are extended to $0(\varepsilon^2)$. Collecting terms in ε^2 the equations for the second order perturbation quantities are:

$$R^{(o)}V^{(2)}_{\lambda} + (R^{(o)'} + 2\frac{R^{(o)}}{\lambda})V^{(2)} + \frac{1}{\lambda}R^{(o)}(W^{(2)}_{\theta} + \cot\theta\ W^{(2)}) + (V^{(o)} - \lambda)R^{(2)}_{\lambda} + (V^{(o)'} + 2\frac{V^{(o)}}{\lambda})R^{(2)} = -[V^{(1)}R^{(1)}_{\lambda} + R^{(1)}V^{(1)}_{\lambda} + \frac{1}{\lambda}W^{(1)}R^{(1)}_{\theta} + \frac{1}{\lambda}R^{(1)}(2V^{(1)} + W^{(1)}_{\theta} + \cot\theta\ W^{(1)})] \quad (B1)$$

$$(V^{(o)} - \lambda)V^{(2)}_{\lambda} + (V^{(o)'} + \frac{n-1}{n})V^{(2)} - \frac{P^{(o)'}}{R^{(o)2}}R^{(2)} + \frac{1}{R^{(o)}}P^{(2)}_{\lambda} = -[V^{(1)}V^{(1)}_{\lambda} + \frac{1}{\lambda}W^{(1)}V^{(1)}_{\theta} - \frac{1}{\lambda}W^{(1)2} - \frac{1}{R^{(o)2}}R^{(1)}P^{(1)}_{\lambda} + \frac{P^{(o)'}}{R^{(o)3}}R^{(1)2}] \quad (B2)$$

$$(V^{(o)} - \lambda)W^{(2)}_{\lambda} + (\frac{V^{(o)}}{\lambda} + \frac{n-1}{n})W^{(2)} + \frac{1}{R^{(o)2}}\frac{1}{\lambda}P^{(2)}_{\theta} = -[V^{(1)}W^{(1)}_{\lambda} + \frac{1}{\lambda}W^{(1)}W^{(1)}_{\theta} + \frac{1}{\lambda}V^{(1)}W^{(1)} - \frac{1}{R^{(o)2}}\frac{1}{\lambda}R^{(1)}P^{(1)}_{\theta}] \quad (B3)$$

$$\gamma P^{(o)}V^{(2)}_{\lambda} + (P^{(o)'} + 2\gamma\frac{P^{(o)}}{\lambda}V^{(2)} + \gamma\frac{P^{(o)}}{\lambda}(W^{(2)}_{\theta} + \cot\theta\ W^{(2)}) + (V^{(o)} - \lambda)P^{(2)}_{\lambda} + (\gamma V^{(o)'} + 2\gamma\frac{V^{(o)}}{\lambda} + 2\frac{n-1}{n})P^{(2)} = -[V^{(1)}P^{(1)}_{\lambda} + \gamma P^{(1)}V^{(1)}_{\lambda} + \frac{1}{\lambda}V^{(1)}P^{(1)}_{\theta} + \frac{1}{\lambda}\gamma P^{(1)}(2V^{(1)} + W^{(1)}_{\theta} + \cot\theta\ W^{(1)})] \quad (B4)$$

The solution of this fourth order linear system is sought as the sum of a complementary solution plus a particular solution. Since the left-hand sides of this system are identical to equations (62) to (65) the complementary solution can be treated in the same way as the first order solution (see Chapter II, Section 3). In particular its behavior near the origin is given by (124) to (127).

B.2. Particular Solution in the Neighborhood of $\lambda = 0$.

Consider the right-hand sides of (B1) to (B4). Their θ - dependence

involves products of Legendre polynomials. If N is the highest harmonic present in the first order solution, developing the product of two $N^{\underline{th}}$ order Legendre polynomials in series yields Legendre polynomials up to order 2 N. The particular solution is thus sought in the form:

$$V^{(2)} = \sum_{\ell=0}^{2N} P_\ell(\cos\theta)\, \bar{\bar{V}}_\ell(\lambda) \tag{B5}$$

$$W^{(2)} \sum_{\ell=0}^{2N} \frac{d}{d\theta} P_\ell(\cos\theta) \bar{\bar{W}}_\ell(\lambda) \tag{B6}$$

$$R^{(2)} = \sum_{\ell=0}^{2N} P_\ell(\cos\theta)\, \bar{\bar{R}}_\ell(\lambda) \tag{B7}$$

$$P^{(2)} = \sum_{\ell=0}^{2N} P_\ell(\cos\theta)\, \bar{\bar{P}}_\ell(\lambda) \tag{B8}$$

In order to find the leading term in the expansions of $\bar{\bar{V}}$ to $\bar{\bar{P}}$ near $\lambda = 0$, only the first term in the expansions of the coefficients is kept on the left-hand side and only the leading terms of the right-hand sides are retained.

Two cases are considered. First suppose that the terms D's are kept in expansions (124) to (127). Table 1 indicates that the strongest singularity m_k' corresponds to the highest harmonic. The leading term on the right-hand side of (B 2) is thus seen to be $\lambda^{2m_N'-1}$. The particular solution then has a λ - dependence:

$$\bar{\bar{V}}_{2N} \sim \lambda^{2m_N' - 1} \tag{B9}$$

$$\bar{\bar{W}}_{2N} \sim \lambda^{2m'_N - 1} \tag{B10}$$

$$\bar{\bar{R}}_{2N} \sim \lambda^{2m'_N - 1 + \alpha - 3} \tag{B11}$$

$$\bar{\bar{P}}_{2N} \sim \lambda^{2m'_N - 1 + \alpha - 1} \tag{B12}$$

Secondly, suppose that D's are set equal to zero. The strongest first order singularity is now given by the first harmonic k = 1. Hence the λ - dependence is given by (B9) to (B12) where m_N' is replaced by $m_{r_1} + im_{i_1}$

It may be noticed that it is physically more acceptable to have the strongest singularity at the origin corresponding to the most asymmetric perturbation i.e. the lowest harmonic rather than the opposite.

The complete second order particular solution has been calculated for the case: D's = 0 and the first order solution limited to its first harmonic. It comes out with $m_r = -0.6253$ and $m_i = 0.5500$:

$$V^{(2)} = \lambda^{2m_r - 1} [\cos^2\theta (X_1 \lambda^{2im_i} + X_1^* \lambda^{-2im_i} + Z_1) + \sin^2\theta (X_1' \lambda^{2im_i} + X_1'^* \lambda^{-2im_i} + Z_1')] \quad \text{(B13)}$$

$$W^{(2)} = \lambda^{2m_r - 1} \sin\theta \cos\theta (X_2 \lambda^{2im_i} + X_2^* \lambda^{-2im_i} + Z_2) \quad \text{(B14)}$$

$$R^{(2)} = \lambda^{2m_r + \alpha - 4} [\cos^2\theta (X_3 \lambda^{2im_i} + X_3^* \lambda^{-2im_i} + Z_3) + \sin^2\theta (X_3' \lambda^{2im_i} + X_3'^* \lambda^{-2im_i} + Z_3')] \quad \text{(B15)}$$

$$P^{(2)} = \lambda^{2m_r + \alpha - 2} [\cos^2\theta (X_4 \lambda^{2im_i} + X_4^* \lambda^{-2im_i} + Z_4) + \sin^2\theta (X_4' \lambda^{2im_i} + X_4'^* \lambda^{-2im_i} + Z_4')] \quad \text{(B16)}$$

The constants X's and Z's are solution of a system of fourteen linear algebraic equations. The numerical values are:

$X_1 = (0.12+i1.88)10^{-3}$ $Z_1 = 1.77\ 10^{-3}$ $X_1' = (-0.06 - i0.94)\ 10^{-3}$ $Z_1' = -0.89\ 10^{-3}$

$X_2 = (1.05+i0.17)10^{-3}$ $Z_2 = 0.22\ 10^{-3}$ $X_3' = (-0.91+i0.39)\ 10^{-3}$ $Z_3' = 2.09\ 10^{-3}$

$X_3 = (0.50-i1.52)10^{-3}$ $Z_3 = -2.34\ 10^{-3}$ $X_4' = (0.12-i0.56)10^{-3}$ $Z_4' = -5.78\ 10^{-3}$

$X_4 = (0.80+i0.04)10^{-3}$ $Z_4 = -4.07\ 10^{-3}$

APPENDIX C

SECOND FORM OF THE FLOW EQUATIONS

The complete non-linear self-similar flow equations (32) to (35) are transformed by defining:

$$R = \frac{1}{S} \tag{C1}$$

$$V = a_o \lambda + v \tag{C2}$$

$$W = w \tag{C3}$$

$$S = \frac{1}{\lambda^{\alpha-1}} \left(\frac{1}{b_1} \lambda + s \right) \tag{C4}$$

$$P = c_o + \lambda^{\alpha-1} (c_1 \lambda + p^*) \tag{C5}$$

With the definition:

$$\Phi \equiv \lambda v_\lambda + 2v + w_\theta + \cot\theta \, w \tag{C6}$$

the system reads:

$$-(\alpha-2)\frac{1}{b_1} v - \frac{1}{b_1} \Phi + (a_o-1)(\lambda s_\lambda - s) + v s_\lambda - (\alpha-1)\frac{vs}{\lambda} + \frac{w s_\theta}{\lambda} - \frac{1}{\lambda} s \Phi = 0 \tag{C7}$$

$$(a_o-1)\lambda v_\lambda + \left(a_o + \frac{n-1}{n}\right) v + \alpha c_1 s + \frac{1}{b_1}[\lambda p^*_\lambda + (\alpha-1) p^*] + v v_\lambda + \frac{1}{\lambda} w v_\theta - \frac{w^2}{\lambda} + \frac{1}{\lambda} s [\lambda p^*_\lambda + (\alpha-1) p^*] = 0 \tag{C8}$$

$$(a_o-1)\lambda w_\lambda + \left(a_o + \frac{n-1}{n}\right) w + \frac{1}{b_1} p^*_\theta + v w_\lambda + \frac{1}{\lambda} w w_\theta + \frac{1}{\lambda} v w + \frac{1}{\lambda} s p^*_\theta = 0 \tag{C9}$$

$$(a_o-1)\alpha c_1 \lambda + \gamma c_o \frac{1}{\lambda^\alpha} \Phi + \alpha c_1 v + \gamma c_1 \Phi + (a_o-1)[\lambda p^*_\lambda + (\alpha-1) p^*] + v p^*_\lambda + (\alpha-1)\frac{p^* v}{\lambda} + \frac{w p^*_\theta}{\lambda} + \gamma \frac{1}{\lambda} p^* \Phi = 0 \tag{C10}$$

In the neighborhood of the origin, equations (C 7) to (C 10) are linearized as follows:

$$\lambda v_\lambda + 2v + w_\theta + \cot\theta w = 0 \tag{C11}$$

$$-(\alpha-2)\frac{1}{b_1} v + (a_o-1)\lambda s_\lambda - (a_o-1) s = 0 \tag{C12}$$

$$(a_o-1)\lambda v_\lambda + \left(a_o + \frac{n-1}{n}\right) v + \alpha c_1 s + \frac{1}{b_1}[\lambda p^*_\lambda + (\alpha-1) p^*] = 0 \tag{C13}$$

$$(a_o-1)\lambda w_\lambda + \left(\frac{n-1}{n} + a_o\right) w + \frac{1}{b_1} p^*_\theta = 0 \tag{C14}$$

As an example the first harmonic of the solution is sought in the form:

$$v = A_1 \lambda^m \cos\theta \tag{C15}$$

$$w = -A_2 \lambda^m \sin\theta \tag{C16}$$

$$s = A_3 \lambda^m \cos\theta \tag{C17}$$

$$p^* = A_4 \lambda^m \cos\theta \tag{C18}$$

The indicial equation is obtained. It is identical to equation (120) for $k = 1$. In conclusion linearizing system (C7) to C 10) specialized to small λ is exactly equivalent to developing system (32) to (35) in powers of ε and specializing to small λ.

Power distribution: $g(\theta) = \frac{1}{4\pi} [1 + \epsilon P_k(\cos\theta)]$

Wave front: $h(\theta) = 1 + \epsilon P_k(\cos\theta) X_k$

Radial velocity behind the wave: $V_d = 1 - f^{(o)} + \epsilon P_k(\cos\theta) C_{Vk}$

Tangential velocity behind the wave: $W_d = -\epsilon \frac{dP_k(\cos\theta)}{d\theta} C_{Wk}$

Density behind the wave: $R_d = \frac{1}{f^{(o)}} + \epsilon P_k(\cos\theta) C_{Rk}$

Pressure behind the wave: $P_d = 1 - f^{(o)} + \epsilon P_k(\cos\theta) C_{Pk}$

k	$P_k(x)$	X_k	C_{Vk}	C_{Wk}	C_{Rk}	C_{Pk}
1	x	.1903	.0491	.0875	-.1297	.1366
2	$\frac{3x^2-1}{2}$	.1754	-.0164	.0806	-.3325	.0642
3	$\frac{5x^3-3X}{2}$	.1589	-.0891	.0730	-.557	-.0161
4	$\frac{34x^4-30x^2+3}{8}$	.1429	-.1586	.0656	-.773	-.0939
5	$\frac{63x^5-70x^3+15x}{8}$	.1288	-.2217	.0591	-.965	-.1625

Note: $X \equiv \cos\theta$

$f^{(o)} = .54041 \quad 1-f^{(o)} = .45959 \quad \frac{1}{f^{(o)}} = 1.8504$

Table I: Spark Shape and Values of Velocities, Density and Pressure Behind the Wave Front

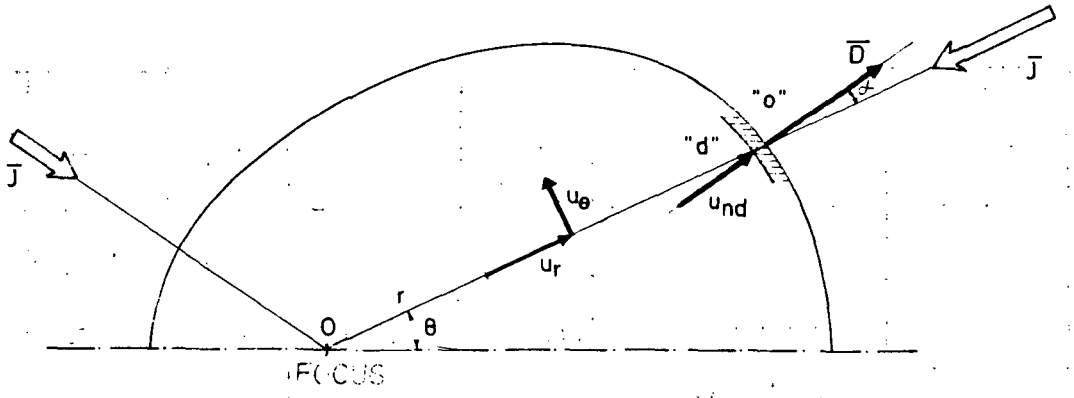

Figure 1. Geometrical arrangement of a laser induced spark.

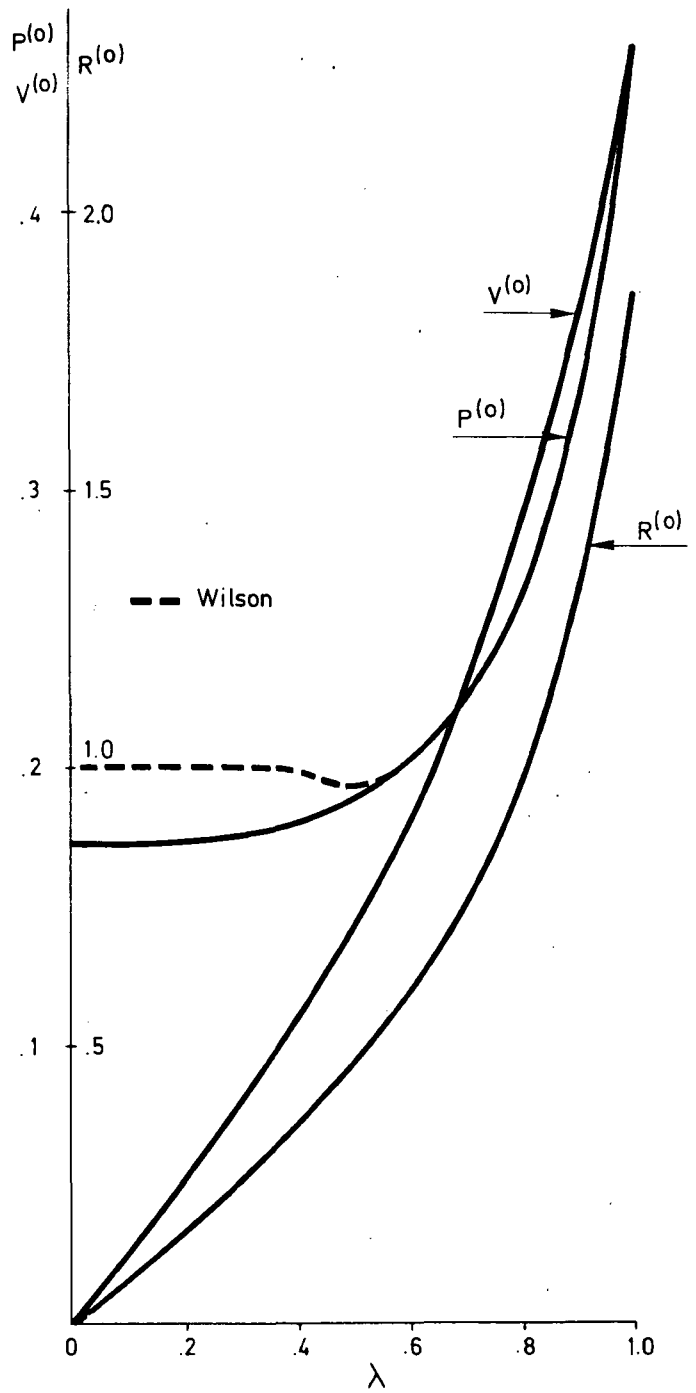

Figure 2. Velocity, density and pressure profiles of a spherically symmetric spark when $\gamma = 5/3$.

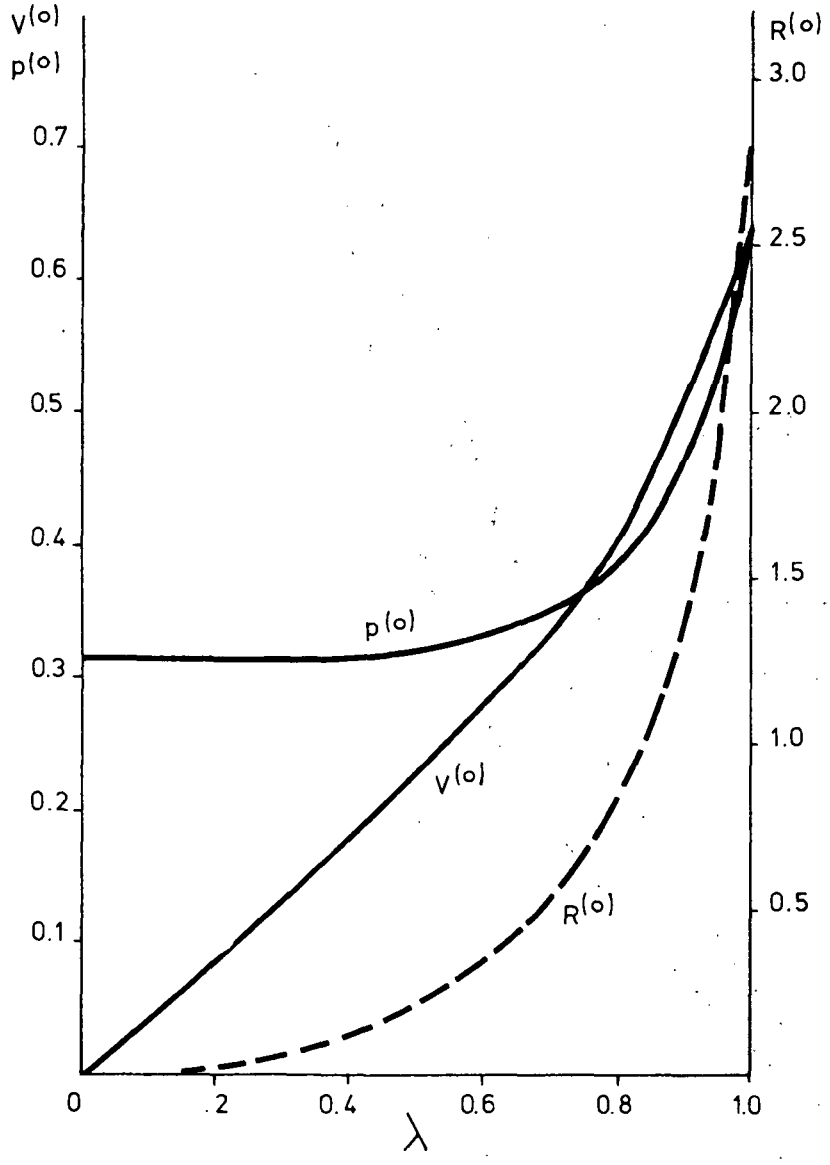

Figure 3. Velocity, density and pressure profiles of a spherically symmetric spark when $\gamma = 1$.

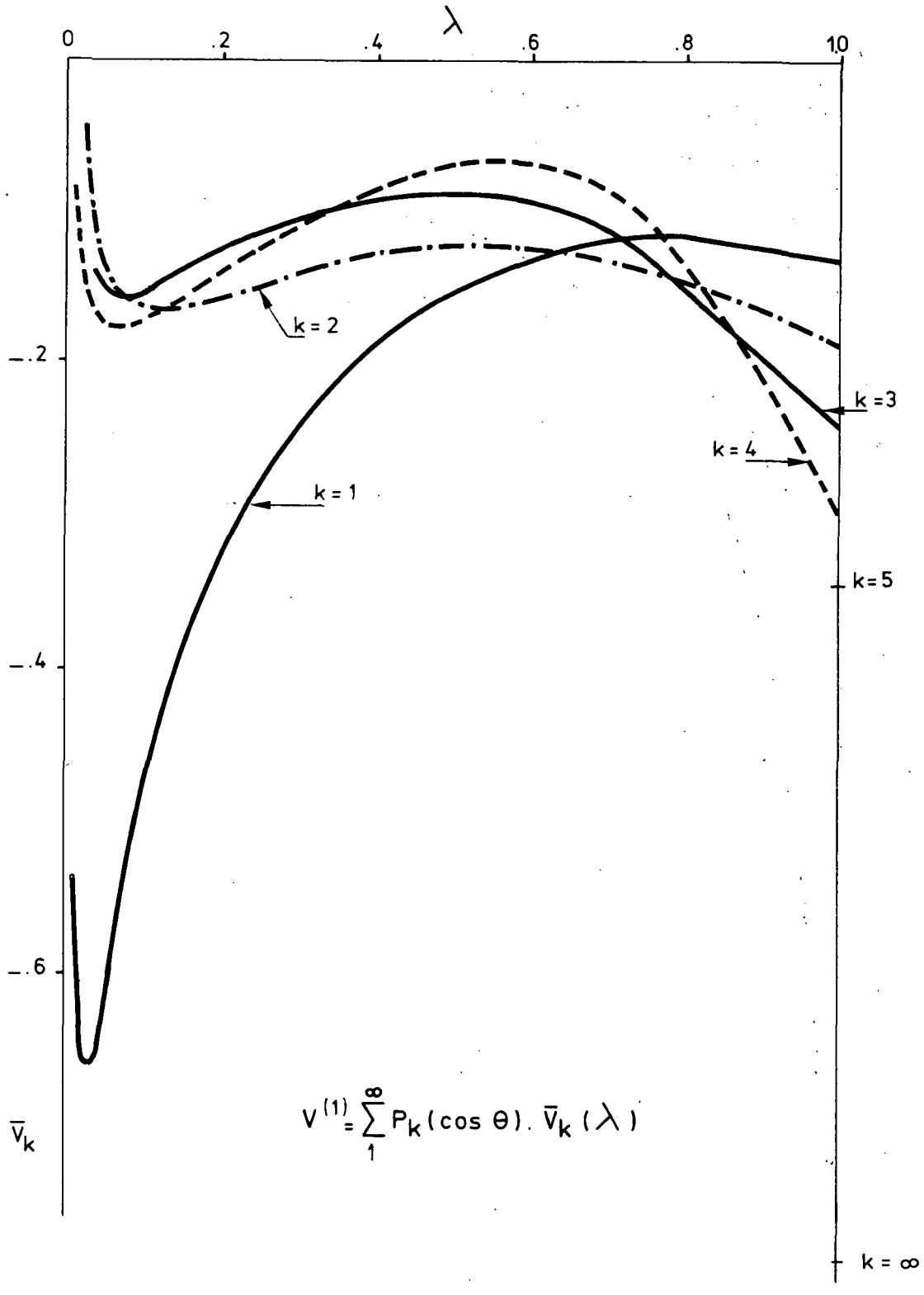

Figure 4. Radial velocity perturbation profiles for harmonics 1 to 4.

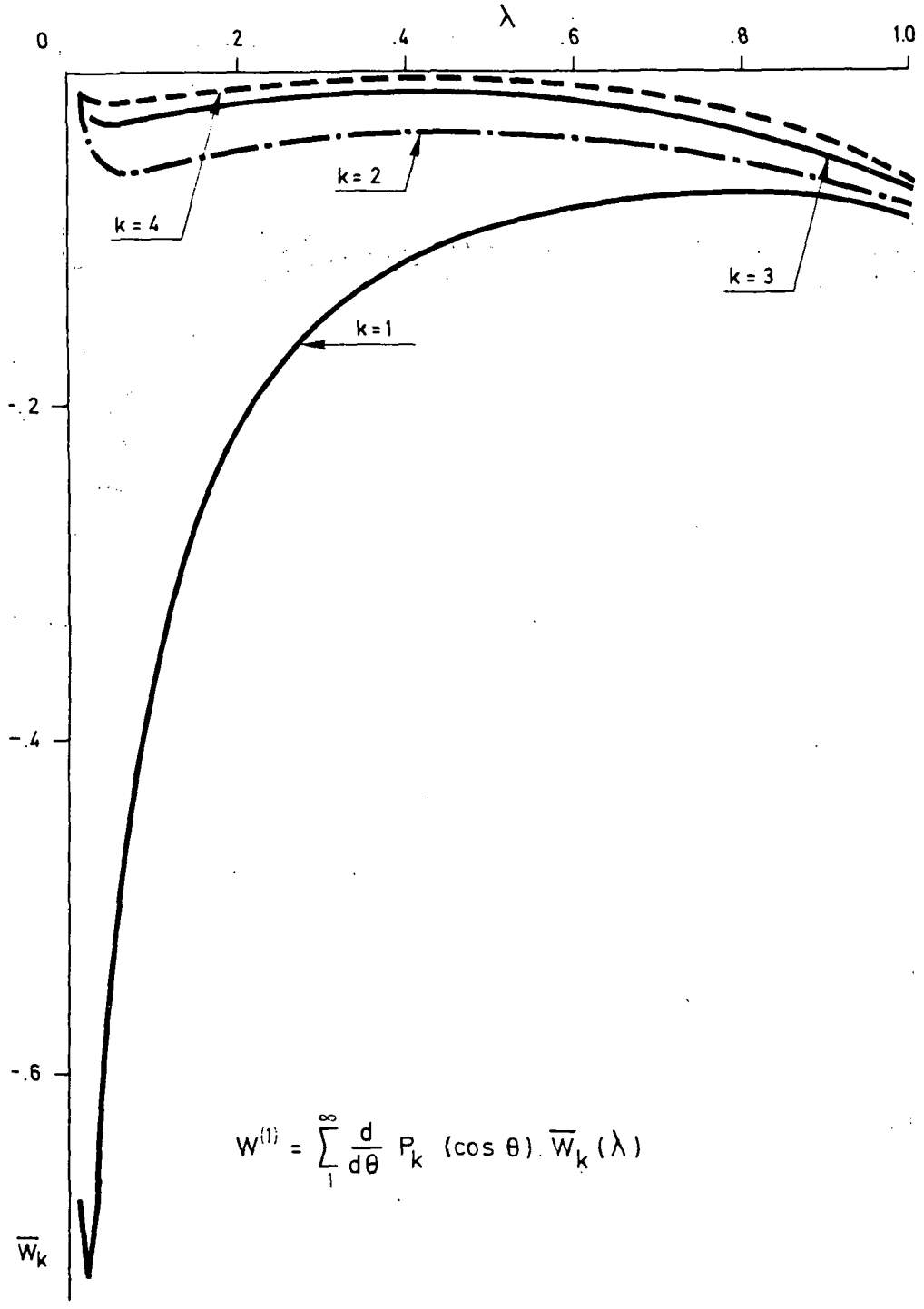

Figure 5. Tangential velocity profiles for harmonics 1 to 4.

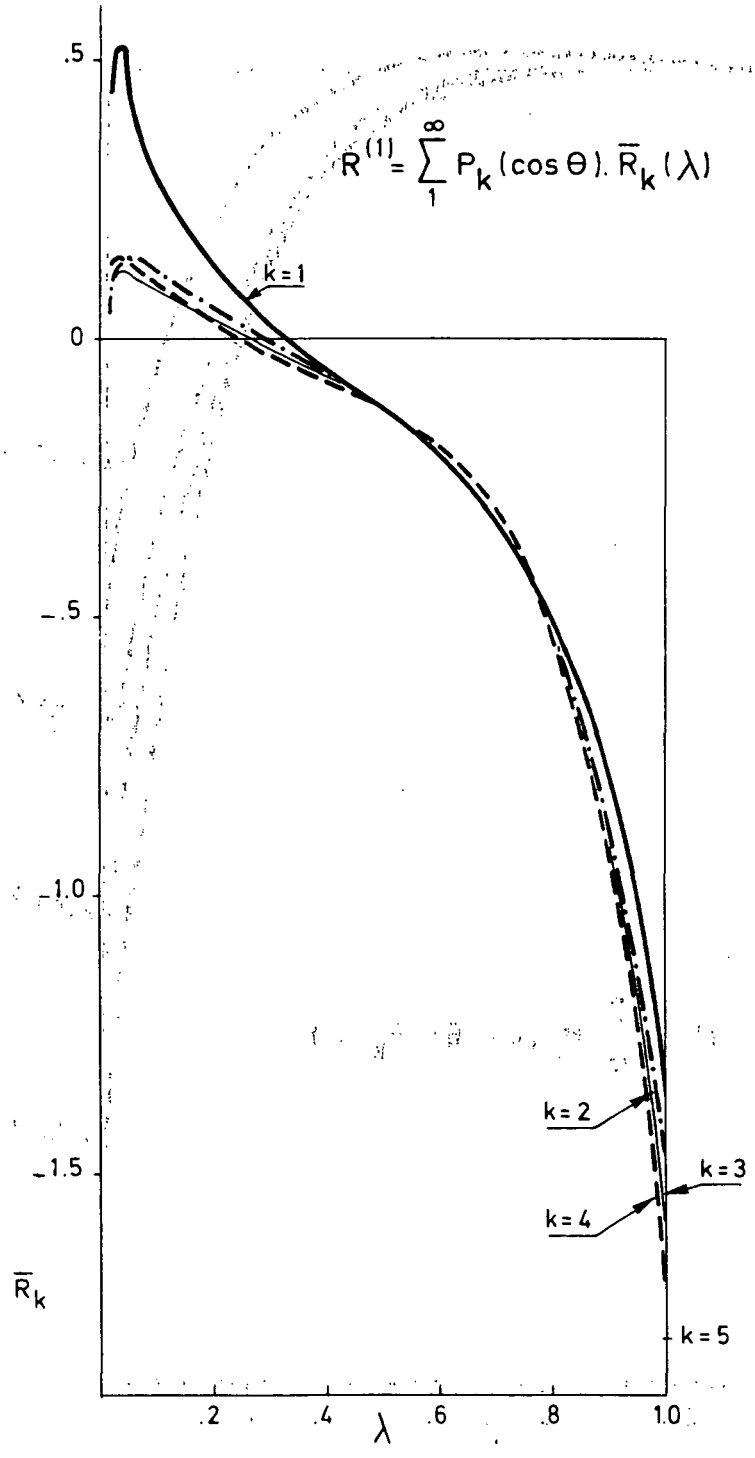

Figure 6. Density perturbation profiles for harmonics 1 to 4.

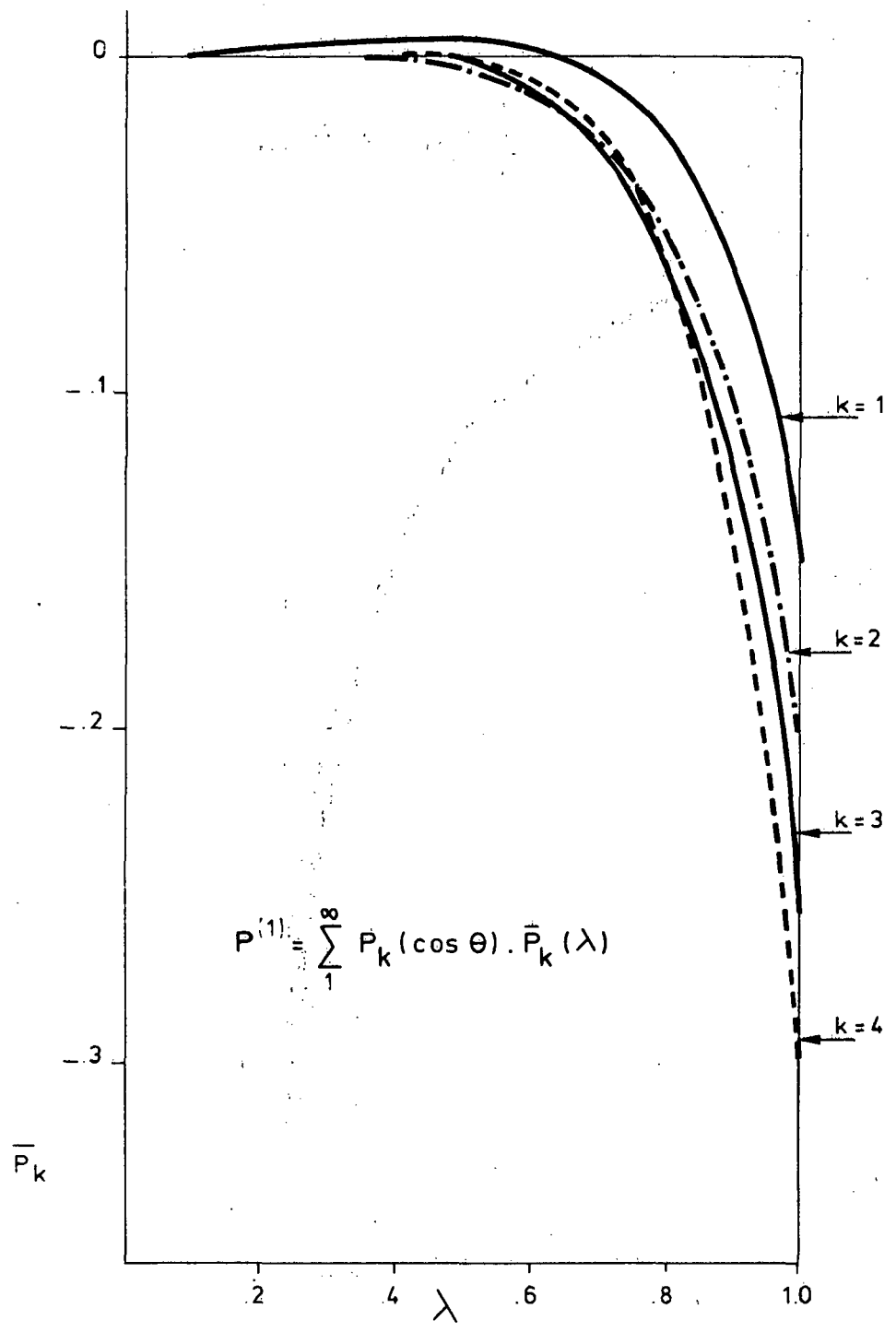

Figure 7. Pressure perturbation profiles for harmonics 1 to 4.

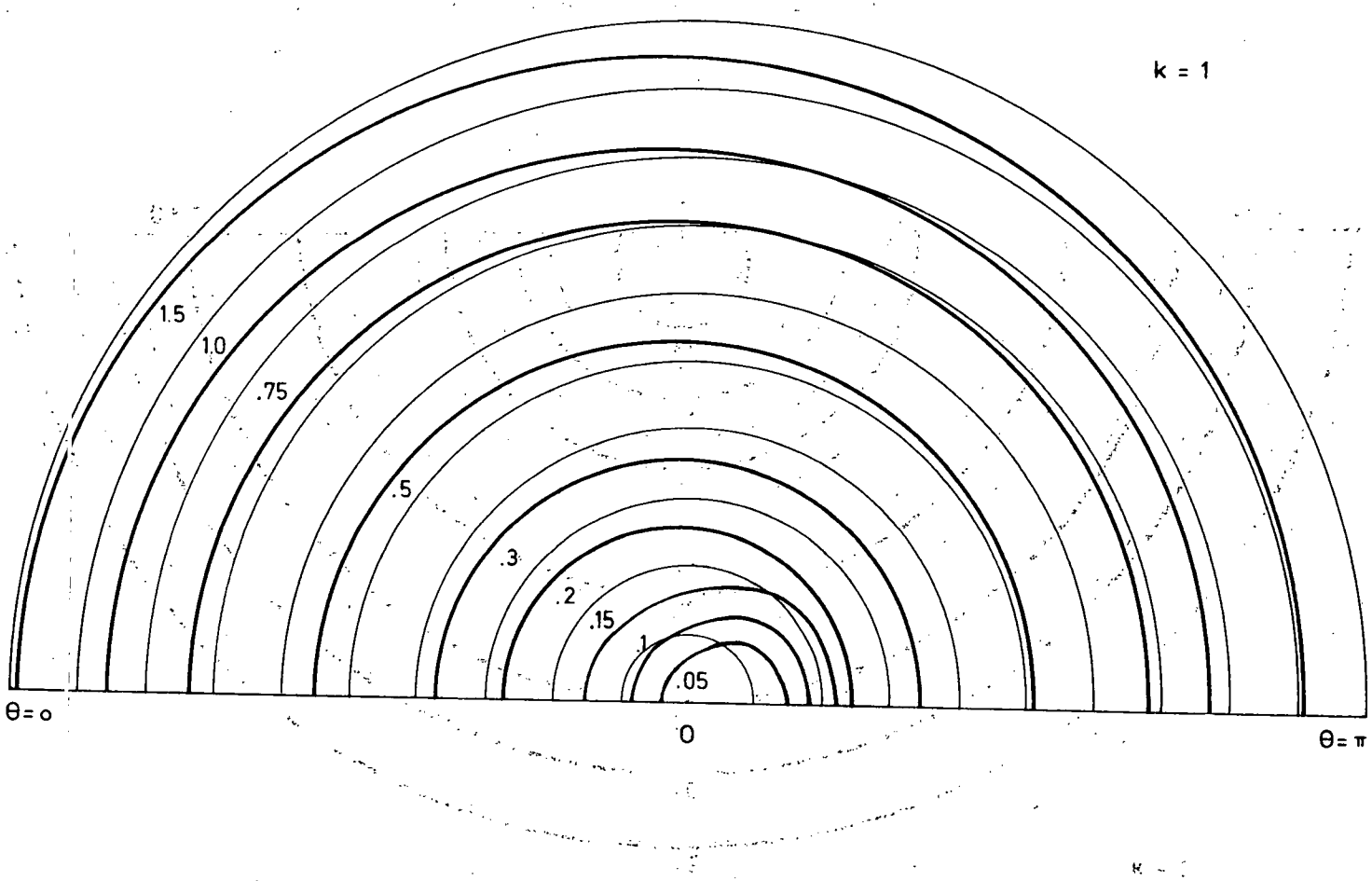

Figure 8. Density map for harmonic 1 when $\varepsilon = 0.2$.

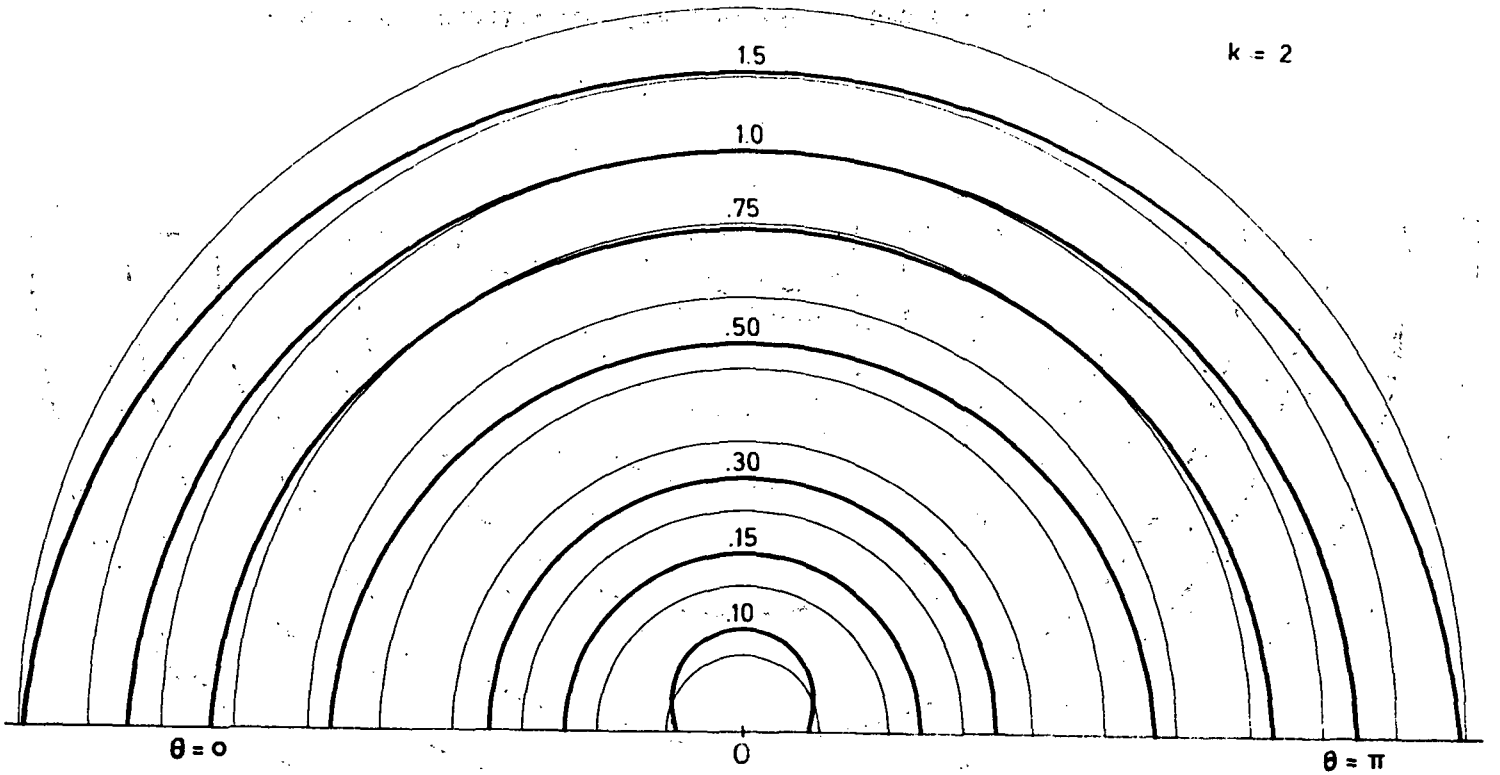

Figure 9. Density map for harmonic 2 when $\varepsilon = 0.2$.

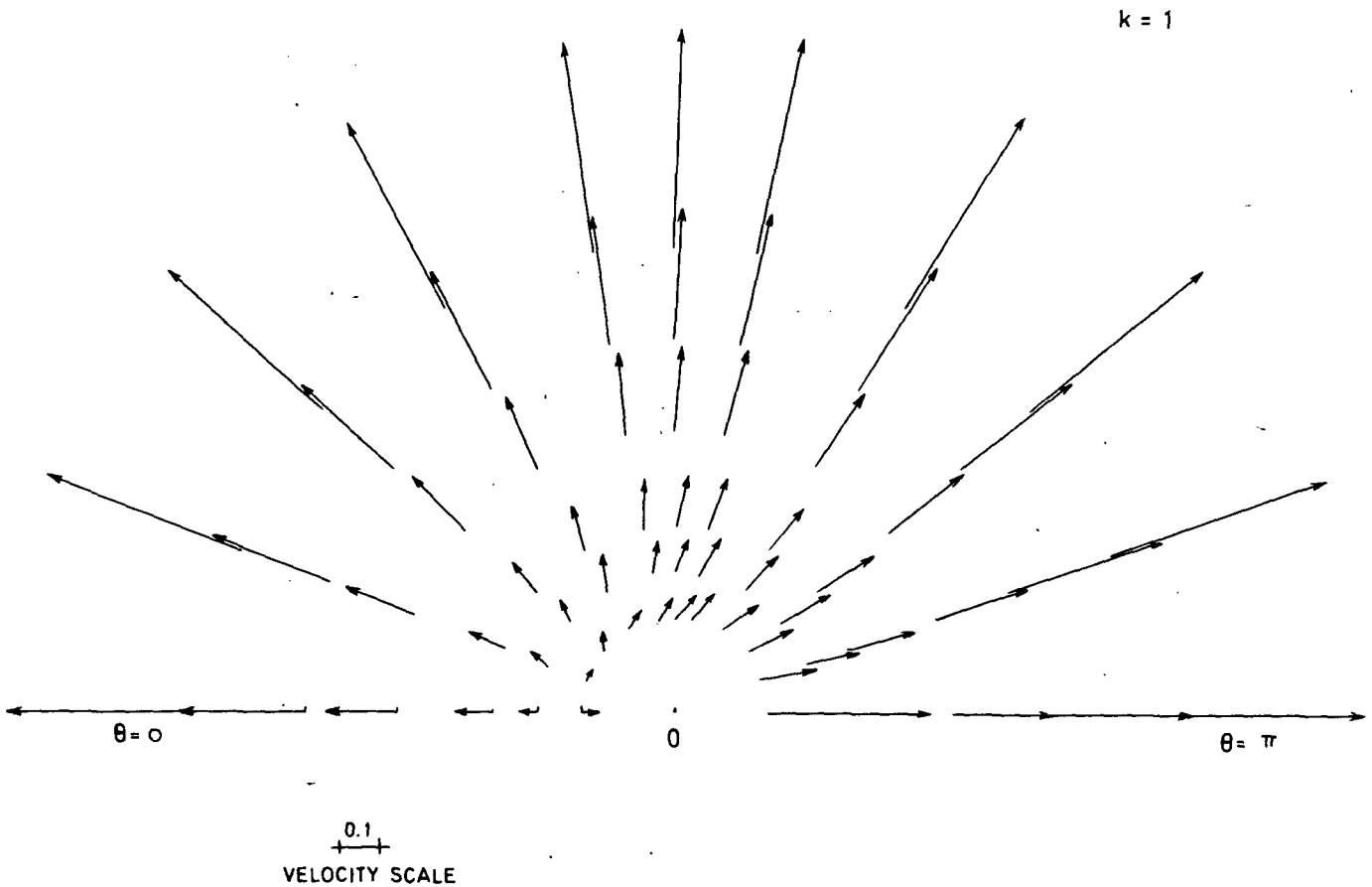

Figure 10. Velocity map for harmonic 1 when $\varepsilon = 0.2$.

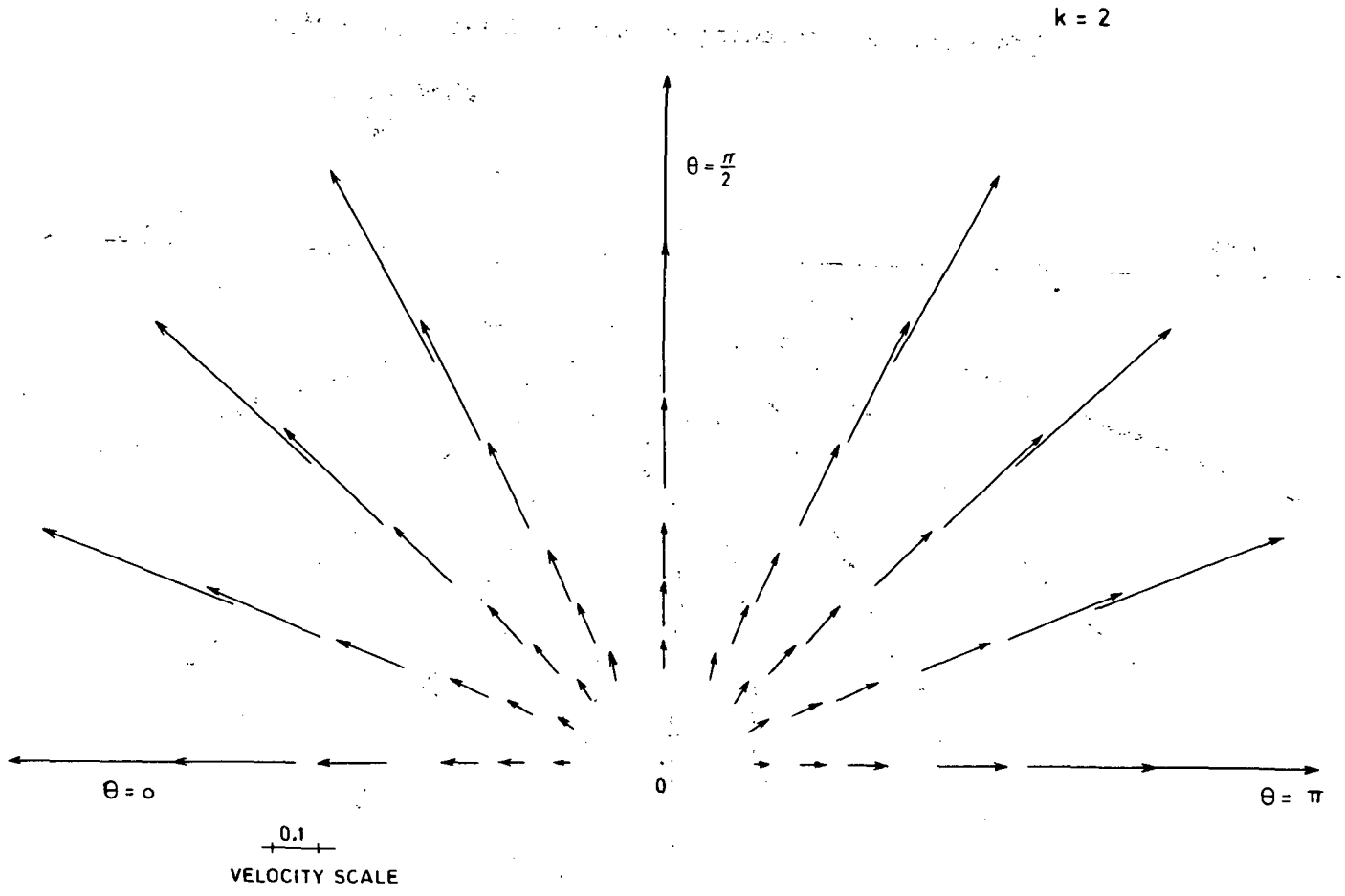

Figure 11. Velocity map for harmonic 2 when $\varepsilon = 0.2$.

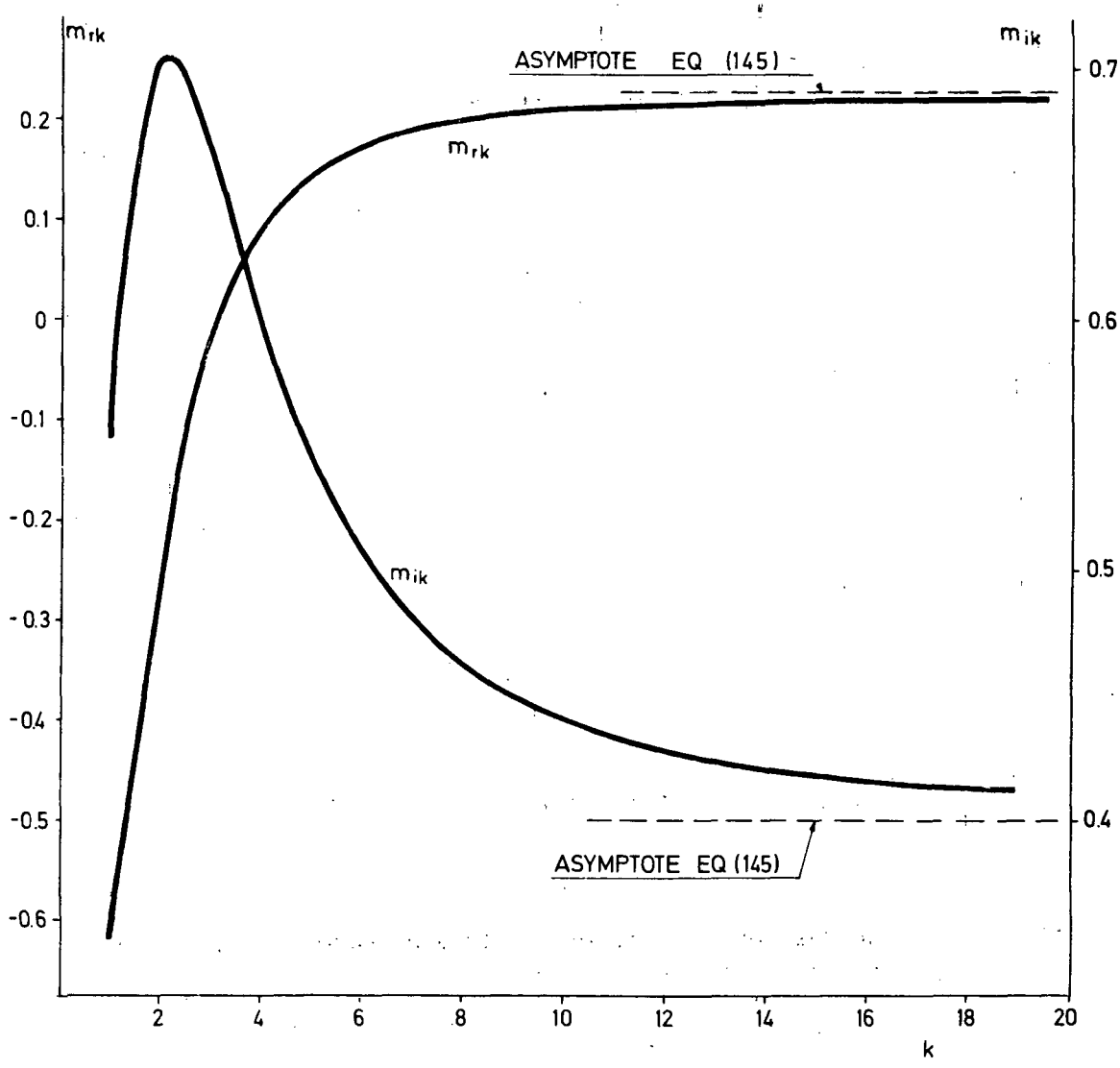

Figure 12. Complex conjugate roots of the characteristic equation near the focus as a function of the harmonic number k.

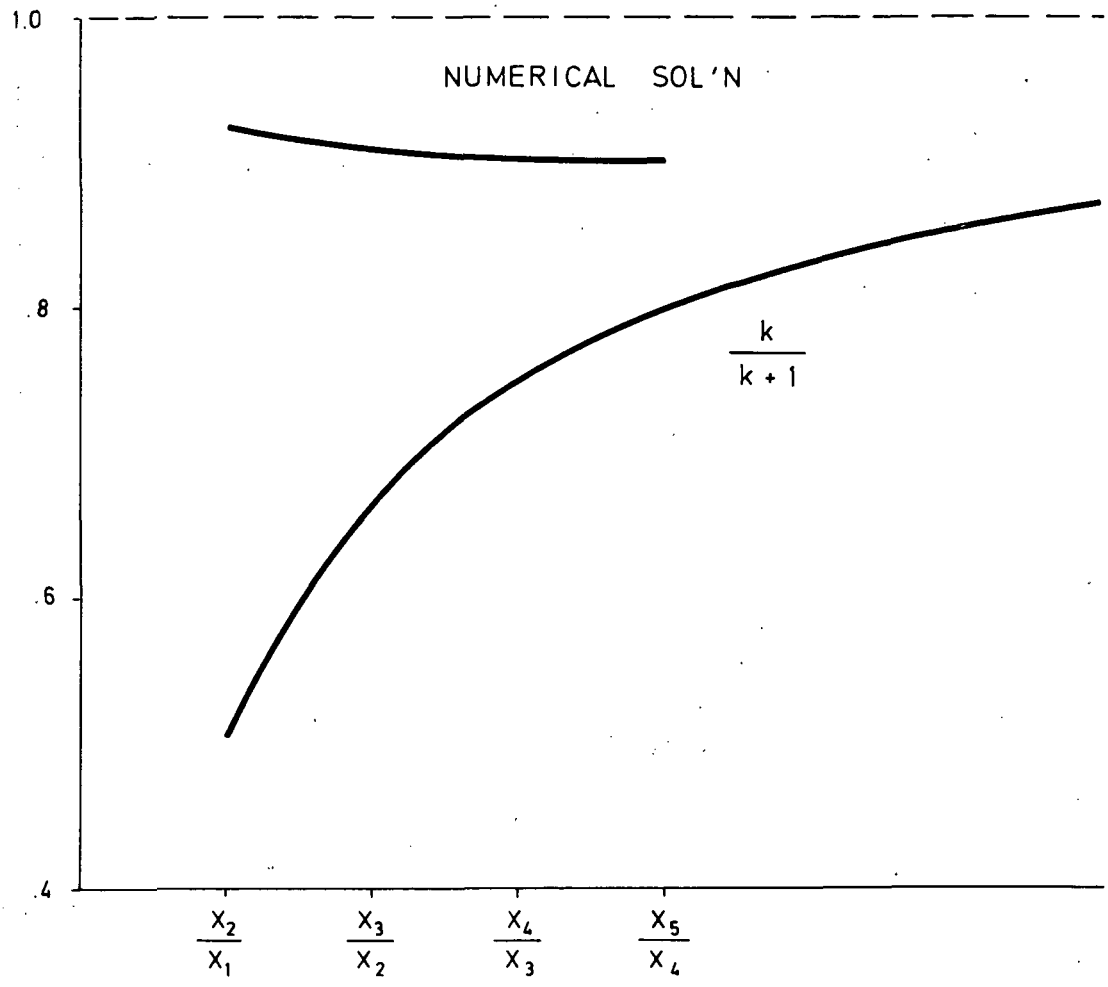

Figure 13. Comparison of numerical values of wave strength with predicted values, for large k.

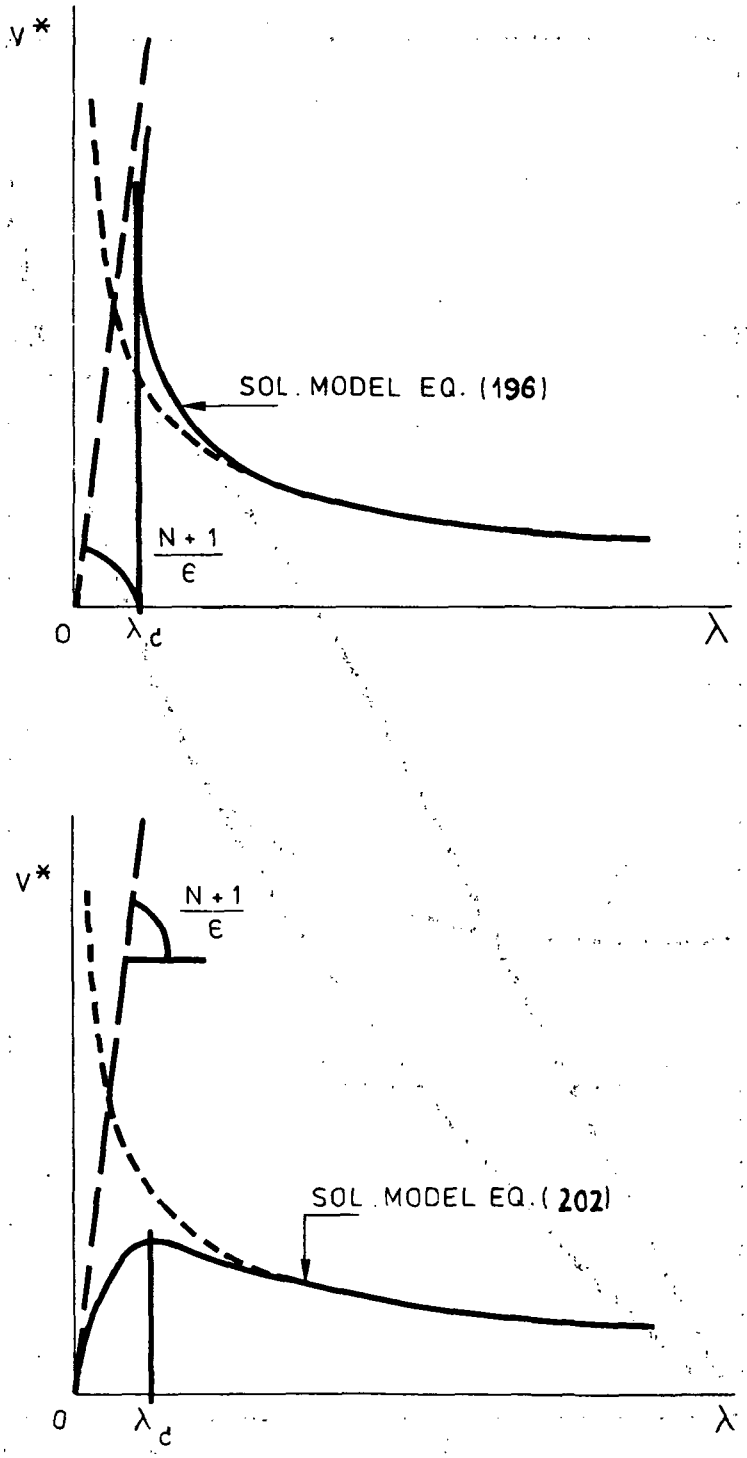

Figure 14. Solutions of two non-linear first order model equations.

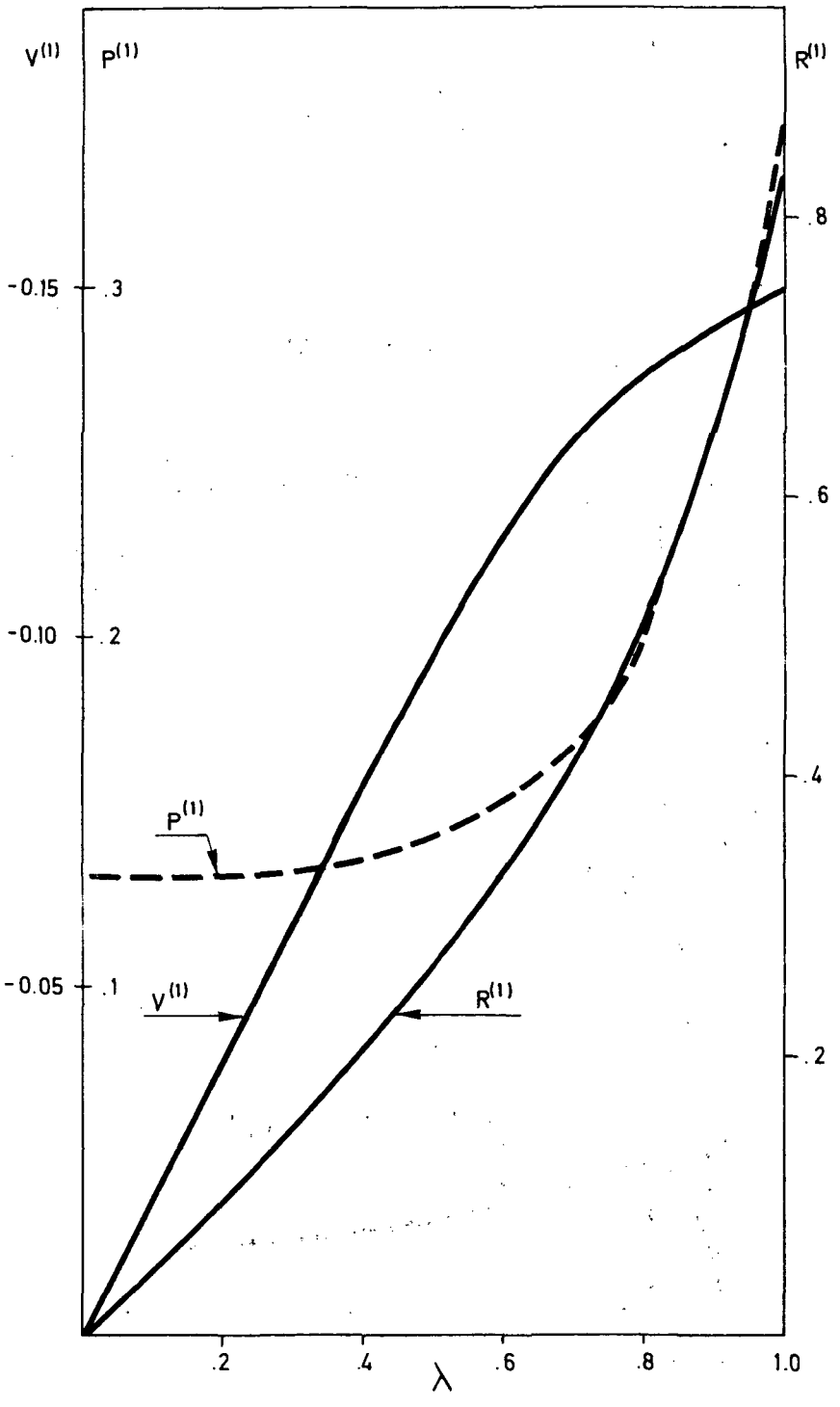

Figure A. Velocity, density and pressure perturbation profiles for finite counterpressure.

NATIONAL AERONAUTICS AND SPACE ADMINISTRATION
WASHINGTON, D.C. 20546

OFFICIAL BUSINESS
PENALTY FOR PRIVATE USE $300

SPECIAL FOURTH-CLASS RATE BOOK

POSTAGE AND FEES PAID
NATIONAL AERONAUTICS AND SPACE ADMINISTRATION
451

U.S.MAIL

POSTMASTER: If Undeliverable (Section 158 Postal Manual) Do Not Return

"The aeronautical and space activities of the United States shall be conducted so as to contribute . . . to the expansion of human knowledge of phenomena in the atmosphere and space. The Administration shall provide for the widest practicable and appropriate dissemination of information concerning its activities and the results thereof."

—NATIONAL AERONAUTICS AND SPACE ACT OF 1958

NASA SCIENTIFIC AND TECHNICAL PUBLICATIONS

TECHNICAL REPORTS: Scientific and technical information considered important, complete, and a lasting contribution to existing knowledge.

TECHNICAL NOTES: Information less broad in scope but nevertheless of importance as a contribution to existing knowledge.

TECHNICAL MEMORANDUMS: Information receiving limited distribution because of preliminary data, security classification, or other reasons. Also includes conference proceedings with either limited or unlimited distribution.

CONTRACTOR REPORTS: Scientific and technical information generated under a NASA contract or grant and considered an important contribution to existing knowledge.

TECHNICAL TRANSLATIONS: Information published in a foreign language considered to merit NASA distribution in English.

SPECIAL PUBLICATIONS: Information derived from or of value to NASA activities. Publications include final reports of major projects, monographs, data compilations, handbooks, sourcebooks, and special bibliographies.

TECHNOLOGY UTILIZATION PUBLICATIONS: Information on technology used by NASA that may be of particular interest in commercial and other non-aerospace applications. Publications include Tech Briefs, Technology Utilization Reports and Technology Surveys.

Details on the availability of these publications may be obtained from:

SCIENTIFIC AND TECHNICAL INFORMATION OFFICE

NATIONAL AERONAUTICS AND SPACE ADMINISTRATION

Washington, D.C. 20546